Tip-over Stability Analysis and Enhancement for Omnidirectional Personal Mobility Robots with Active Dual-wheel Caster Assemblies

2014, March

Muhammad Juhairi Aziz Bin Safar

Graduate School of
Natural Sciences and Technology
(Doctor's Course)
OKAYAMA UNIVERSITY

This page is intentionally left blank.

Abstract

This thesis focuses on the tip-over stability study for a personal mobility robot with a holonomic and omnidirectional capability. The design of this personal mobility robot is based on the principle of omnidirectional mobile robots with active dual-wheel caster assemblies. A unit consisting of one active dual-wheel caster (ADWC) enables two degrees of freedom motion at the steering axle for forward and lateral direction. By attaching two units of ADWC to a mobile body, it enables three degrees of freedom motion at the center of the line connected between both steering axles. The ADWC mechanism is chosen instead of the conventional specialized wheel due to the implementation of standard wheel with rubber tire. It offers a better traction power without any disturbing vibration as produced by most specialized wheels. The design of the wheel also does not require any specific expertise. However, the personal mobility robot with ADWCs possesses dynamic footprints in return for the rapid changes of the ADWCs in order to produce the holonomic and omnidirectional motion. In contrary to the existing on-road vehicles and the omnidirectional mobile robots with specialized wheels, the prediction of the tip-over occurrence in this personal mobility robot is difficult due to the rapid changes in the footprint. Therefore, this thesis is presented to solve this problem by introducing a tip-over prediction method and a tip-over stability enhancement method for this type of personal mobility robot.

The robot's footprint is estimated by finding the solution of the convex polygon of n-ground contact points. Here, the value of n depends on the number of wheels used. At any position, the convex polygon for a six-wheeled robot can be evaluated either as tetragon, pentagon or hexagon. The possibility of tip-over occurrence for any instant is measured by using the tip-over stability metrics. Two types of tip-over stability metrics have been examined: i.e., moment stability measure and force-angle stability measure. The force-angle stability measure is superior in the sense of correctness to the moment stability measure since it is also sensitive to the changes of height of the center of gravity (CoG). The candidate of the tip-over axis is evaluated using these stability metrics incorporated with the dynamical model. This dynamical model is derived based on the solution of the Newtonian equilibrium to estimate the reaction ground forces of the wheels.

The summation of the reaction ground forces in the z-axis direction is later used to estimate the acting net-force at the CoG, which works in the perpendicular direction of the candidate tip-over axes. It is evaluated with the force-angle stability measure to find the most potential tip-over axis. The potential tip-over direction is described by a line

connecting the CoG to the potential tip-over axis perpendicularly. For a better representation, this potential tip-over direction is measured by using the angle between this perpendicular line and the longitudinal direction of the robot. However, the occurrence of the tip-over incident is only predicted if the stability metric is less than zero. For a safety reason, a threshold is set to a positive stability value. The tip-over stability enhancement system is activated for the value less than the preset threshold.

Two types of tip-over stability enhancement are proposed: i.e., the alteration of the acceleration input and the implementation of the gyroscopic torque device. Both approaches are considered for the personal mobility robot because an additional motion is unnecessary during the travel to avoid the collision with human and other objects. In the former method, the input is altered to comply with the preset stability metrics. This method is more suitable for being taken into the robot path planning instead of instantaneous tip-over prevention. Meanwhile, the latter method is more suitable for the real-time operation. A gyroscopic torque device is used to produce the counter torque against the tip-over direction. This gyroscopic torque device is realized by implementing a single-gimbal control moment gyro. Both methods are proven to be capable for enhancing the tip-over stability of the personal mobility robot as shown by simulation results. The performance of the latter method is also proven to be superior in travel time cost to the former method.

Acknowledgements

First and foremost, I would like to express my sincere gratitude to my advisor, Professor Keigo Watanabe, for his continuous support and his excellent guidance for my doctoral study and research. Honestly, I have gained a lot of knowledge and priceless research experience that are so beneficial for my future.

A special thank to the Ministry of Education Malaysia (previously Ministry of Higher Education Malaysia) and Universiti Malaysia Perlis (UniMAP) for giving the opportunity and providing the fund for my PhD study. I will try as much as possible to convert all of the knowledge and experience that I gained during my study for the development of Malaysia.

My sincere thanks also goes to Dr. Shoichi Maeyama and Dr. Isaku Nagai for their support during my stay in the laboratory. Many thanks to my research colleagues including the current and former members of Mechatronics System Laboratory.

I would like also to express my very great appreciation to my family especially my mother, my late father, my wife and my daughters for their full support and continuous encouragement throughout my study. To my friends, thank you for listening, offering me advice, and supporting me through this entire process.

Above all, I owe it all to Almighty God for granting me the wisdom, health and strength to undertake this research task and enabling me to its completion.

Contents

List of Figures

List of Tables

Chapter 1

Introduction

1.1 Background

The importance of robots in human environment is progressively increasing. The robot sale between year 2013 to 2016 for industrial and service robots is estimated to continuously increase [1]. The use of robot also is no longer limited to the industrial field but already invades into every aspect of human life including a domestic area for personal use. Robots are utilized to assist human to make every job easier, decreasing the labor power and also provide the satisfaction to the completeness. One of the main streams in current robotics technology is the mobile robotics. At present, a countless number of applications and designs can be easily found in human surroundings. Most of these mobile robots are widely used for transportation [2], inspection [3, 4] and surveillance [5, 6, 7]. The importance of these mobile robots cannot be neglected, especially for their contribution to the improvement of human life.

In recent trend, many researchers are pursuing on the green technology and eco-friendly technology. A number of paradigm-shifting technical approaches can be noted in various fields to reduce the burden of environmental problems by managing the greenhouse gases and waste. Recent report shows that road transports were among the largest contributors to the global warming problem. In the year 2011, transport (including shipping and aviation) was responsible for 22% of CO_2 emissions globally [8]. Meanwhile according to the Japanese Ministry of the Environment report [9] as summarized in Table 1.1, the transport in Japan has contributed 18.8% of CO_2 emission locally which equal to 227 megatons for the year 2012. This percentage is expected to grow in near future according to the increased demand of transportation for the economic and personal activities in both developed and developing countries.

TABLE 1.1: CO_2 emissions produced by Japan within each sector in year 2012 [9]

Sector	**Amount** (Mt-CO_2)
Industries (factories, etc)	431
Transport (cars, etc)	227
Commercial and other (commerce, service, office, etc)	259
Residential	203
Energy Industries (power plants, etc)	86.3
Total	1207

In the automotive field, the introduction of new technologies like hybrid vehicles, electric-powered vehicles and environmentally friendly fuel was among the solution provided by the automotive makers. These kind of vehicles may offer better CO_2 emission in comparison to the conventional gasoline engine. These approaches may reduce the environmental pollution brought about by the conventional transportation. However, other problems such as traffic congestion problem especially in big cities continue to be unsolved. Most people prefer to use their own cars instead of the public transports and the carpooling system even for a very short distance travel. According to our survey, most of the automotive makers tend to show interest in developing alternative fuels and engines. This may solve the first given problem on managing the pollution issues. However, only a few automotive makers were interested on developing miniature sized vehicles of a single passenger or two passengers in concern to the second mentioned problem. These miniature sized vehicles for personal transportation are expected to improve the existing motorized systems in near future.

1.2 Personal mobility

The term of personal mobility (PM) can be defined as the ability to transport the human from one place to another place. It can be related to the use of personal transportation such as bicycles, skateboards, scooters, wheelchairs, etc. However, the modern term of personal mobility is always referring to the vehicles of a solo passenger or two passengers which are normally operated by an electrical system [10]. It can be referred in many literature by other names like Personal Transporter (PT) [2, 11, 12], Personal Vehicle (PV) [13], Personal Electric Vehicle (PEV) [14], Personal Mobility Device (PMD) [15], Personal Mobility Vehicle (PMV) [16, 17, 18] or Personal Mobility Robot (PMR) [19, 20, 21]. The first vehicle used the term 'personal mobility' as a name can be found as early in late

1980s [22]. It takes almost two decades before this term became famous when the Segway Corporation introduced their first two-wheeled personal transporter which is called as Segway Human Transporter or Personal Transporter in 2001.

The personal mobility vehicles can offer several potential benefits to the consumers and society as the replacement to the existing automobiles such as:

- Reduction of air pollution by using clean energy and green technology. Most of the personal mobility vehicles were half or fully powered by an electrical system using batteries. Almost no harmful wastes were produced by them.
- Lower total operating costs than the conventional automobiles. Most of the personal mobility vehicles can be purchased at a very cheap price in comparison to the conventional vehicles. Other expenditures such as for licensing, insurance, parking or maintenance were also quite minimal.
- Free from noise pollution. Many existing personal mobility vehicles were electrical powered where the electrical motors were adopted in replacement to the conventional gasoline engine. Electrical motors produced a non-annoying sound with very minimal noise which is acceptable even in a traffic congestion.
- Reduction of traffic congestion problems. Many people tend to move with their individual car even when they drive alone or for a short distance travel. The use of personal mobility vehicles can reduce the spaces needed on the road and possible to improve the traffic even during the peak hours. Other associate problems with the traffic congestion such as air pollution, noise, consumption of non-renewable resources and traffic accidents also can be reduced.
- Reduction of parking spaces. With the miniature size, the area needed for a parking is smaller than the size of the standard on-road vehicles. Currently available parking spaces can support more parking lots which are possible to eliminate the waiting time and reduce the traffic congestion problem due to a long parking queue.
- Multipurpose transportation for indoor and outdoor application. The personal mobility vehicles can be used for both outdoor and indoor activities without or with a very light modification.
- Mobility for those with limited ability to walk especially disabled people, sick people and elder community.

Today, a number of existing products and ongoing researches regarding the personal mobility vehicles can be easily found from markets and websites. There are overlapping interest

in automotive industries and robotic fields. Giant automotive companies like General Motors, Toyota and Honda were among the pioneers in the current personal mobility vehicles together with other specialized companies like Segway etc. Many researchers in academia also played a big role for the current achievement in personal mobility vehicles. Every personal mobility vehicle has its own special characteristics. For example, the Segway Personal Transporters (Segway PTs) were built based on the two-wheeled differential drive architecture with a self-balancing capability which was achieved by the implementation of the inverted pendulum model. The passenger of the Segway PTs can steadily stand still in a static condition or even in the existing of dynamics in the maneuver mode. Many of the later researches have been benefited from this concept. Toyota Motor offers various models of its personal mobility technology. One of the series offered from the Toyota Motor is similar to the design of the Segway PT but with smaller packaging is known as Toyota Winglet. Other models from Toyota Motor applied three or four wheels for better stability with amazing adjustable mechanisms for different driving modes and cornering safety. Meanwhile, Honda Motor is focused on a single-wheeled personal mobility vehicles but capable for omnidirectional motion. Other products of personal mobility vehicles can be found as four-wheeled compact cars, wheelchairs and scooters. Some of these personal mobility vehicles will be introduced in detail in the following chapter.

There are several challenges and issues in the development of personal mobility vehicles as the future transportation. Among these challenges, there are two major concerns that we are interested in: (1) the ability of the personal mobility vehicles to move in a very limited area especially in a crowded pedestrian area and narrow spaces in the domestic area, and (2) the safety aspect related to the stability and the tip-over occurrences with respect to the existing of dynamic properties. Due to these concerns, several existing mechanisms that offer the full ability to perform two dimensional planar motions, i.e. holonomic and omnidirectional mechanisms, were examined. There are various existing arrangements which give a three degrees of freedom motion such as Mecanum wheels, orthogonal wheels, chains of spherical or cylindrical wheels and ball wheels. Most of the mechanisms, except vehicles with the ball wheels, have discontinuous ground contact which leads to the undesirable vibration and shocks. Although the current trend tends to the application of these specialized wheel mechanisms, the implementation of omnidirectional mechanism with the standard tire is more desirable in order to improve the traction power of the wheel drive and to obtain a smoother maneuver. The application of the standard wheel also allows the motion on a slightly uneven terrain which will be suited for both indoor and outdoor applications.

The safety aspect regarding the tip-over occurrences of the personal mobility vehicles can be realized by providing a tip-over prevention system. Therefore, a continuous stability

measuring, tip-over prediction and tip-over prevention are essential for this purpose. There are several existing methods to assess and evaluate the stability such introduced in the following chapter. However, according to the existence of dynamical effects such as instant acceleration and braking in the real environment, personal mobility vehicles should be able to resist the tip-over incident and maintain the upright position in all conditions. Thus, a tip-over prediction for the personal mobility vehicles, which are sensitive to the changes in the dynamic properties, is necessary. In order to prevent collision with the people or the surrounding objects during the tip-over prevention, an additional motion such implemented in the inverted pendulum model is undesirable. Thus, tip-over prevention mechanisms that are possible to maintain the trajectory and the pose of the personal mobility vehicles are more attractive.

1.3 Contribution

In general, this thesis introduces the solutions for the above mentioned issues. A holonomic and omnidirectional platform with active dual-wheel caster assemblies is proposed as a personal mobility robot. This structure uses the standard wheels with rubber tires which enable better traction and are capable of overcoming slightly uneven terrains or steps. Due to the application of the active dual-wheel casters, the personal mobility robot possesses a dynamic footprint. Tip-over prediction method and prevention method for this kind of personal mobility robots are proposed.

The contribution of this thesis can be discussed in detail as follows:

- Derivation of the dynamical equations to estimate the wheel reaction forces for two types of the omnidirectional personal mobility robots with active dual-wheel caster assemblies, i.e., four-wheeled architecture and six-wheeled architecture. Wheel reaction forces are used to estimate the net-force and its components on each boundary of a support polygon for the vehicle's footprint.
- The moment-stability measure (MSM) is introduced as an alternative tip-over stability metric using the wheel reaction forces. This metric is evaluated using the four-wheeled omnidirectional mobile robot.
- The prediction of the tip-over occurrence is introduced using the derived dynamical model and the tip-over stability measures, i.e., the MSM and the force-angle stability measure (FASM). Estimation of the possible tip-over axis and the tip-over direction is presented.

- Tip-over stability enhancement methods without additional motion, i.e., the alteration of the acceleration input and the production of gyroscopic torque using a single-gimbal control moment gyro, are introduced.

1.4 Thesis organization

After describing this introduction in Chapter 1, this thesis is organized as follows:

Chapter 2 introduces the background study of the personal mobility robots. The previous and existing works of various personal mobility robots were presented and discussed regarding their design, problems and also the concern of safety in term of tip-over stability. Several types of omnidirectional mechanism in mobile robotics including the specialized wheel and the standard wheel with rubber tire were also presented. The idea of implementing the holonomic omnidirectional mechanism with standard wheel in personal mobile robot is discussed in detail. Other concerns in the personal mobility robot including the safety aspect regarding the tip-over stability are also explained.

Chapter 3 introduces the model of the personal mobility robot. The kinematic model of active dual-wheel caster and the omnidirectional mobile robot with active dual-wheel caster assemblies are explained. The motion control based on the kinematic model under the resolved velocity control is also presented. These kinematic equations and the resolved velocity control are the preliminary basis for our study. In this chapter, the personal mobility robot is modeled in two designs: (1) four-wheeled architecture and (2) six-wheeled architecture. The derivation of dynamical models for both architectures is explained to estimate the wheel reaction forces.

Chapter 4 describes the tip-over prediction method for the holonomic omnidirectional mobile robot with active dual-wheel caster assemblies. Several methods to measure the tip-over stability are provided and discussed in detail. In consideration with the existence of dynamical effects, the force-moment stability measure and the force-angle stability measure were applied to the four-wheeled architecture and the six-wheeled architecture respectively. The model to estimate the value of the net-force is also presented by using the dynamical model as explained in the previous chapter. At the end of this chapter, the concept of tip-over prediction including the prediction of the tip-over axis and the estimation of the tipping direction is explained in detail. The performance of these prediction methods is evaluated with other techniques.

Chapter 5 explains the tip-over prevention method and the tip-over stability enhancement method for the holonomic omnidirectional mobile robot with active dual-wheel caster assemblies. Two possible approaches for tip-over stability enhancement are discussed: (1) alteration of pre-planned velocity and acceleration input and (2) gyroscopic torque device using single-gimbal control moment gyros. The evaluation of both approaches is also presented at the end of this chapter.

Chapter 6 summarizes the developed methodology proposed in the thesis and gives the future works in the direction of this research.

Chapter 2

Literature Review

2.1 Introduction

Humans have made use of the personal mobility vehicles for some hundred years. Their contribution to society is well known. Modern personal mobility vehicles which are related to the robotics field can be represented by wheelchairs and scooters. The improvement in their technologies is very great, from a wooden structure and human powered to the recent motorized technology. The first electric wheelchair was invented in 1950 by a Canadian inventor which was specifically designed for quadriplegics. Meanwhile, mobility scooters were first introduced in 1960s. In 1970s, mobility scooters became a very popular alternative to the powered wheelchairs. Mobility scooters are more intended for people who are able to walk for a short distance, but it is found to be painful to do so over extended periods of time. Nowadays, the wheelchairs and the scooters are very advanced. Some of

(a) Motorized wheelchair (b) Mobility scooter

FIGURE 2.1: Example of current motorized wheelchair and mobility scooter [23]

the wheelchairs now are capable of step climbing and some are equipped with omnidirectional ability. Most of the existing wheelchairs and scooters are purposely designed for the disabled and elder people.

2.2 Previous work

Recent personal mobility vehicles are enriched with artificial intelligence and robotics technology. These kind of personal mobility vehicles are also known as personal mobility robots. While vehicles such as motorized wheelchairs and mobility scooters had existed since a long time ago, the modern personal mobility had become the focus of the world when the Segway introduced their first Segway Personal Transporter (Segway PT) in the Good Morning America program in year 2001 [24]. Since then, the personal mobility is not only known as transportation but also recognized as an enjoyable riding device.

The Segway PT is designed as a two-wheeled vehicle using the differential drive concept. It is equipped with a self-balancing system using the inverted pendulum model. The rider has to be in the standing mode during maneuver and able to change the moving direction just by leaning the handle towards the desired direction without collapse. Segway also has produced several models of personal transporter using the same basis but with variety of accessories according to the user needs. Under cooperation with General Motors, this machine has been extended into two passenger road vehicle named Personal Urban Mobility and Accessibility (PUMA) [25] in 2009 as a proposal for a short distance eco-friendly urban transport. In the year 2011, General Motors and Segway improved the PUMA with active safety technologies such as adaptive cruise control, side blind zone warning and automatic park assist. This new personal mobility is called Chevrolet EN-V (Electric Networked-Vehicle) [26].

(a) Segway PT (i2) [27] (b) PUMA [25] (c) Chevrolet EN-V [26]

FIGURE 2.2: Segway PT based technologies

The impact of the Segway PT is too great. Most of the successors in the personal mobility robot has been adapting its technology into their designs. A numerous papers that discussing the similar layout of Segway robot can be found until today [28, 19, 29]. Most of them focused on the development of balancing control using the inverted pendulum model [30].

Toyota Motor is the only vehicle makers that show a great interest in developing personal mobility robots [31]. Since year 2003, Toyota Motor has introduced at least six models of their concept mobility robots/vehicles such as Toyota PM [32], i-Unit [10], i-Swing [33], i-Real [34], Winglet series [35] and i-Road [36]. The first Toyota's mobility robot, Toyota PM, is introduced in year 2003 as a one passenger vehicle with smaller cabin than the conventional car. It comes with a four-wheeled layout with a rear motor driven and impressive front steerable hollow-center wheel. The Toyota PM also features three driving modes – the "high-speed" mode sees the posture drop lower for a more aerodynamic profile, in "city" mode the posture of the vehicle is raised a better view at low speed and the "entry/exit mode" enables the left and right rear wheels to turn in opposite directions, creating an awesome turning circle for parking just about anywhere. A further evolution of the Toyota Personal Mobility concept called the "i-Unit" is introduced in year 2005. Some improvement on the design concept and the intelligence such as personalized recognition system according to the individual's preferences and emotions were made. The basic package for the i-Unit contains two modes: a low-speed mode and a high-speed mode. It can maneuver equally well within rooms and on ordinary streets, and was developed to offer "personal mobility" for a single driver.

The second generation of personal mobility by Toyota Motor which featured by i-Swing is also introduced in year 2005. It comes with dual driving modes – a two-wheeled drive in city area which also enables the user to chat while walking with other pedestrians at the same face level, and a three-wheeled drive for a more aggressive movement. The rear wheels are adjustable during turning to increase the stability. The approach for driving and balancing in the two-wheeled mode is the same as the Segway PT. Later in the year 2007, Toyota has introduced a new model named "i-Real". It is a three-wheeled vehicle, with two wheels in the front and one in the back, and is capable of switching driving modes between walking mode and cruising mode. It requires a drive controller to enable operability regardless of the driver's physical abilities. Anyone can easily operate it even with one hand. Also, an "active lean" system is adopted, which is an innovative balance controller that enables stable acceleration, deceleration, and turns as well as superior dynamic performance. There are numerous safety measures, such as a perimeter monitoring sensor that detects obstacles and alerts others of your presence through the pleasing use of lights and sound. There are likewise other functions that make traveling

(a) Toyota PM [37] (b) i-Unit [37] (c) i-Swing [37]

(d) Winglet series [35] (e) i-Real [37] (f) i-Road [36]

FIGURE 2.3: Toyota personal mobility robots

more fun, such as a communication display capable of sending and receiving blogs and local information as well as sharing information with other i-Real drivers.

In August 2008, Toyota Motor has announced the development of the "Winglet" series, a personal transport assistance robot ridden in a standing position. The Winglet consists of a body that houses an electric motor, two wheels and internal sensors that constantly monitor the user's position and make adjustments in power to ensure stability. Meanwhile, a unique parallel link mechanism allows the rider to go forward, backward and turn simply by shifting body weight, making the vehicle safe and useful even in tight spaces or crowded environments. Toyota has created three models, the "L", "M" and "S", each having different handling features that allow consumers to select a model appropriate to their needs – from "practical" to "hands-free sporty". In the year 2013, Toyota Motor presented their latest model, i-Road, as an alternative transportation to negotiate with busy city streets. It can cut through the congested traffic like a motorbike, but with a comfortable drive like a car. The i-Road comes with a standard motorbike size which can also fit to two passengers.

Another vehicle maker from Japan, Honda Motor has also introduced at least three models

(a) U3-X [38] (b) UNI-CUB [40] (c) 3R-C [41]

FIGURE 2.4: Honda personal mobility robots

of their personal mobility devices. The first model is U3-X [38], a single-wheeled experimental device providing seated transportation for a single user which released in the year 2009. The most remarkable features of the U3-X are its innovative balance-control mechanism and the ability to move laterally. The U3-X can still remain in an upright position whether with the passenger or not. It adopts the stability technology which applied in the famous ASIMO bipedal robot. The U3-X not only enables the motion in the lateral direction on a single wheel, but it enables the motion in any desired direction using the Honda Omni Traction Drive System [39]. The wheel of the Honda Omni Traction Drive System is structured by a series of motorized small wheels which attached to the main large-diameter wheel like the conventional omni-wheels. The main wheel is used to move forwards and backwards, while the smaller wheels rotate perpendicular to the main wheel for moving side to side. Combining both functions, it is possible to cause the U3-X to move diagonally. In May 2011, Honda unveiled the prototype of UNI-CUB [40], a personal mobility device offering enhanced ease of control and mobility. This new model is just an improved version of the previous U3-X model. The new system introduced a new traction system with an additional turning wheel at the back. This turning wheel moves laterally to ease the turning of the robot and enables an instantaneous turn at its center. Honda Motor also introduced a three-wheeled concept vehicle for one passenger named 3R-C [41] in the year 2010. At a glance, this 3R-C vehicle is almost alike to the Toyota's i-Road. It has a flexible canopy for weather and safety protection. However, the details of the driving mechanism and other specialties were remained unknown until today.

A famous Korean vehicle maker, Hyundai Motor, has introduced their first personal mobility vehicle named E4U [42] on March, 2013. The initial letter "E" represents "egg," "evolution," "ecology," etc. It can be moved in any direction with a motor that rotates only in one direction. Instead of tires, the vehicle uses a rotating semispherical part. When the part is vertical to the ground and rotating in the horizontal direction, a force is produced to spin the vehicle. To prevent the vehicle from spinning, it has two safety

wheels on the rear side. At this point, the vehicle does not move even though the semispherical part is spinning because of the frictional force generated by the safety wheels. So, the wheels function like the tail rotor of a helicopter. On the other hand, when the semispherical part is tilted, it becomes possible to move the vehicle because the rotative force is transmitted to the ground. The semispherical part rotates counterclockwise. And the direction of travel can be controlled by using the feet placed on the part to tilt it.

FIGURE 2.5: Hyundai E4U [42]

FIGURE 2.6: Hitachi Ropits [43]

In the same month, Hitachi also has announced the development of a mobility-support robot named Robot for Personal Intelligent Transportation System (ROPITS) [43]. Although at a quick glance the ROPITS may seem similar as other miniature four-wheeled vehicles without any remarkable futuristic design, the ROPITS actually is developed for a specific purpose to autonomously navigate within a specified arbitrary point with autonomous pick-up and drop-off function. In order to work autonomously, ROPITS is equipped with a variety of navigation tools including a GPS, a gyro sensor, and laser sensors. The most significant feature of ROPITS is the implementation of active suspensions which were mounted at each wheel so that the vehicle can be kept in a comfortable upright position even on the uneven ground.

In this section, only a few personal mobility robots were presented. Yet there are still many personal mobility vehicles that exist as the future concept cars. Some were examined and some are still progressing in the development stage. There are also numerous designs and layouts provided by the academia around the globe such mentioned in [16, 19].

2.2.1 Challenges in the personal mobility robots

The development of personal mobility robots will continuously progress toward a better solution for the existing transportation problems. At least, there are four major problems of the existing transportation that were identified and focused by many researchers which are air pollution, energy consumption, traffic congestion and road accidents. These major problems are estimated to decrease by implementing the personal mobility robots as the alternative to the current transportation. At present, there are many ongoing projects to study and analyze the possibility to use them in public. In Japan, a specific zone for the experimental purpose located in Tsukuba City which is known as Tsukuba Mobility Robot Experimental Zone [44] is opened since March, 2011. A few models are tested in this area like Segway PT, Toyota Winglet and Hitachi ROPITS. Another example for a public test has been conducted by Toyota in public areas such as airports and industrial facilities since 2008 [45].

A new personal mobility should also consider a few improvements in automation, electrification, battery, system integration and locomotion system. Most of the above mentioned personal mobility robots are unique and have their own specialties. However, in consideration to the realization of better maneuvering in crowded and narrow areas, the ability to move in a holonomic and omnidirectional motion is desirable for a new personal mobility robot. All the above mentioned personal mobility robots, except Honda U3X and UNI-CUB, did not consider a holonomic and omnidirectional motion in their locomotion systems. The Honda U3X and UNI-CUB offered this capability but restricted to a single-wheel structure which might not be suitable for uneven grounds. There are numerous examples for omnidirectional and holonomic mechanisms that actually existed in mobile robotics field. Several mechanisms are discussed and introduced in the following section.

2.3 Holonomic and omnidirectional locomotion system

A major achievement for any vehicle or mobile robot is the ability to move freely in any direction and performing rotation at any arbitrary position and orientation. This can be realized by obtaining a locomotion system with the ability to perform a holonymy and omnidirectional motion. Both abilities are necessary for realizing better maneuver in a crowded area or restricted space. A non-holonomic omnidirectional mechanism [46, 47] requires preliminary maneuvering for reorientation of steering wheel which may affect the time-travel cost and the spaces needed. The holonomic omnidirectional mechanism has better mobility and also less complexity in design compared with a non-holonomic omnidirectional mechanism.

There are several well-known holonomic omnidirectional platforms which adapting the following wheel or mechanism:

- mecanum wheels - Swedish, universal wheel
- orthogonal wheels
- crawler mechanisms
- spherical/ ball wheel
- syncho-drive
- offset driving/ caster wheel

2.3.1 Mecanum wheels

Berg Ilon [48] patented the first mecanum wheel which also known as Swedish wheel in 1975 for an omnidirectional vehicle. The patented design has several passive rollers arranged at certain angle along the outer rim of the wheel. A driving velocity of the wheel produces a lateral direction force at the rollers which then produce driving forces in longitudinal and lateral direction of the wheel itself. There are two popular variations of mecanum wheel; 45 deg and 90 deg configurations. The 90 deg mecanum wheels did not produce lateral forces according to the elimination of non-holonomic velocity constraint. This kind of mecanum wheel also called as universal wheel or omni-wheel. Typical design of omnidirectional platforms with both wheels [49] are shown in Fig. 2.7. Some papers also introduced the omnidirectional mobile robots with four omni-wheels design [50]. Many vehicles or mobile robots with mecanum wheels are developed according to these arrangements. In addition, Chugo et. al. introduced a stair climbing omnidirectional mobile platform with mecanum wheels using passive linkages [51, 52]. Seven units of omni-wheels were adopted into their design in consideration to the stability during climbing. While there are also a few approaches to actuate all small rollers in the conventional omni-wheel to obtain a longitudinal and lateral motion within a single wheel [40, 53]. By actuating both small rollers and the outer wheel, it can move in any desired direction.

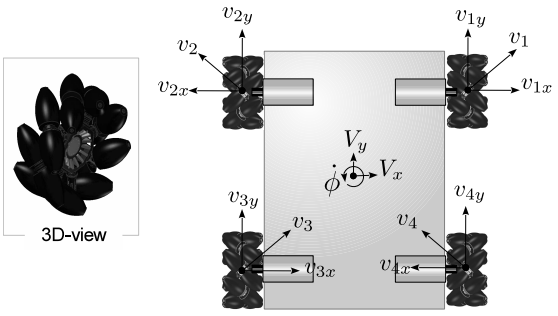

(a) Mecanum wheel

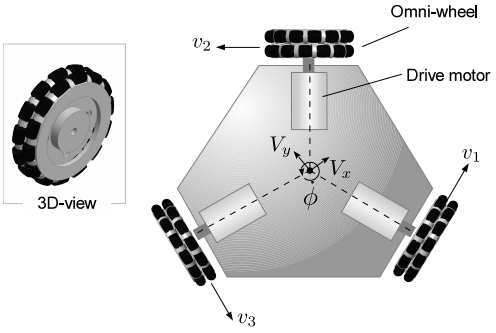

(b) Omni-wheel

FIGURE 2.7: Conventional mecanum wheels [49]

2.3.2 Orthogonal wheels

Pin and Killough [54] presented a novel locomotion system based on orthogonal wheels as shown in Fig. 2.8. The idea is that a pair of sliced spherical wheels is placed at the driving axle in an orthogonal configuration. These wheels can freely rotate at the driving axle and produce a rolling force in the driving direction while at the same time produce a pure free rolling in the orthogonal direction. With this arrangement, the contact with the ground can be assured at all times to produce a better traction force compared to the mecanum wheel. They have presented the orthogonal wheel with two types of wheel assembly: longitudinal assembly and lateral assembly. Using at least three pairs of those assemblies will produce an omnidirectional motion. The concepts and kinematics model for both assemblies are presented in [55]. Meanwhile, the dynamical model and control methods for omnidirectional mobile robots with orthogonal wheels are presented in [56, 57]. Two similar architectures to the longitudinal assembly type of orthogonal wheel are presented in [58, 59]. In replacement to the sliced ball in the conventional orthogonal wheel, these two architectures proposed an assembly of crown slices, i.e. two and four crown slices, to form a ball. Each crown slice can rotate freely around its center. These approaches are insensitive to fragments and irregularities on the floor but have a higher payload capacity than the conventional orthogonal wheels.

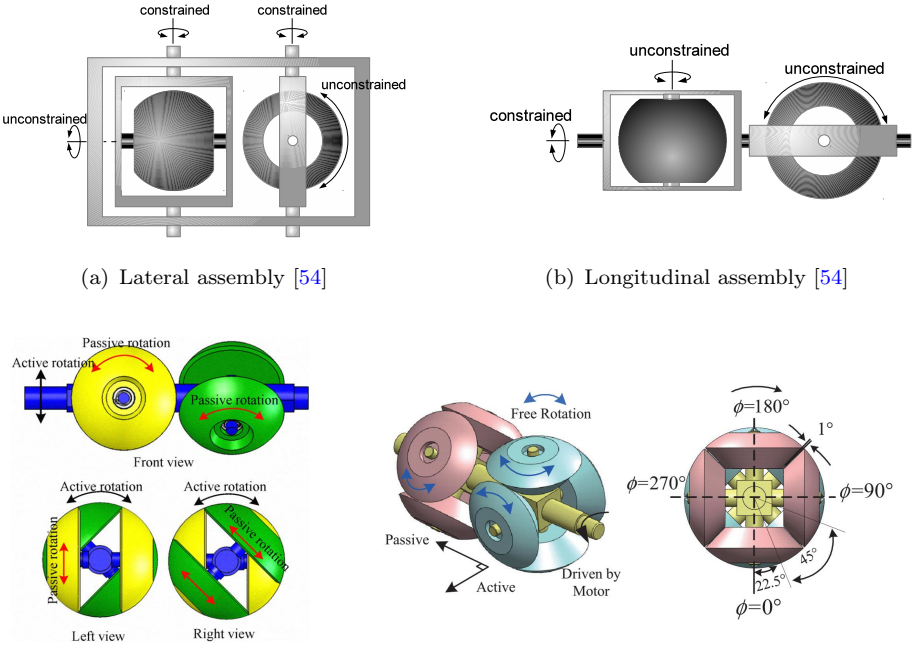

(a) Lateral assembly [54]

(b) Longitudinal assembly [54]

(c) My wheel [58]

(d) My wheel-II [59]

FIGURE 2.8: Orthogonal wheels and its variant

2.3.3 Spherical and ball wheels

West and Asada [60] and Ferriere [61] presented a three ball wheels of omnidirectional mobile robot. West and Asada used ring bearing and rollers to control the rotation and translation of the ball wheels. Ferriere replaced the bearing which used for controlling the rotation of the ball wheel by applying omni-wheel to each of the ball wheel as shown in Fig. 2.9(a). Similar layouts also are presented by Ghariblu [62] and Ishida [63]. Mascaro et. al. introduced a four-wheeled structure of ball wheel mechanism for wheelchair and bed system [64, 65]. Instead of a fix footprint, Wada et. al. [66, 67, 68] introduced an improvement to the design of Mascaro et.al. by applying a re-configurable footprint mechanism as shown in Fig. 2.9(b). The shape of the footprint will change depending on the space of maneuver. In a small space, the robot ables to change the width of the robot to adapt with the surroundings. The manipulation of ball in each ball wheel unit is similar to the design of West and Asada. Recently, Ok et. al. [69] introduced a link-driven spherical mechanism in two layouts named SO(2) and SO(3). Another interesting mechanism named omni-ball by Tadakuma et. al. [70, 71] solved the discontinuous ground contact point problem in the conventional omni-wheel design. Statically unstable layout of a single spherical wheel mechanism is presented by Nagarajan et. al. [72]. A dynamical control is essential to keep the mobile robot stable during maneuver.

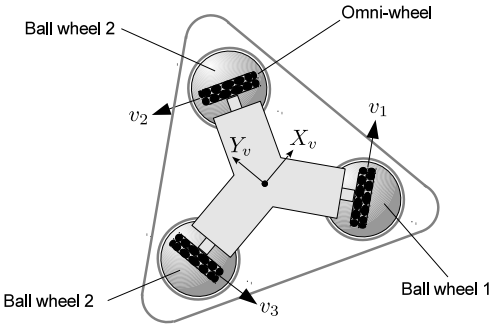

(a) Ball wheels locomotion with driving omni-wheels by Ghariblu [62]

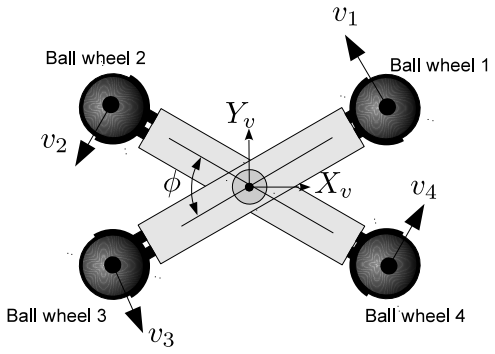

(b) Ball wheels locomotion with variable footprint by Wada et. al. [66, 73]

FIGURE 2.9: Spherical and ball wheels platform

2.3.4 Crawler mechanism

Nishikawa et. al. [74] presented a holonomic omnidirectional mobile robot using a crawler mechanism constructed by spherical balls as shown in Fig. 2.10. The vehicle comprises of two parallel tracks at the side which hold the spherical balls. The spherical balls are arranged into a circulating chain that controls forward and backward movement. At the same time, the spherical balls hold the load from the body through two controlled parallel rods. By rotating the rods the mobile platform can be moved in the desired sideways direction. Combining both mechanisms enabled an omnidirectional motion. However, this mechanism has significant sideways slippage and loss of contact with the ground especially during turns or uneven ground.

Hirose and Amano [75] developed an improved version of this crawler named Vuton by replacing the spherical wheel with cylindrical free rollers as shown in Fig. 2.11(a). This crawler has four units of track with wider contact surface to the ground. It has eliminated the sideways slippage and able to work with high payload. Another version of Vuton named Vuton II has been developed later by Damoto and Hirose et. al. [76] as shown in Fig. 2.11(b) using the four sets of active Omni-disc. Each Omni-disc comprised of several

casters and gears. This new vehicle is designed to be lower in cost and shorter in stature than the Vuton-I, but still maintains a reasonably high payload capacity.

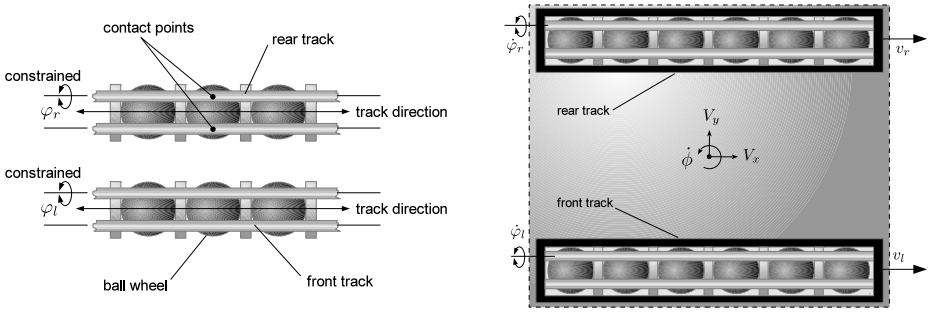

(a) Crawler track from upper view (b) Principle of the crawler (front view)

FIGURE 2.10: Crawler mechanism by Nishikawa et. al. [74]

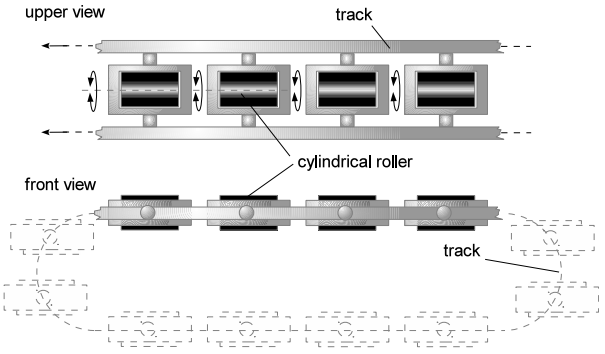

(a) Free roller track for Vuton [75]

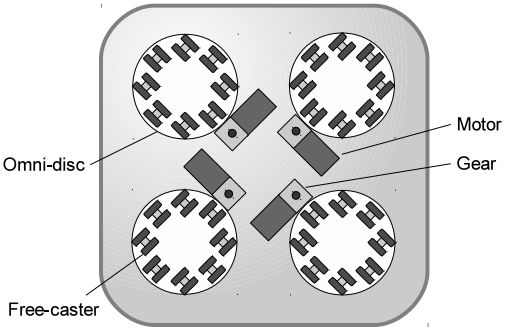

(b) Vuton II with omni-disc [76]

FIGURE 2.11: Crawlers for Vuton platform

2.3.5 Synchro-drive mechanism

Wada et. al. [77] introduced a synchro-drive caster mechanism as shown in Fig. 2.12. Wheel sprockets of all drive-casters are mechanically coupled by a drive belt and simultaneously driven by a wheel motor. Steering sprockets are coupled by another drive belt as well and driven by a steering motor. Since all drive-casters are driven and steered by common two actuators, each wheel executes the same motions at all times. Then each wheel gives an equal and parallel velocity vector to the drive unit, a resultant velocity vector of the drive unit would be identical to the wheel velocity vector. Another motor is added to the rotational stage to control the rotation of a vehicle frame relating to the drive unit to produce a holonomic motion.

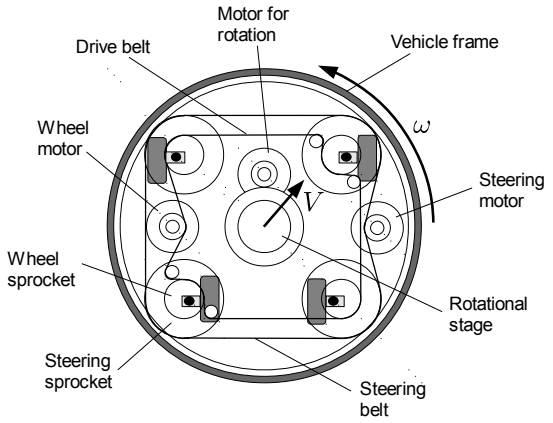

FIGURE 2.12: Holonomic synchro-drive mechanism proposed by Wada et. al.[77]

2.3.6 Offset driving and caster wheel

Wada and Mori [78, 79] developed a holonomic and omnidirectional mobile robot using two steered driving wheels, in which the wheel has the offset distance between the axle and steering axis like a caster and can use a normal tire such as a rubber tire and a pneumatic tire, instead of a specialized wheel mechanism. An active dual-wheel caster assembly was suggested by Han et. al. [80, 81], in which a wheeled mechanism has a passive steering axis with offset arranged on the front of a conventional two independent driving wheels mechanism, and a holonomic and omnidirectional mobile robot was realized by using two or more of these assemblies. This assembly can generate two-degrees of freedom velocity on the passive steering axis, because of the difference between the angular velocities of the left and right wheels. In addition, it can of course use a normal tire and is simple in structure. Another similar mechanism to Han et. al. is proposed by Yu et. al. [82] in the name of Active Split Caster Offset (ASOC). The improved version of this mechanism for uneven and rough terrain by exploiting the suspension and its control system is mentioned

in [83, 84]. Four units of ASOC are applied for better stability on rough terrain. Wada [85, 86] introduced the mechanism and control of a 4WD holonomic and omnidirectional wheelchairs. The mechanism consists of two standard differential drive mechanisms in rear position and another two omni-wheels at the front. Both omni-wheels at the front are connected with the belt to the respected actuator for the rear differential drive. The concept is similar to the offset driving caster principle as explained above. The front omni-wheels produced an additional traction force while at the same time allowing the movement in the lateral direction.

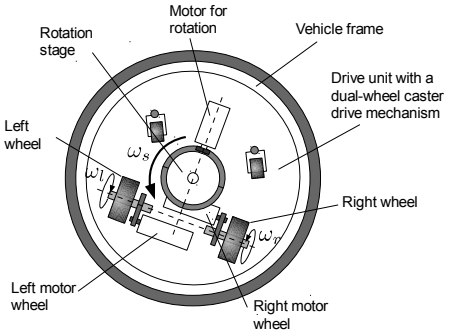

(a) Offset driving caster by Wada [78, 79]

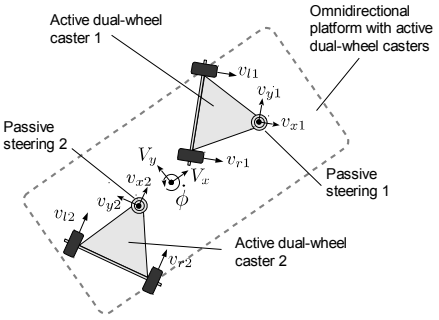

(b) Omnidirectional mobile robot by Han et.al. [80]

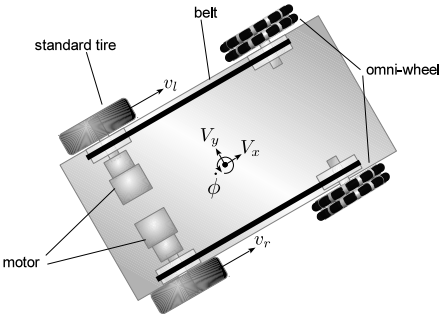

(c) Offset driving caster with omni-wheels by Wada [85, 86]

FIGURE 2.13: Caster wheel based omnidirectional platform

2.3.7 Problem and issues

Most of the above mentioned locomotion systems used special wheels to obtain the holonomicity and the omnidirectional functionality. The designs provided by the existing special wheels are too complicated and require a lot of expertise. Although most people are attracted to the uniqueness of the special wheels and their impressive motion, there are several deficiencies in their application such as:

i. slippery and lack of traction force due to small ground contact region,

ii. undesirable vibration and scratch due to discontinuous ground contact,

iii. high maintenance as the dirt and tiny objects can easily penetrate and stuck between spaces in the wheel, and

iv. low performance for outdoor application especially handling the steps and uneven terrain.

In order to solve the above mentioned problems, an omnidirectional platform in which a special wheel mechanism is not used and which is using normal tires seems to be more attractive. Thus, the desired personal mobility robot can be realized using this platform. With respect to the safety aspect of a personal mobility robot, it should be equipped with reliable safety systems that at least manage the obstacle avoidance and rollover (tip-over) avoidance. The research in obstacle avoidance is already advanced and it is possible to offer many reliable systems. However, the tip-over aspect has always been neglected due to the assumption of slow motion and statically stable. The following section will introduce some of the available methods involving the tip-over stability measurement.

2.4 Tip-over stability measurement

Stability is one of the essential abilities required for the vehicles or mobile robots especially for those involved with humans. The absent of stability control may lead to an undesired accident, injuries and damage to the machines and surrounding objects. There are continuous efforts by researchers for finding the best method to measure, monitor and prevent the instability in vehicles. In current automobile technology, Static Stability Factor (SSF) is used to evaluate the static stability of the vehicles. It is defined as the ratio of the vehicle width to CoG height [87] as described by

$$S_{SSF} = \frac{w}{2h} \tag{2.1}$$

where, w is the distance between the right and left wheel, and h is the height of the center of gravity. A higher SSF value equates to a more stable, less top-heavy vehicle. Other metrics such as Side Pull Ratio (SPR) and Tilt Table Ratio (TTR) are also available [88]. There are also various studies on the dynamics approach to prevent the roll over incidents in on-road vehicles [89, 90]. However, most of these approaches are specially developed for a fixed footprint such provided by cars and trucks. The stability of multi-legged vehicles for instant, which depends on different type of gaits may not be suitable for these approaches. Therefore, other methods that are versatile to the changes in the

support polygon are more desired. There are varieties of continuous work in mobile robotics which discussed both static and dynamic stability measurements. Some of them will be introduced in the next subsection.

2.4.1 Static stability

The first static stability criterion is proposed by McGhee and Frank in 1968 for an ideal walking vehicle at a constant speed along a predefined constant direction on a flat terrain [91]. The vehicle is considered statically stable if the center of mass lies within the support polygon which is formed by connecting the footprints. The work also proposed the use of the shortest horizontal distance between the center of mass to the boundary of the support polygon in the direction of motion to show the static stability. This definition was later redefined with respect to the concern of vehicle motion on uneven terrain [92]. Zhang [93, 94] has extended this technique by introducing longitudinal stability margin (LSM) and crab longitudinal stability margin (CLSM)

The above mentioned stability measures only consider the geometrical aspect of the support polygon and the position of the center of mass. Non of the kinematic and dynamic parameters were considered. All of these definitions however are very useful in gaits studies for walking machines in the consideration of slow motion [95, 96].

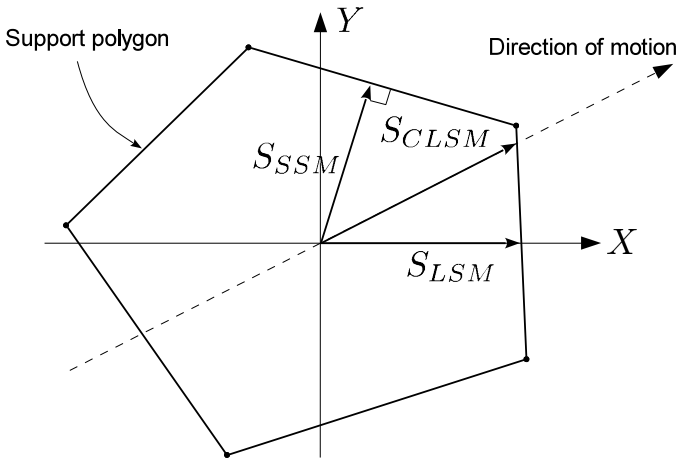

FIGURE 2.14: Basic static stability margins

Messuri and Klein introduced another stability measure named Energy Stability Margin (ESM) [97]. The Energy Stability Margin is defined as the potential energy that required to tumble the robot around an edge of the support polygon. This approach includes the effect of vertical position of the center of mass and the consideration of top-heaviness. It can be described by

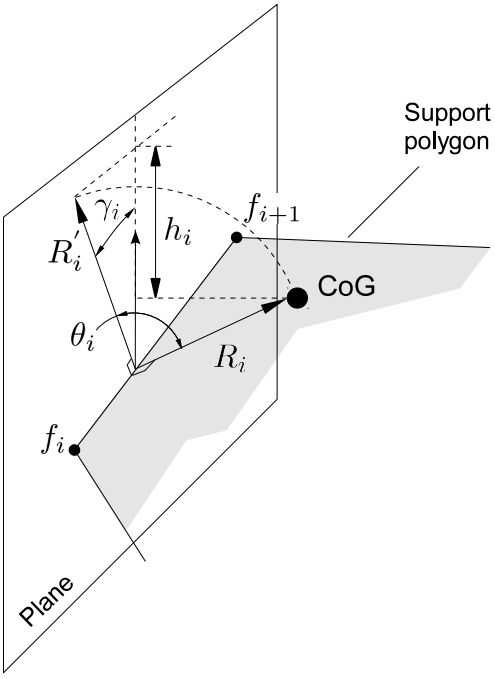

FIGURE 2.15: Energy stability margin

$$S_{ESM} = \min_{i}^{N}(mgh_i) \tag{2.2}$$

where i denotes the segment of the support polygon considered as the rotation axis, N is the number of distinct contact points of the posture, m is the robot's weight and h_i is the variation of the CoG height during the tip-over which can be derived as

$$h_i = R_i(1 - \cos\theta_i)\cos\gamma_i.$$

where R_i is the distance from the CoG to the rotation axis, θ_i is the angle that R_i forms with the vertical axis and γ_i is the inclination angle of the rotation axis relative to the horizontal plane. Later, Nagy [98] proposed the extension of the ESM named as Compliant Stance Stability Measure (CSSM) to consider the motion on soft and compliant terrain. It is described by

$$S_{CSSM} = \min_{i}^{N}(mgh_i) + \sum_{i=1}^{N} E_{\mathrm{spr}_i} \tag{2.3}$$

where the E_{spr_i} represents the change of potential energy in the spring i. He also introduced the Rigid Walker Stability Measure (RWSM) and Compliant Walker Stability Measure (CWSM) to consider the stabilizing effect of a foot that is in the air for rigid and compliant terrain, respectively. This is followed by the proposal of the Normalized Energy Stability Margin (NESM) by Hirose et. al. [99] in the consideration of the robot weight. The NESM metric is described by

$$S_{NESM} = \frac{S_{ESM}}{mg} = \min_{i}^{N}(h_i) \tag{2.4}$$

2.4.2 Dynamic stability

In consideration to the existence of dynamical effects, especially for those related to high speed vehicles, the dynamic stability measurement is extremely important. The first attempt for examining the stability and the dynamic effect using the crawl gaits for quadruped was introduced by Orin in 1976 [100]. Lin and Song [101] defined the Dynamic Stability Margin (MSD) as the minimum resultant moments for every candidate tip-over axis in the support polygon normalized by the weight of the system. The dynamic stability margin is given by the following equation

$$\begin{aligned} S_{DSM} &= \min_{i}^{N}\left(\frac{M_i}{mg}\right) \\ M_i &= E_i * (F_R \times P_i + R_m) \end{aligned} \tag{2.5}$$

where E_i is a unit vector along the boundary positive in clockwise direction, P_i is the position vector between the center of mass and any point at the boundary. F_R is the resultant force acting at the center of gravity and R_m is the resultant moment also acting on the center of gravity. Yoneda and Hirose [102] propose a similar method named Tumble Stability Margin (TSM). TSM claims that if all moments relative to a unit vector are positive, the whole system will remain stable. The Tumble Stability Margin around the i-th axis can be written as

$$\begin{aligned} S_{TSM} &= \min_{i}^{N}\left(\frac{M_i}{mg}\right) \\ M_i &= \bar{M} \cdot \frac{(p_i - p_{i-1})}{|p_i - p_{i-1}|} + \bar{F} \cdot \frac{(p_i \times p_{i-1})}{|p_i - p_{i-1}|} \end{aligned} \tag{2.6}$$

where the force $\bar{F}$ and the moment $\bar{M}$ can be defined as

$$\bar{F} = F_\alpha - F_g - F_o$$
$$\bar{M} = M_\alpha - M_g - M_o.$$

Here, F_α and M_α are the sum of forces and moments required in acceleration and deceleration of all parts, F_g and M_g are the force and moment which are the sum total of the gravity which works on each part in a planned posture, and that F_o and M_o are the sum total of the manipulation counter-forces in the planned manipulation. Zhou et. al. [103] introduced the use of force sensors to obtain the resultant force and moment. This measurement method is called as Leg-end Supporting Moment (LSM). This stability margin is similar to the TSM method.

Papadopolous and Rey [104] then introduced a different kind of measurement method named as Force-angle Stability Measure (FASM). The principle of two-dimensional FASM can be illustrated as shown in Fig. 2.16. The FASM metric can be expressed as

$$S_{FASM} = \min_i (\theta_i \cdot |d_i| \cdot |F_r|) \tag{2.7}$$

where F_r is the resultant force acting at the CoG.

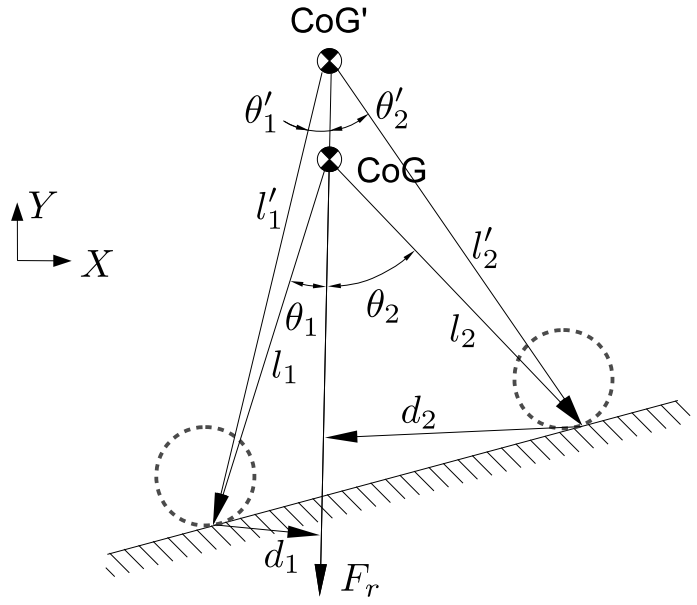

FIGURE 2.16: 2D Force-angle stability measure (FASM)

In this example, the vehicle is expected to tip-over more at the front wheel in comparison to the rear wheel due to $\theta_1 < \theta_2$ and $|d_1| < |d_2|$. This stability criterion also considers the top heaviness of the robot. By changing the position of the center of gravity from CoG to a new position at COG', the angle between the resultant force to the wheels are decreased. This caused the S_{FASM} to be so sensitive with the changes of the CoG height.

2.5 Summary

Some of the previous works related to the personal mobility robots have been examined. Although their representations are very unique, most of them did not consider the ability of motion in a very constrained area. In consideration of this, the implementation of a holonomic and omnidirectional mechanism is very desirable. Among the existing omnidirectional and holonomic locomotion systems, the mechanism with normal tire is very attractive in comparison with other special wheel mechanisms. The safety aspect related to the tip-over stability also is one of the concerns that should be considered. Many of the existing mobile robots with omnidirectional capability neglected this aspect due to the assumption of statically stable platform.

Chapter 3

A Personal Mobility Robot with Active Dual-wheel Casters

3.1 Introduction

The best known ability of a personal mobility robot is to move in a crowded place and narrow area without facing any difficulties to avoid the humans, obstacles and wall. Many of the existing researches in mobile robotics already proposed several techniques for anti-collision system using sensors to measure and monitor surrounding objects and incorporate with some avoidance algorithms. The results presented by these techniques were very promising for the implementation in the personal mobility robot applications. However, in the hardware side, the mechanical design and the capability of the locomotion system provided by the vehicle also were among the important aspects to be taken into account. Most of the existing driving systems for personal mobility robots were developed based on the differential drive system due to the simplicity of the structure and the ability for performing instantaneous rotation. However, due to the mechanical restriction in the differential drive system, it can only produce one degree of freedom (1-DOF) motion in the forward direction.

The implementation of a holonomic and omnidirectional mechanism in personal mobility robots is very attractive to increase the mobility. Although there are various holonomic and omnidirectional mechanisms that can be found recently, the implementation of the normal tire is more attractive than the special wheels due to the higher traction power and the suitability for outdoor applications especially in rough terrains. In this thesis, the holonomic and omnidirectional platform using active dual-wheel caster assemblies is proposed for a personal mobility robot to obtain the holonomic and omnidirectional capability.

In this chapter, the principle of an active dual-wheel caster mechanism with an offset steering is presented at the beginning. A design of the personal mobility robot is proposed with an active dual-wheel caster assemblies. Then, the kinematics model of the robot is discussed. Finally, the derivation of the dynamical model to estimate the wheel reaction forces is presented in detail.

3.2 Active dual-wheel caster

The general idea of the active dual-wheel caster (ADWC) has been introduced by Han et.al. [80] and Yamada et.al. [105] as an alternative to the design represented by Wada et.al. [78]. A similar architecture also has been proposed by Yu et.al. which named as active split offset castors (ASOC) [82]. All of these represented architectures applied the standard rubber wheel to reproduce the same traction power as the conventional vehicle and to improve the existing standard differential drive system.

In a standard differential drive system, only one degree of freedom motion (1-DOF), i.e. forward velocity, can be produced at the center of the wheel axle. A typical design of the differential drive mechanism is shown in Fig. 3.1(a). In order to move to a sideway direction as shown in Fig. 3.1(b), an instantaneous rotation at the center of the wheel axle

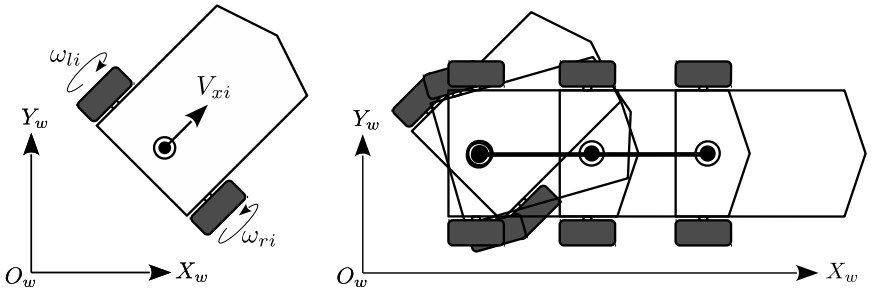

(a) Differential drive (b) Trajectory of differential drive

FIGURE 3.1: Kinematical model of standard differential drive mechanism

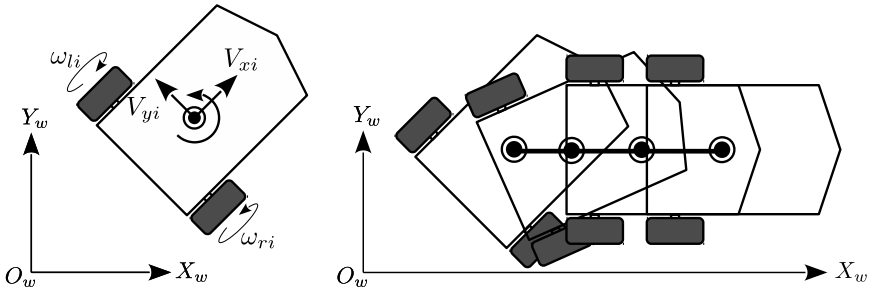

(a) Active dual-wheel caster (b) Trajectory of active dual-wheel caster

FIGURE 3.2: Kinematical model of active dual-wheel caster

must be performed first before translating to the sideway direction. However, by moving the control position from the existing center position to a new position along the x_i-axis with an offset distance, a two degrees of freedom motion (2-DOF), i.e. forward and sideway velocity, can be generated at the new reference position as shown in Fig. 3.2(a). Thus, it enables the active dual-wheel caster to perform a simultaneous translation and rotation motion at the same time as shown in Fig. 3.2(b).

3.2.1 Kinematics model

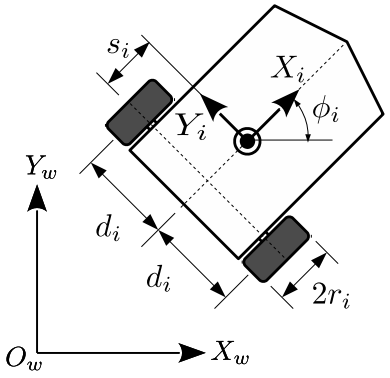

FIGURE 3.3: Setting of active dual-wheel caster

TABLE 3.1: List of nomenclatures for ADWC

$\Sigma_w\,(O_w - X_wY_w)$	absolute coordinate system
$\Sigma_i\,(O_i - X_iY_i)$	coordinate sytem of the active dual-wheel caster unit
s_i	offset distance between the steering axle and the wheel axis
d_i	distance between the center of the wheel and X_i-axis
r_i	radius of the wheel
ω_{ri}, ω_{li}	angular velocity of the right and left wheel of the ADWC
x_i, y_i	the position of steering axle for active dual-wheel caster in Σ_w coordinate system
ϕ_i	orientation of the active dual-wheel caster in Σ_w coordinate system

By defining the state variable for the dual-wheel caster as $\boldsymbol{x}_i = [x_i\ y_i]^T$ and the angular velocity of the wheels as $\boldsymbol{\omega}_i = [\omega_{ri}\ \omega_{li}]^T$, the forward kinematic model of the dual-wheel caster is given by

$$\dot{\boldsymbol{x}}_i = \boldsymbol{A}_i\boldsymbol{\omega}_i \tag{3.1}$$

where,

$$\boldsymbol{A} = \frac{r_i}{2}\begin{bmatrix} \cos\phi_i - \frac{s_i}{d_i}\sin\phi_i & \cos\phi_i + \frac{s_i}{d_i}\sin\phi_i \\ \sin\phi_i + \frac{s_i}{d_i}\cos\phi_i & \sin\phi_i - \frac{s_i}{d_i}\cos\phi_i \end{bmatrix}.$$

The rotational velocity of the active dual-wheel caster is given by

$$\dot{\phi}_i = \frac{r_i}{2d_i}(\omega_{ri} - \omega_{li}) \tag{3.2}$$

Meanwhile, the inverse kinematics model can be derived from the above mentioned forward kinematic model as

$$\boldsymbol{\omega}_i = \boldsymbol{A}_i^{-1}\dot{\boldsymbol{x}}_i \tag{3.3}$$

where,

$$\boldsymbol{A}_i^{-1} = \frac{1}{r_i}\begin{bmatrix} \cos\phi_i - \frac{d_i}{s_i}\sin\phi_i & \sin\phi_i + \frac{d_i}{s_i}\cos\phi_i \\ \cos\phi_i + \frac{d_i}{s_i}\sin\phi_i & \sin\phi_i - \frac{d_i}{s_i}\cos\phi_i \end{bmatrix}.$$

Here, the rotational velocity can be obtained by

$$\dot{\phi}_i = \frac{1}{s_i}\dot{y}_i\cos\phi_i - \frac{1}{s_i}\dot{x}_i\sin\phi_i \tag{3.4}$$

3.3 A holonomic omnidirectional personal mobility robot

A holonomic and omnidirectional personal mobility robot can be realized by applying a holonomic and omnidirectional mobile platform as the base for locomotion. There are several possible arrangements of the active dual-wheel caster assemblies in order to obtain the holonomicity as presented in [106]. By considering the mobile platform or the vehicle as a rigid body which travels on a plane, its motion can be described in three degrees of freedom motion (x, y and ϕ). These can be fully defined by controlling the linear velocities in $xy-$axis direction at least at any two separated points.

3.3.1 A holonomic and omnidirectional mobile platform

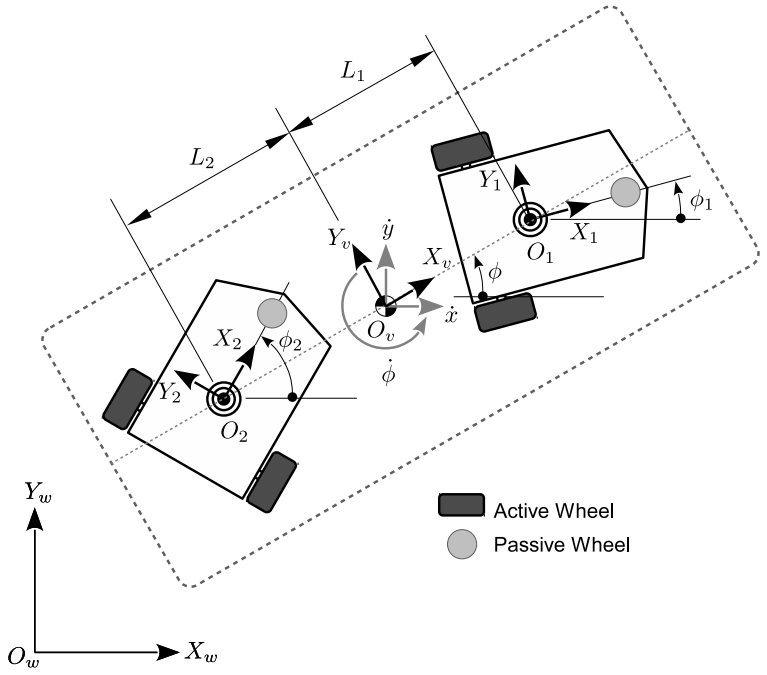

FIGURE 3.4: Omnidirectional mobile platform with active dual-wheel caster assemblies

Figure 3.4 shows a holonomic and omnidirectional mobile platform which comprises two units of active dual-wheel casters that are arranged in the longitudinal direction of the platform. The center of each active dual-wheel caster, O_i, is attached to the platform by a revolute joint (passive steering) without any rotation constraint. Thus, the ADWCs are freely rotated around the steering axles while at the same time generating velocities in X_i and Y_i direction. The existence of the two degrees of freedom (2-DOF) motion at both steering axles induces a holonomic motion to the center of the mobile platform, O_v, where the velocity in X_w-axis direction, $\dot{x}$, velocity in Y_w-axis direction, $\dot{y}$, and the instantaneous rotation, ϕ were produced. As the static stability is concerned, additional

passive wheels such as passive caster wheels can be embedded into the structure to enhance the stability.

3.3.1.1 Kinematics solution

Letting the pose of the omnidirectional mobile platform be $\boldsymbol{x} = [x\, y\, \phi]^T$, the pose of each steering axis be $\boldsymbol{x}_i = [x_i\, y_i]^T$ and $\boldsymbol{x}_a = [\boldsymbol{x}_1^T\ \boldsymbol{x}_2^T]$, the motion of this omnidirectional mobile platform can be described by the following forward kinematics equation:

$$\dot{\boldsymbol{x}} = \boldsymbol{G}\dot{\boldsymbol{x}}_a \tag{3.5}$$

where,

$$\boldsymbol{G} = \frac{1}{L}\begin{bmatrix} L_2 & 0 & L_1 & 0 \\ 0 & L_2 & 0 & L_1 \\ -\sin\phi & \cos\phi & \sin\phi & -\cos\phi \end{bmatrix}$$

In addition, setting the angular velocity of the wheels as $\boldsymbol{\omega} = [\boldsymbol{\omega}_1^T\ \boldsymbol{\omega}_2^T]^T$ and combining Eqs. (3.1) and (3.5), we obtain

$$\dot{\boldsymbol{x}} = \boldsymbol{G}\boldsymbol{A}\boldsymbol{\omega} \tag{3.6}$$

where,

$$\boldsymbol{A} = \begin{bmatrix} \boldsymbol{A}_1 & \boldsymbol{0}_{2\times 2} \\ \boldsymbol{0}_{2\times 2} & \boldsymbol{A}_2 \end{bmatrix}.$$

Meanwhile the inverse kinematics equation can be solved by

$$\boldsymbol{\omega} = \boldsymbol{A}^{-1}\boldsymbol{G}^*\dot{\boldsymbol{x}} \tag{3.7}$$

where,

$$\boldsymbol{G}^* = \begin{bmatrix} 1 & 0 & -L_1 \sin\phi \\ 0 & 1 & L_1 \cos\phi \\ 1 & 0 & L_2 \sin\phi \\ 0 & 1 & -L_2 \cos\phi \end{bmatrix}$$

$$\boldsymbol{A}^{-1} = \begin{bmatrix} \boldsymbol{A}_1^{-1} & \boldsymbol{0}_{2\times 2} \\ \boldsymbol{0}_{2\times 2} & \boldsymbol{A}_2^{-1} \end{bmatrix}.$$

Here, $\boldsymbol{G}^*$ is not the inverse matrix of $\boldsymbol{G}$ as $\boldsymbol{G}$ is not square and therefore not invertible. The $\boldsymbol{G}^*$ is derived from kinematics relations and constraints of the system.

3.3.2 Control of the omnidirectional mobile robot

The omnidirectional mobile platform is controlled based on the above mentioned kinematical model using the resolved velocity control [106] as shown in Fig. 3.5. When introducing the desired values $\boldsymbol{x}_d = [x_d \ y_d \ \phi_d]^T$ of the position and posture of the omnidirectional mobile platform, the output error vector $\boldsymbol{e} = [e_x \ e_y \ e_\phi]^T$ is defined as follows:

$$\boldsymbol{e} = \boldsymbol{x}_d - \boldsymbol{x} \tag{3.8}$$

where $\boldsymbol{x}_d$ is the reference vector. The revised reference velocity vector added to the desired velocity vector $\dot{\boldsymbol{x}}_d$ is expressed by

$$\dot{\boldsymbol{x}}_d^* = \dot{\boldsymbol{x}}_d - K\boldsymbol{e} \tag{3.9}$$

where $\boldsymbol{K} > 0$ is the proportional gain. Finally, the input vector should be provided by

$$\dot{\boldsymbol{x}}_a = \boldsymbol{G}^* \dot{\boldsymbol{x}}_d^* \tag{3.10}$$

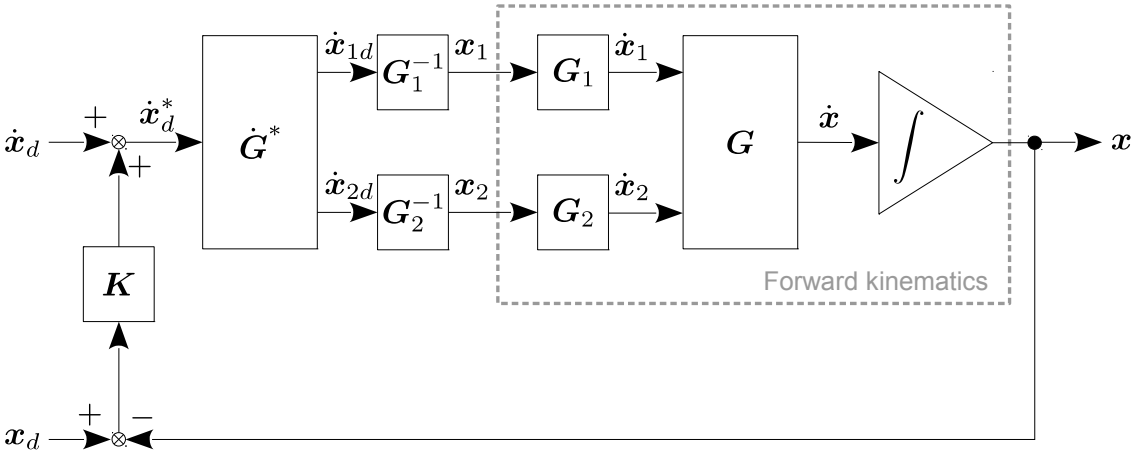

FIGURE 3.5: Resolved velocity control

3.3.3 Modeling the holonomic and omnidirectional personal mobility robot

Figure 3.6 illustrates the mobile platform for the holonomic and omnidirectional personal mobility robot. The passenger can be set as in standing position or in sitting position. In this thesis, we have considered a personal mobility robot with seat which is similar to wheelchairs.

Two types of omnidirectional mobile platform model were examined for stability analysis and tip-over prevention. The basic design of both types are shown in Figs. 3.7 and 3.8. Both of them were built with two units of active dual-wheel caster (ADWC). The first model consists of four active wheels. On the other hand, the second model has additional of two passive wheels. The existence of these passive wheels provide better supporting

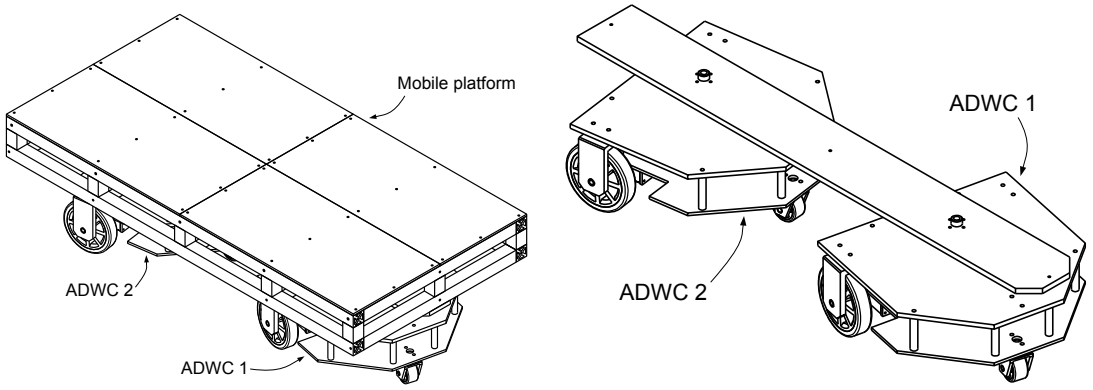

(a) Six-wheeled omnidirectional mobile platform (b) Active dual-wheel casters without platform

FIGURE 3.6: Three-dimensional model for a holonomic omnidirectional mobile platform with active dual-wheel caster assemblies

and is assumed to produce better stability.

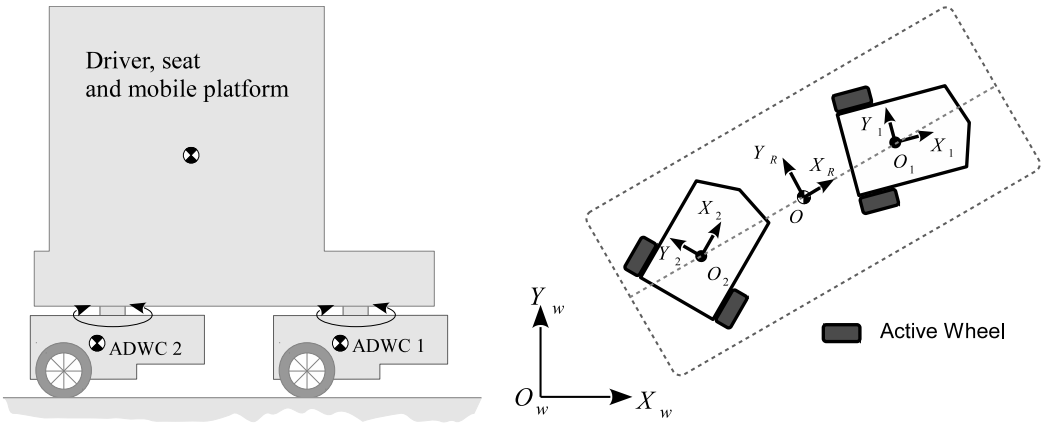

(a) Four-wheeled architecture (b) Kinematic diagram of four-wheeled architecture

FIGURE 3.7: Holonomic omnidirectional mobile robot with four active wheels

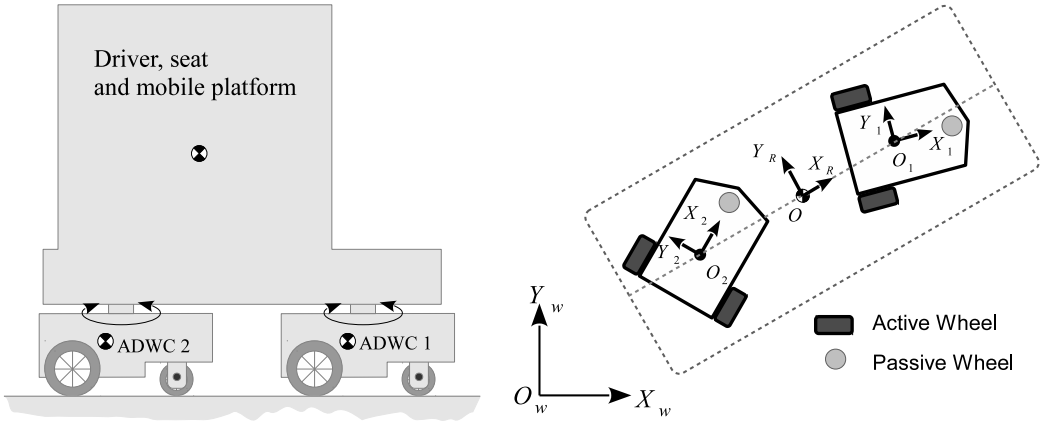

(a) Six-wheeled architecture (b) Kinematic diagram of six-wheeled architecture

FIGURE 3.8: Holonomic omnidirectional mobile robot with four active wheels and two passive wheels

3.4 Derivation of dynamical model

The goal of this section is to derive a relationship between the dynamical properties of the personal mobility robot and the normal forces acting on each wheel. Two dynamical models for the personal mobility robots, i.e. four-wheeled and six-wheeled architectures, were derived and described in this section. These derivations also were presented in [107, 108].

In order to derive this relationship, the following assumptions is made:

1. the mobile robot can operate in omnidirectional direction with the holonomic motion of $[\dot{x}\ \dot{y}\ \dot{\phi}]$, and
2. the mobile robot is kept in a stabilizing condition in vertical direction and maintains equilibrium of moments around x- and y-direction.
3. other forces such as drag force is neglected and the mobile robot is assumed to work on a plane ground.

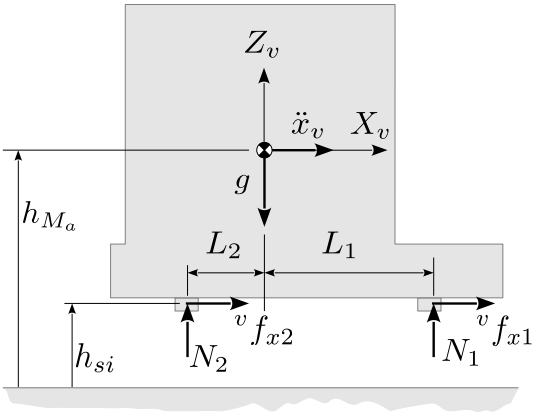

FIGURE 3.9: Dynamical model of upper vehicle

TABLE 3.2: List of nomenclatures for upper part of vehicle

M_a	mass of the driver, seat and mobile platform, i.e., the total mass of upper vehicle
L_i	distance between i-th steering axis and CoG of the mass M_a
N_i	normal forces acting on steering axis
h_{M_a}	height of CoG of the mass M_a
h_{si}	height of steering axis
$\ddot{x}_v, \ddot{y}_v$	accelerations at CoG of the mass M_a in Σ_v
g	gravitational acceleration
$^v f_{xi}, ^v f_{yi}$	force acting on steering axis in Σ_v

Both design share a similarity where two passive steering supporting the upper part of the personal mobility robot. With reference to Fig. 3.9, we can derive the motion for the accelerating personal mobility robot from Newton's equations in X_v- and two static equilibrium equation in Z_v-direction and moments around Y_v-axis by:

$$\sum {}^{v}F_x = M_a\ddot{x}_v \tag{3.11}$$

$$\sum {}^{v}F_z = 0 \tag{3.12}$$

$$\sum {}^{v}n_y = 0 \tag{3.13}$$

Expanding these equations yields:

$${}^{v}f_{x1} + {}^{v}f_{x2} = M_a\ddot{x}_v \tag{3.14}$$

$$N_1 + N_2 - M_a g = 0 \tag{3.15}$$

$$N_2L_2 - N_1L_1 - ({}^{v}f_{x1} + {}^{v}f_{x2})(h_{M_a} - h_{si}) = 0 \tag{3.16}$$

Finally, solving Eq.(3.11)–(3.13) by eliminating unnecessary components produces

$$N_1 = \tfrac{1}{L}(M_a g L_2 - M_a\ddot{x}_v h_a) \tag{3.17}$$

$$N_2 = \tfrac{1}{L}(M_a g L_1 + M_a\ddot{x}_v h_a) \tag{3.18}$$

where $L = L_1 + L_2$ and $h_a = h_{M_a} - h_{si}$.

3.4.1 Four-wheeled omnidirectional mobile platform

Let us consider the dynamical model for two-wheeled ADWC as shown in Fig. 3.10 as our reference.

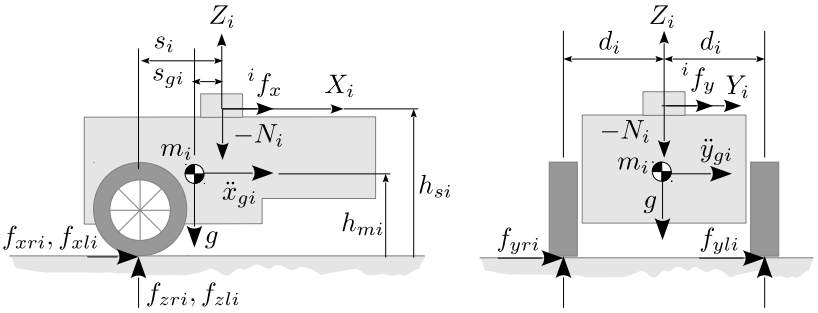

(a) Side view (X_iZ_i-frame) (b) Front view (Y_iZ_i-frame)

FIGURE 3.10: Dynamical model for two-wheeled ADWC

TABLE 3.3: List of nomenclatures for two-wheeled ADWC

m_i	mass of the i-th dual-wheel caster
h_{mi}	height of CoG of the dual-wheel caster
$\ddot{x}_{gi}, \ddot{y}_{gi}$	accelerations at CoG of dual-wheel caster
f_{xi}, f_{yi}	force acting on steering axis in Σ_w
${}^i f_x, {}^i f_y$	force acting on steering axis in Σ_i
f_{xri}, f_{xli}	driving forces of the wheel
f_{yri}, f_{yli}	sideway forces of the wheel
f_{zri}, f_{zli}	normal forces of the wheel

From Fig. 3.10(a) we obtain that the sum of forces in X_i-direction, $\Sigma^i F_x$, the sum of forces in Z_i-direction, $\Sigma^i F_z$ and the sum of moments around Y_i-direction at the CoG, $\Sigma^G n_y$ by

$$\sum {}^i F_x = m_i \ddot{x}_{gi} + {}^i f_x \tag{3.19}$$

$$\sum {}^i F_z = 0 \tag{3.20}$$

$$\sum {}^G n_y = 0 \tag{3.21}$$

Expanding these equations produces

$$f_{xri} + f_{xli} = m_i \ddot{x}_{gi} + {}^i f_x \tag{3.22}$$

$$f_{zri} + f_{zli} + N_i - m_i g = 0 \tag{3.23}$$

$$(f_{zri} + f_{zli}) s_{ai} + {}^i f_x h_{smi} - N_i s_{gi} - (f_{xri} + f_{xli}) h_{mi} = 0 \tag{3.24}$$

where $s_{ai} = s_i - s_{gi}$ and $h_{smi} = h_{si} - h_{mi}$.

Inserting Eq. (3.22) into Eq. (3.24) yields

$$\begin{aligned}(f_{zri} + f_{zli})s_{ai} + {}^{i}f_x h_{smi} - N_i s_{gi} - (m_i \ddot{x}_{gi} + {}^{i}f_x)h_{mi} = 0 \\ f_{zri} + f_{zli} = \frac{1}{s_{ai}}\{{}^{i}f_x h_{ci} + N_i s_{gi} + m_i \ddot{x}_{gi} h_{mi}\}\end{aligned} \tag{3.25}$$

where $h_{ci} = 2h_{mi} - h_{si}$.

The additional Newton's equations can be derived from Fig. 3.10(b) by

$$\sum {}^{i}F_y = m_i \ddot{y}_{gi} + {}^{i}f_y \tag{3.26}$$

$$\sum {}^{G}n_{x,l} = 0 \tag{3.27}$$

$$\sum {}^{G}n_{x,r} = 0 \tag{3.28}$$

where $\Sigma^i F_y$ is the sum of forces in y-direction, while $\Sigma^G n_{x,r}$ and $\Sigma^G n_{x,l}$ is the sum of moments around x-direction at the ground contact point of the right wheel and left wheel.

Which can be expanded as

$$f_{yri} + f_{yli} = m_i \ddot{y}_{gi} + {}^{i}f_y \tag{3.29}$$

$$f_{zri}(2d_i) + {}^{i}f_y h_{si} + m_i \ddot{y}_{gi} h_{mi} - (m_i g - N_i)d_i = 0 \tag{3.30}$$

$$-f_{zli}(2d_i) + {}^{i}f_y h_{si} + m_i \ddot{y}_{gi} h_{mi} + (m_i g - N_i)d_i = 0 \tag{3.31}$$

From Eqs. (3.30)–(3.31) we obtain

$$f_{zri} = \frac{1}{2d_i}\{-{}^{i}f_y h_{si} - m_i \ddot{y}_{gi} h_{mi} + (m_i g - N_i)d_i\} \tag{3.32}$$

$$f_{zli} = \frac{1}{2d_i}\{{}^{i}f_y h_{si} + m_i \ddot{y}_{gi} h_{mi} + (m_i g - N_i)d_i\} \tag{3.33}$$

Inserting Eqs. (3.32) and (3.33) into Eq. (3.25) produces

$$f_{zri} = \tfrac{1}{s_{ai}}H_{ai} - \tfrac{1}{2d_i}H_{bi} + \tfrac{1}{2s_{ai}}H_{ci} \tag{3.34}$$

$$f_{zli} = \tfrac{1}{s_{ai}}H_{ai} + \tfrac{1}{2d_i}H_{bi} + \tfrac{1}{2s_{ai}}H_{ci} \tag{3.35}$$

where,

$$
\begin{aligned}
H_{ai} &= {}^{i}f_x h_{ci} + m_i \ddot{x}_{gi} h_{mi} \\
H_{bi} &= {}^{i}f_y h_{si} + m_i \ddot{y}_{gi} h_{mi} \\
H_{ci} &= N_i s_{bi} - m_i g s_{ai} \\
s_{bi} &= s_i + s_{gi}
\end{aligned}
$$

By defining $\ddot{\boldsymbol{x}}_v = [\ddot{x}_v \ \ddot{y}_v \ \ddot{\phi}_v]^T$ and $\ddot{\boldsymbol{x}} = [\ddot{x} \ \ddot{y} \ \ddot{\phi}]^T$, the relationship between $\ddot{\boldsymbol{x}}_v$ and $\ddot{\boldsymbol{x}}$ can be expressed by

$$
\ddot{\boldsymbol{x}} = {}^{w}\boldsymbol{T}_v \ddot{\boldsymbol{x}}_v \tag{3.36}
$$

where

$$
{}^{w}\boldsymbol{T}_v = \begin{bmatrix} \cos\phi & -\sin\phi & 0 \\ \sin\phi & \cos\phi & 0 \\ 0 & 0 & 1 \end{bmatrix}
$$

Taking into account that ${}^{w}\boldsymbol{T}_v$ is an orthogonal matrix, the inverse equation of this relationship can be derived by

$$
\ddot{\boldsymbol{x}}_v = {}^{w}\boldsymbol{T}_v^T \ddot{\boldsymbol{x}} \tag{3.37}
$$

Therefore, defining $\boldsymbol{f}_{zi} = [f_{zri} \ f_{zli}]^T$, ${}^{i}\boldsymbol{f} = [{}^{i}f_x \ {}^{i}f_y]^T$, ${}^{i}\ddot{\boldsymbol{x}}_{gi} = [\ddot{x}_{gi} \ \ddot{\phi}_i]^T$ and replacing $\ddot{y}_{gi}$ with the time derivative of the non-holonomic constraint, $\ddot{y}_{gi} = s_{ai}\ddot{\phi}_i$, the following equation is obtained by combining Eqs. (3.34)–(3.35)

$$
\boldsymbol{f}_{zi} = \boldsymbol{A}_i {}^{i}\boldsymbol{f} + \boldsymbol{B}_i {}^{i}\ddot{\boldsymbol{x}}_{gi} + \boldsymbol{C}_i {}^{w}\boldsymbol{T}_v^T \ddot{\boldsymbol{x}} + \boldsymbol{D}_i \tag{3.38}
$$

where,

$$\boldsymbol{A}_i = \begin{bmatrix} \frac{h_{ci}}{s_{ai}} & -\frac{h_{si}}{2d_i} \\ \frac{h_{ci}}{s_{ai}} & \frac{h_{si}}{2d_i} \end{bmatrix}, \boldsymbol{B}_i = m_i h_{mi} \begin{bmatrix} \frac{1}{s_{ai}} & -\frac{s_{ai}}{2d_i} \\ \frac{1}{s_{ai}} & \frac{s_{ai}}{2d_i} \end{bmatrix}$$

$$\boldsymbol{C}_1 = \begin{bmatrix} -c_1 & 0 & 0 \\ -c_1 & 0 & 0 \end{bmatrix}, \boldsymbol{C}_2 = \begin{bmatrix} c_2 & 0 & 0 \\ c_2 & 0 & 0 \end{bmatrix}, c_i = \frac{s_{bi} M_a h_a}{2 s_{ai} L}$$

$$\boldsymbol{D}_1 = \begin{bmatrix} \frac{s_{b1} M_a g L_2}{2 s_{a1} L} - \frac{m_1 g}{2} \\ \frac{s_{b1} M_a g L_2}{2 s_{a1} L} - \frac{m_1 g}{2} \end{bmatrix}, \boldsymbol{D}_2 = \begin{bmatrix} \frac{s_{b2} M_a g L_1}{2 s_{a2} L} - \frac{m_2 g}{2} \\ \frac{s_{b2} M_a g L_1}{2 s_{a1} L} - \frac{m_2 g}{2} \end{bmatrix}$$

Then, introducing the coordinate transformation matrix from Σ_i to Σ_w as ${}^w\boldsymbol{T}_i$, defining the normal force vector $\boldsymbol{f}_z = [\boldsymbol{f}_{z1}^T \ \boldsymbol{f}_{z2}^T]^T$ for the wheel, setting $\boldsymbol{f} = [\boldsymbol{f}_1^T \ \boldsymbol{f}_2^T]^T$, and $\ddot{\boldsymbol{x}}_g = [{}^1\ddot{\boldsymbol{x}}_{g1}^T \ {}^2\ddot{\boldsymbol{x}}_{g2}^T]^T$ gives

$$\boldsymbol{f}_z = \boldsymbol{A}\boldsymbol{f} + \boldsymbol{B}\ddot{\boldsymbol{x}}_g + \boldsymbol{C}\ddot{\boldsymbol{x}} + \boldsymbol{D} \tag{3.39}$$

where,

$$\boldsymbol{A} = \begin{bmatrix} \boldsymbol{A}_1 {}^w\boldsymbol{T}_1^T & \boldsymbol{0}_{2\times 2} \\ \boldsymbol{0}_{2\times 2} & \boldsymbol{A}_2 {}^w\boldsymbol{T}_2^T \end{bmatrix}, {}^w\boldsymbol{T}_i = \begin{bmatrix} \cos\phi_i & -\sin\phi_i \\ \sin\phi_i & \cos\phi_i \end{bmatrix}$$

$$\boldsymbol{B} = \begin{bmatrix} \boldsymbol{B}_1 & \boldsymbol{0}_{2\times 2} \\ \boldsymbol{0}_{2\times 2} & \boldsymbol{B}_2 \end{bmatrix}, \boldsymbol{C} = \begin{bmatrix} \boldsymbol{C}_1 {}^w\boldsymbol{T}_v^T \\ \boldsymbol{C}_2 {}^w\boldsymbol{T}_v^T \end{bmatrix}, \boldsymbol{D} = \begin{bmatrix} \boldsymbol{D}_1 \\ \boldsymbol{D}_2 \end{bmatrix}$$

Also the dynamic property for the omnidirectional mobile robot also can be described as:

$$\boldsymbol{M}\ddot{\boldsymbol{x}} = \boldsymbol{E}\boldsymbol{f} \tag{3.40}$$

with

$$\boldsymbol{M} = \mathrm{diag}(M_a, M_a, I)$$

$$\boldsymbol{E} = \begin{bmatrix} 1 & 0 & 1 & 0 \\ 0 & 1 & 0 & 1 \\ -L_1 \sin\phi & L_1 \cos\phi & L_2 \sin\phi & -L_2 \cos\phi \end{bmatrix}$$

where, I is the moment of inertia for the upper vehicle.

Inserting the inverse equation of Eq. (3.40) into Eq. (3.39) yields

$$\boldsymbol{f}_z = \boldsymbol{A}\boldsymbol{E}^*\boldsymbol{M}\ddot{\boldsymbol{x}} + \boldsymbol{B}\ddot{\boldsymbol{x}}_g + \boldsymbol{C}\ddot{\boldsymbol{x}} + \boldsymbol{D} \tag{3.41}$$

where $\boldsymbol{E}^*$ denotes the pseudoinverse of matrix $\boldsymbol{E}$ as described by

$$\boldsymbol{E}^* = \frac{1}{L}\begin{bmatrix} L_2 + \alpha_{cc}(\phi) & \alpha_{sc}(\phi) & -\sin\phi \\ \alpha_{sc}(\phi) & L_2 + \alpha_{ss}(\phi) & \cos\phi \\ L_1 - \alpha_{cc}(\phi) & -\alpha_{sc}(\phi) & \sin\phi \\ -\alpha_{sc}(\phi) & L_1 - \alpha_{ss}(\phi) & -\cos\phi \end{bmatrix}$$

$$\begin{aligned} \alpha_{ss}(\phi) &= \tfrac{1}{2}(L_1 - L_2)\sin^2\phi \\ \alpha_{sc}(\phi) &= \tfrac{1}{2}(L_1 - L_2)\sin\phi\cos\phi \\ \alpha_{cc}(\phi) &= \tfrac{1}{2}(L_1 - L_2)\cos^2\phi \end{aligned}$$

Also the relationship between ${}^i\dot{\boldsymbol{x}}_{gi}$ and $\dot{\boldsymbol{x}}_i$ can be written as

$${}^i\dot{\boldsymbol{x}}_{gi} = \boldsymbol{F}_i\dot{\boldsymbol{x}}_i \tag{3.42}$$

where,

$$\boldsymbol{F}_i = \begin{bmatrix} \cos\phi_i & \sin\phi_i \\ -\frac{1}{s_i}\sin\phi_i & \frac{1}{s_i}\cos\phi_i \end{bmatrix}$$

Letting $\boldsymbol{x}_a = [\boldsymbol{x}_1^T\ \boldsymbol{x}_2^T]^T$ and referring to Eq. (3.42), the following equation is satisfied:

$$\dot{\boldsymbol{x}}_g = \boldsymbol{F}\dot{\boldsymbol{x}}_a \tag{3.43}$$

where,

$$\boldsymbol{F} = \begin{bmatrix} \boldsymbol{F}_1 & \boldsymbol{0}_{2\times 2} \\ \boldsymbol{0}_{2\times 2} & \boldsymbol{F}_2 \end{bmatrix}$$

Combining Eqs. (3.43) and (3.7) gives

$$\dot{\boldsymbol{x}}_g = \boldsymbol{F}\boldsymbol{G}^*\dot{\boldsymbol{x}} \tag{3.44}$$

Hence differentiating Eq. (3.44) with respect to time, we obtain

$$\ddot{\boldsymbol{x}}_g = (\dot{\boldsymbol{F}}\boldsymbol{G}^* + \boldsymbol{F}\dot{\boldsymbol{G}}^*)\dot{\boldsymbol{x}} + \boldsymbol{F}\boldsymbol{G}^*\ddot{\boldsymbol{x}} \tag{3.45}$$

Replacing Eq. (3.45) into Eq. (3.41) and rearranging the equation yields

$$\boldsymbol{f}_z = \boldsymbol{K}'\dot{\boldsymbol{x}} + \boldsymbol{K}''\ddot{\boldsymbol{x}} + \boldsymbol{D} \tag{3.46}$$

where,

$$\boldsymbol{K}' = \boldsymbol{B}(\dot{\boldsymbol{F}}\boldsymbol{G}^* + \boldsymbol{F}\dot{\boldsymbol{G}}^*)$$
$$\boldsymbol{K}'' = \boldsymbol{A}\boldsymbol{E}^*\boldsymbol{M} + \boldsymbol{B}\boldsymbol{F}\boldsymbol{G}^* + \boldsymbol{C}$$

3.4.2 Six-wheeled omnidirectional mobile platform

Let us consider the dynamical model for three-wheeled ADWC as shown in Fig. 3.11 as our reference.

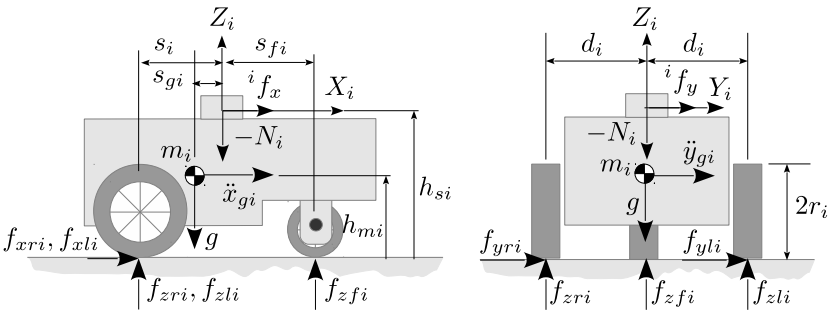

(a) Side view (X_iZ_i-frame) (b) Front view (Y_iZ_i-frame)

FIGURE 3.11: Dynamical model for three-wheeled ADWC

TABLE 3.4: List of nomenclatures for three-wheeled ADWC

m_i	mass of the i-th dual-wheel caster
h_{mi}	height of CoG of the dual-wheel caster
$\ddot{x}_{gi}, \ddot{y}_{gi}$	accelerations at CoG of dual-wheel caster
f_{xi}, f_{yi}	force acting on steering axis in Σ_w
${}^i f_x, {}^i f_y$	force acting on steering axis in Σ_i
f_{xri}, f_{xli}	driving forces of the wheel
f_{yri}, f_{yli}	sideway forces of the wheel
$f_{zri}, f_{zli}, f_{zfi}$	normal forces of the wheel

From Fig. 3.11(a) we obtain that the sum of forces in x-direction, $\Sigma^i F_x$, the sum of forces in z-direction, $\Sigma^i F_z$ and the sum of moments around y-direction at the CoG, $\Sigma^G n_y$ by

$$\sum {}^i F_x = m_i \ddot{x}_{gi} + {}^i f_x \tag{3.47}$$

$$\sum {}^i F_z = 0 \tag{3.48}$$

$$\sum {}^G n_y = 0 \tag{3.49}$$

Expanding these equations produces

$$f_{xri} + f_{xli} = m_i \ddot{x}_{gi} + {}^i f_x \tag{3.50}$$

$$f_{zri} + f_{zli} + f_{zfi} + N_i - m_i g = 0 \tag{3.51}$$

$$(f_{zri} + f_{zli}) s_{ai} + {}^i f_x h_{smi} - N_i s_{gi} - f_{zfi} s_{bi} - (f_{xri} + f_{xli}) h_{mi} = 0 \tag{3.52}$$

where $s_{ai} = s_i - s_{gi}$, $s_{bi} = s_{fi} + s_{gi}$ and $h_{smi} = h_{si} - h_{mi}$.

Inserting Eqs. (3.50) and (3.51) into Eq. (3.52) yields

$$(m_i g - f_{zfi} - N_i)s_{ai} + {}^i f_x h_{smi} - N_i s_{gi} - f_{zfi} s_{bi} - (m_i \ddot{x}_{gi} + {}^i f_x)h_{mi} = 0 \tag{3.53}$$

This equation can be rearranged into

$$f_{zfi}(\underbrace{s_{ai} + s_{bi}}_{s_i + s_{fi}}) = m_i g s_{ai} - N_i(\underbrace{s_{ai} + s_{gi}}_{s_i}) + {}^i f_x(\underbrace{h_{smi} - h_{mi}}_{h_{si} - 2h_{mi}}) - m_i \ddot{x}_{gi} h_{mi} \tag{3.54}$$

Here, we obtain

$$f_{zfi} = \tfrac{1}{s_{ci}}(m_i g s_{ai} - N_i s_i) - \tfrac{1}{s_{ci}}({}^i f_x h_{ci} + m_i \ddot{x}_{gi} h_{mi}) \tag{3.55}$$

where $s_{ci} = s_i + s_{fi}$ and $h_{ci} = 2h_{mi} - h_{si}$.

Then, similarly from Fig. 3.11(b) we obtain the remaining Newton's and static equilibrium equations

$$\sum {}^i F_y = m_i \ddot{y}_{gi} + {}^i f_y \tag{3.56}$$

$$\sum {}^G n_x = 0 \tag{3.57}$$

These equations can be expanded as

$$f_{yri} + f_{yli} = m_i \ddot{y}_{gi} + {}^i f_y \tag{3.58}$$

$$(f_{zri} - f_{zli})d_i + {}^i f_y h_{smi} - (f_{yri} + f_{yli})h_{mi} = 0 \tag{3.59}$$

Inserting Eq. (3.58) into Eq. (3.59) produces

$$(f_{zri} - f_{zli})d_i + {}^i f_y h_{smi} - (m_i \ddot{y}_{gi} + {}^i f_y)h_{mi} = 0$$

which can be simplified as

$$f_{zri} = f_{zli} + \tfrac{1}{d_i}({}^i f_y h_{ci} + m_i \ddot{y}_{gi} h_{mi}) \tag{3.60}$$

$$f_{zli} = f_{zri} - \tfrac{1}{d_i}({}^i f_y h_{ci} + m_i \ddot{y}_{gi} h_{mi}) \tag{3.61}$$

While from Eq. (3.51) we obtain

$$f_{zri} = m_i g - f_{zfi} - N_i - f_{zli} \tag{3.62}$$

$$f_{zli} = m_i g - f_{zfi} - N_i - f_{zri} \tag{3.63}$$

Here, the value of f_{zri} and f_{zli} can be derived from Eqs.(3.60)–(3.63).

Replacing f_{zli} in Eq. (3.62) with Eq. (3.61):

$$\begin{aligned} f_{zri} &= m_i g - f_{zfi} - N_i - \{f_{zri} - \tfrac{1}{d_i}({}^i f_y h_{ci} + m_i \ddot{y}_{gi} h_{mi})\} \\ &= \tfrac{1}{2}(m_i g - f_{zfi} - N_i) + \tfrac{1}{2d_i}({}^i f_y h_{ci} + m_i \ddot{y}_{gi} h_{mi}) \end{aligned} \tag{3.64}$$

Replacing f_{zri} in Eq. (3.63) with Eq. (3.60):

$$\begin{aligned} f_{zli} &= m_i g - f_{zfi} - N_i - \{f_{zli} + \tfrac{1}{d_i}({}^i f_y h_{ci} + m_i \ddot{y}_{gi} h_{mi})\} \\ &= \tfrac{1}{2}(m_i g - f_{zfi} - N_i) - \tfrac{1}{2d_i}({}^i f_y h_{ci} + m_i \ddot{y}_{gi} h_{mi}) \end{aligned} \tag{3.65}$$

The first part of Eqs. (3.64) and (3.65) can be simplified by replacing the f_{zif} from Eq.(3.55)

$$\begin{aligned} & m_i g - N_i - f_{zfi} \\ &= m_i g - N_i - \{\tfrac{1}{s_{ci}}(m_i g s_{ai} - N_i s_i) - \tfrac{1}{s_{ci}}({}^i f_x h_{ci} + m_i \ddot{x}_{gi} h_{mi})\} \\ &= \tfrac{1}{s_{ci}}\{s_{ci}(m_i g - N_i) - m_i g s_{ai} + N_i s_i\} + \tfrac{1}{s_{ci}}({}^i f_x h_{ci} + m_i \ddot{x}_{gi} h_{mi}) \\ &= \tfrac{1}{s_{ci}}\{m_i g(\underbrace{s_{ci} - s_{ai}}_{s_{bi}}) + N_i(\underbrace{s_i - s_{ci}}_{-s_{fi}})\} + \tfrac{1}{s_{ci}}({}^i f_x h_{ci} + m_i \ddot{x}_{gi} h_{mi}) \\ &= \tfrac{s_{bi}}{s_{ci}} m_i g - \tfrac{s_{fi}}{s_{ci}} N_i + \tfrac{1}{s_{ci}}({}^i f_x h_{ci} + m_i \ddot{x}_{gi} h_{mi}) \end{aligned}$$

Finally, replacing back this value into Eqs. (3.64)–(3.65) and rearranging Eq. (3.55) yields

$$f_{zri} = \tfrac{1}{2s_{ci}} H_{ai} + \tfrac{1}{2d_i} H_{bi} + \tfrac{1}{2s_{ci}} H_{ci} \tag{3.66}$$

$$f_{zli} = \tfrac{1}{2s_{ci}} H_{ai} - \tfrac{1}{2d_i} H_{bi} + \tfrac{1}{2s_{ci}} H_{ci} \tag{3.67}$$

$$f_{zfi} = -\tfrac{1}{s_{ci}} H_{ai} + \tfrac{1}{s_{ci}} H_{di} \tag{3.68}$$

where,

$$H_{ai} = {}^{i}f_x h_{ci} + m_i \ddot{x}_{gi} h_{mi} \tag{3.69}$$

$$H_{bi} = {}^{i}f_y h_{ci} + m_i \ddot{y}_{gi} h_{mi} \tag{3.70}$$

$$H_{ci} = m_i g s_{bi} - N_i s_{fi} \tag{3.71}$$

$$H_{di} = m_i g s_{ai} - N_i s_i \tag{3.72}$$

By defining $\ddot{\boldsymbol{x}}_v = [\ddot{x}_v \ \ddot{y}_v \ \ddot{\phi}_v]^T$ and $\ddot{\boldsymbol{x}} = [\ddot{x} \ \ddot{y} \ \ddot{\phi}]^T$, the relationship between $\ddot{\boldsymbol{x}}_v$ and $\ddot{\boldsymbol{x}}$ can be expressed by

$$\ddot{\boldsymbol{x}} = {}^{w}\boldsymbol{T}_v \ddot{\boldsymbol{x}}_v \tag{3.73}$$

where

$${}^{w}\boldsymbol{T}_v = \begin{bmatrix} \cos\phi & -\sin\phi & 0 \\ \sin\phi & \cos\phi & 0 \\ 0 & 0 & 1 \end{bmatrix}$$

Taking into account that ${}^{w}\boldsymbol{T}_v$ is an orthogonal matrix, the inverse equation of this relationship can be derived by

$$\ddot{\boldsymbol{x}}_v = {}^{w}\boldsymbol{T}_v^T \ddot{\boldsymbol{x}} \tag{3.74}$$

Therefore, defining $\boldsymbol{f}_{zi} = [f_{zri} \ f_{zli} \ f_{zfi}]^T$, ${}^{i}\boldsymbol{f} = [{}^{i}f_x \ {}^{i}f_y]^T$, ${}^{i}\ddot{\boldsymbol{x}}_{gi} = [\ddot{x}_{gi} \ \ddot{\phi}_i]^T$ and replacing $\ddot{y}_{gi}$ with the time derivative of the non-holonomic constraint ($\ddot{y}_{gi} = s_{ai}\ddot{\phi}_i$), Eqs. (3.66) and (3.67) can be introduced into matrix equation by

$$\boldsymbol{f}_{zi} = \boldsymbol{A}_i {}^{i}\boldsymbol{f} + \boldsymbol{B}_i {}^{i}\boldsymbol{x}_{gi} + \boldsymbol{C}_i {}^{w}\boldsymbol{T}_v^T \ddot{\boldsymbol{x}} + \boldsymbol{D}_i \tag{3.75}$$

where,

$$\boldsymbol{A}_i = \begin{bmatrix} \frac{h_{ci}}{2s_{ci}} & \frac{h_{ci}}{2d_i} \\ \frac{h_{ci}}{2s_{ci}} & -\frac{h_{ci}}{2d_i} \\ -\frac{1}{s_{ci}} & 0 \end{bmatrix}, \boldsymbol{B}_i = m_i h_{mi} \begin{bmatrix} \frac{1}{2s_{ci}} & \frac{s_{ai}}{2d_i} \\ \frac{1}{2s_{ci}} & -\frac{s_{ai}}{2d_i} \\ -\frac{1}{s_{ci}} & 0 \end{bmatrix}$$

$$\boldsymbol{C}_1 = \begin{bmatrix} \frac{s_{f1}}{2}c_1 & 0 & 0 \\ \frac{s_{f1}}{2}c_1 & 0 & 0 \\ s_1 c_1 & 0 & 0 \end{bmatrix}, \boldsymbol{C}_2 = \begin{bmatrix} -\frac{s_{f2}}{2}c_2 & 0 & 0 \\ -\frac{s_{f2}}{2}c_2 & 0 & 0 \\ -s_2 c_2 & 0 & 0 \end{bmatrix}, c_i = \frac{M_a h_a}{s_{ci} L}$$

$$\boldsymbol{D}_1 = g \begin{bmatrix} \frac{m_1 s_{b1}}{2s_{c1}} - \frac{s_{f1} M_a L_2}{2s_{c1} L} \\ \frac{m_1 s_{b1}}{2s_{c1}} - \frac{s_{f1} M_a L_2}{2s_{c1} L} \\ \frac{m_1 s_{a1}}{s_{c1}} - \frac{s_1 M_a L_2}{s_{c1} L} \end{bmatrix}, \boldsymbol{D}_2 = g \begin{bmatrix} \frac{m_2 s_{b2}}{2s_{c2}} - \frac{s_{f2} M_a L_1}{2s_{c2} L} \\ \frac{m_2 s_{b2}}{2s_{c2}} - \frac{s_{f2} M_a L_1}{2s_{c2} L} \\ \frac{m_2 s_{a2}}{s_{c2}} - \frac{s_2 M_a L_1}{s_{c2} L} \end{bmatrix}$$

Then, introducing the coordinate transformation matrix from Σ_i to Σ_w as ${}^w\boldsymbol{T}_i$, defining the normal force vector $\boldsymbol{f}_z = [\boldsymbol{f}_{z1}^T \ \boldsymbol{f}_{z2}^T]^T$ for the wheel, setting $\boldsymbol{f} = [\boldsymbol{f}_1^T \ \boldsymbol{f}_2^T]^T$, $\ddot{\boldsymbol{x}}_g = [{}^1\ddot{\boldsymbol{x}}_{g1}^T \ {}^2\ddot{\boldsymbol{x}}_{g2}^T]^T$ gives

$$\boldsymbol{f}_z = \boldsymbol{A}\boldsymbol{f} + \boldsymbol{B}\ddot{\boldsymbol{x}}_g + \boldsymbol{C}\ddot{\boldsymbol{x}} + \boldsymbol{D} \tag{3.76}$$

$$\boldsymbol{A} = \begin{bmatrix} \boldsymbol{A}_1 {}^w\boldsymbol{T}_1^T & \boldsymbol{0}_{3\times 2} \\ \boldsymbol{0}_{3\times 2} & \boldsymbol{A}_2 {}^w\boldsymbol{T}_2^T \end{bmatrix}, {}^w\boldsymbol{T}_i = \begin{bmatrix} \cos\phi_i & -\sin\phi_i \\ \sin\phi_i & \cos\phi_i \end{bmatrix}$$

$$\boldsymbol{B} = \begin{bmatrix} \boldsymbol{B}_1 & \boldsymbol{0}_{3\times 2} \\ \boldsymbol{0}_{3\times 2} & \boldsymbol{B}_2 \end{bmatrix}, \boldsymbol{C} = \begin{bmatrix} \boldsymbol{C}_1 {}^w\boldsymbol{T}_v \\ \boldsymbol{C}_2 {}^w\boldsymbol{T}_v \end{bmatrix}, \boldsymbol{D} = \begin{bmatrix} \boldsymbol{D}_1 \\ \boldsymbol{D}_2 \end{bmatrix}$$

Also the dynamic property for the omnidirectional mobile robot also can be described as:

$$\boldsymbol{M}\ddot{\boldsymbol{x}} = \boldsymbol{E}\boldsymbol{f} \tag{3.77}$$

with

$$\boldsymbol{M} = \mathrm{diag}(M_a, M_a, I),$$

$$\boldsymbol{E} = \begin{bmatrix} 1 & 0 & 1 & 0 \\ 0 & 1 & 0 & 1 \\ -L_1 \sin\phi & L_1 \cos\phi & L_2 \sin\phi & -L_2 \cos\phi \end{bmatrix}$$

where I is the moment of inertia for upper vehicle.

Inserting the inverse equation of Eq. (3.77) into Eq. (3.76) yields

$$\boldsymbol{f}_z = \boldsymbol{A}\boldsymbol{E}^*\boldsymbol{M}\ddot{\boldsymbol{x}} + \boldsymbol{B}\ddot{\boldsymbol{x}}_g + \boldsymbol{C}\ddot{\boldsymbol{x}} + \boldsymbol{D} \tag{3.78}$$

where $\boldsymbol{E}^*$ denotes the pseudoinverse of matrix $\boldsymbol{E}$ as described by

$$\boldsymbol{E}^* = \frac{1}{L}\begin{bmatrix} L_2 + \alpha_{cc}(\phi) & \alpha_{sc}(\phi) & -\sin\phi \\ \alpha_{sc}(\phi) & L_2 + \alpha_{ss}(\phi) & \cos\phi \\ L_1 - \alpha_{cc}(\phi) & -\alpha_{sc}(\phi) & \sin\phi \\ -\alpha_{sc}(\phi) & L_1 - \alpha_{ss}(\phi) & -\cos\phi \end{bmatrix}$$

$$\begin{aligned} \alpha_{ss}(\phi) &= \tfrac{1}{2}(L_1 - L_2)\sin^2\phi \\ \alpha_{sc}(\phi) &= \tfrac{1}{2}(L_1 - L_2)\sin\phi\cos\phi \\ \alpha_{cc}(\phi) &= \tfrac{1}{2}(L_1 - L_2)\cos^2\phi \end{aligned}$$

Also the relationship between ${}^i\dot{\boldsymbol{x}}_{gi}$ and $\dot{\boldsymbol{x}}_i$ can be written as

$${}^i\dot{\boldsymbol{x}}_{gi} = \boldsymbol{F}_i\dot{\boldsymbol{x}}_i \tag{3.79}$$

where,

$$\boldsymbol{F}_i = \begin{bmatrix} \cos\phi_i & \sin\phi_i \\ -\frac{1}{s_i}\sin\phi_i & \frac{1}{s_i}\cos\phi_i \end{bmatrix}$$

Letting $\boldsymbol{x}_a = [\boldsymbol{x}_1^T \ \boldsymbol{x}_2^T]^T$ and referring to Eq. (3.79), the following equation is satisfied:

$$\dot{\boldsymbol{x}}_g = \boldsymbol{F}\dot{\boldsymbol{x}}_a \tag{3.80}$$

where,

$$\boldsymbol{F} = \begin{bmatrix} \boldsymbol{F}_1 & \boldsymbol{0}_{2\times2} \\ \boldsymbol{0}_{2\times2} & \boldsymbol{F}_2 \end{bmatrix}$$

Combining Eqs. (3.80) and (3.7) gives

$$\dot{\boldsymbol{x}}_g = \boldsymbol{F}\boldsymbol{G}^*\dot{\boldsymbol{x}} \tag{3.81}$$

Hence differentiating Eq. (3.81) with respect to time, we obtain

$$\ddot{\boldsymbol{x}}_g = (\dot{\boldsymbol{F}}\boldsymbol{G}^* + \boldsymbol{F}\dot{\boldsymbol{G}}^*)\dot{\boldsymbol{x}} + \boldsymbol{F}\boldsymbol{G}^*\ddot{\boldsymbol{x}} \tag{3.82}$$

where,

$$\dot{\boldsymbol{F}} = \begin{bmatrix} \dot{\boldsymbol{F}}_1 & \boldsymbol{0}_{2\times2} \\ \boldsymbol{0}_{2\times2} & \dot{\boldsymbol{F}}_2 \end{bmatrix}, \ \dot{\boldsymbol{F}}_i = \begin{bmatrix} -\dot{\phi}_i \sin\phi_i & \dot{\phi}_i \cos\phi_i \\ -\frac{\dot{\phi}_i}{s_i}\cos\phi_i & -\frac{\dot{\phi}_i}{s_i}\sin\phi_i \end{bmatrix},$$

$$\dot{\boldsymbol{G}}^* = \begin{bmatrix} 0 & 0 & -L_1\dot{\phi}_i\cos\phi \\ 0 & 0 & -L_1\dot{\phi}_i\sin\phi \\ 0 & 0 & L_2\dot{\phi}_i\cos\phi \\ 0 & 0 & L_2\dot{\phi}_i\sin\phi \end{bmatrix}$$

Replacing Eq. (3.82) into Eq. (3.78) and rearranging the equation yields

$$\boldsymbol{f}_z = \boldsymbol{K}'\dot{\boldsymbol{x}} + \boldsymbol{K}''\ddot{\boldsymbol{x}} + \boldsymbol{D} \tag{3.83}$$

where,

$$\boldsymbol{K}' = \boldsymbol{B}(\dot{\boldsymbol{F}}\boldsymbol{G}^* + \boldsymbol{F}\dot{\boldsymbol{G}}^*)$$
$$\boldsymbol{K}'' = \boldsymbol{A}\boldsymbol{E}^*\boldsymbol{M} + \boldsymbol{B}\boldsymbol{F}\boldsymbol{G}^* + \boldsymbol{C}$$

3.5 Summary

This chapter has introduced the fundamental knowledge about a personal mobility robot with active dual-wheel caster assemblies. It presented an omnidirectional mobile platform with two architectures: four-wheeled architecture and six-wheeled architecture. The six-wheeled architecture differed from the four-wheeled architecture in the additional passive wheels. The general kinematic equations for both architectures were discussed. A control method using the kinematic equations named resolved velocity control was explained. Finally, we derived the dynamical equations for both architectures to find the relationship between the dynamical properties and the support forces. These equations will be employed in the following chapter for predicting the net-force.

Chapter 4

Tip-over Prediction

4.1 Introduction

This thesis is to present two major concerns in the development of personal mobility robots: i.e., ability to locomote on the ground with holonomic motion and the safety aspect regarding the tip-over stability. In the previous chapter, a personal mobility robot with active dual-wheel caster assemblies has been presented. Both active dual-wheel casters which freely rotate around their steering axles produce dynamic footprints. As far as the tip-over stability is concerned, the stability monitoring and the estimation of tip-over occurrence are extremely important. The existing works related to the tip-over stability are mostly concentrated on high-speed vehicles and mobile robots [109, 110]. Certainly, most of high-speed vehicles and mobile robots were fully facilitated with the stability monitoring and tip-over avoidance system. Meanwhile, most of the existing vehicles and mobile robots with low velocity ignore the possibility of tip-over occurrence as long as the CoG is inside the support polygon and the static stability is obtained. However, in reality, the dynamical effects such as instant braking and disturbances could also appear at any instant without prior warning. Due to the dynamic footprints, it is somehow difficult to predict the tip-over occurrence for the personal mobility robots with active dual-wheel caster assemblies.

In this chapter, the tip-over prediction method is explained for the omnidirectional personal mobility robot with active dual-wheel caster assemblies. Two types of stability metrics are introduced to measure the stability margin, i.e., the moment stability margin (MSM) and the force-angle stability measure (FASM). The tip-over direction and the use of the tip-over angle are also presented. Finally, the simulation results are discussed for both architectures.

4.2 Predicting the tip-over occurrence

4.2.1 Estimating the support polygon

With the assumption of a flat trajectory ground, the omnidirectional personal mobility robot has a number of ground contact points equal to the number of wheels at any position as long as the personal mobility robot is in a stable condition. The outermost ground contact points of its footprint form a convex support polygon. All interior angles of the convex support polygon are lesser than 180 deg. Unlike most vehicles, the shape of the support polygon for this personal mobility robot is changed according to the posture of the ADWCs and the given trajectory profile. There are numerous possible patterns even for the same body posture. Figure 4.1 shows some examples of the support polygon for a four-wheeled structure at the orientation of 90 deg. The shape of the support polygon is either triangle or tetragon. However, if both of the ADWCs are totally aligned at 0 deg or 180 deg, the ground contact points are also aligned. A line is formed instead of a support polygon. The personal mobility robot at this moment is considered as in a critical stability position. The personal mobility robot may continue to fall if there is no other action to stabilize the personal mobility robot is taken.

Figure 4.2 shows some examples of the support polygon for the six-wheeled architecture which has similar orientation as the four-wheeled architecture in Fig. 4.1. The shape of the support polygon for the six-wheeled architecture can be classified into three shapes: tetragon, pentagon and hexagon. The personal mobility robot with the six-wheeled structure has three advantages over the four-wheeled structure: (i) larger support polygon, (ii) the position of the CoG is kept inside the support polygon at any moment, and (iii) the footprint will never be existed as a line. These advantages have made the personal mobility robot to be a statistically stable structure. It can stand still in any posture without tumbling as long as the dynamical effect is minimal.

The shape of the support polygon is correlated to the stability of the personal mobility robot and also essential in determining the direction of the tip-over incident. Thus, finding the shape of the support polygon is essential for the tip-over prediction. The shape of the support polygon can be determined by finding the convex hull solution of the ground contact points. The convex hull solution [111] for a set of points $Q = \{p_1, p_2, ..., p_n\}$ can be described by Eq. 4.1. In our case, the value of n can be either $n = 4$ or $n = 6$, depending on the number of wheels involved in the robot structure.

$$P_{ch} \triangleq \left\{ \sum_{j=1}^{N} \lambda_j p_j : \lambda_j \geq 0 \text{ for all } j \text{ and } \sum_{j=1}^{N} \lambda_j = 1 \right\}. \tag{4.1}$$

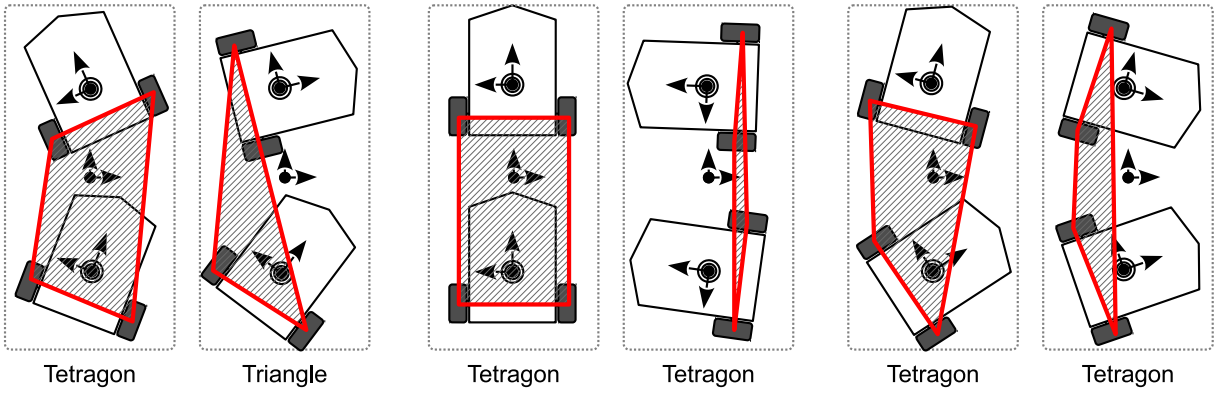

FIGURE 4.1: Support polygon for four-wheeled architecture

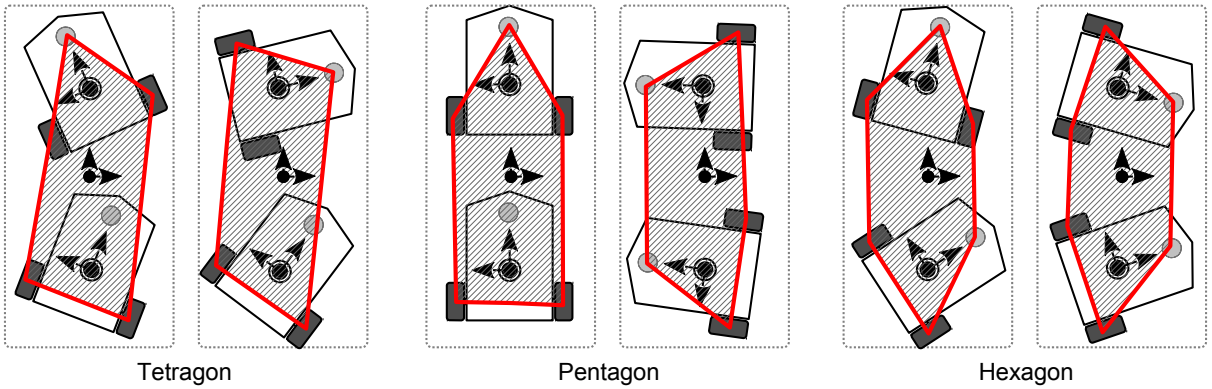

FIGURE 4.2: Support polygon for six-wheeled architecture

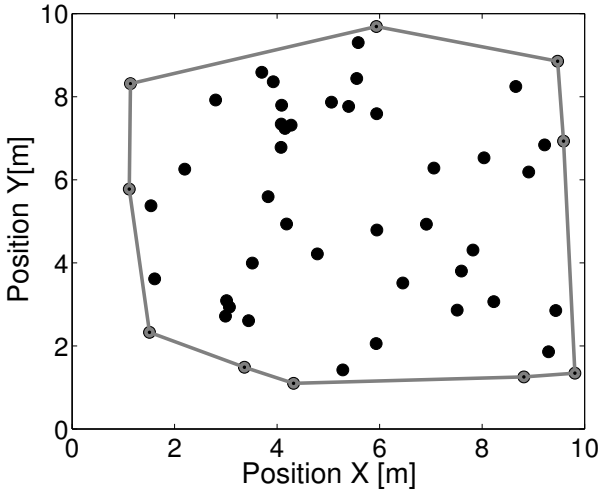

FIGURE 4.3: Example of convex polygon for a set of points $Q = \{p_1, p_2, ..., p_{50}\}$

Algorithm 1: Quickhull algorithm for the convex hull

1. Find the points with the minimum and maximum value of x, those are bound to be part of the convex.
2. Use the line formed by the two points to divide the set in two subsets of points, which will be processed recursively.
3. Determine the point, on one side of the line, with the maximum distance from the line. The two points found before along with this one form a triangle.
4. The points lying inside of that triangle cannot be part of the convex hull and can therefore be ignored in the next steps.
5. Repeat the previous two steps on the two lines formed by the triangle.
6. Keep on doing so on until no more points are left, the recursion has come to an end and the points selected constitute the convex hull.

4.2.2 Evaluating the tip-over axis

Due to the rapid changes in the support polygon as shown in Fig. 4.4, a continuous monitoring on the shape is very important. A normal tip-over incidence may take place at one of the edge of the support polygon. The edge where the tip-over take place is called a tip-over axis. A continuous measuring of stability metrics on each edges of the support polygon is made to evaluate the tendency of the tip-over occurrence. Normally, the candidate of the tip-over axis is determined by the minimum value from all measurements.

There have been several studies conducted to study the stability and the metric representation to show the tendency of the tip-over occurrence such mentioned in the introduction.

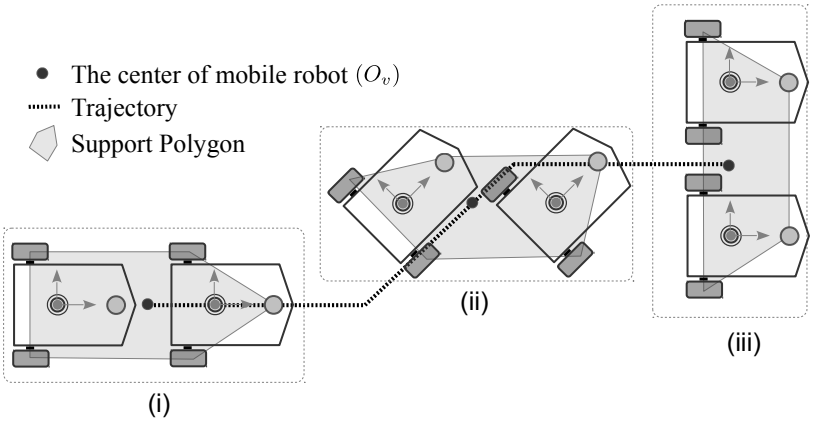

FIGURE 4.4: Support polygon with robot trajectory

We also examined some other existing variances [112, 113, 114]. A few papers also presented the comparison of these metrics based on their robot applications [115]. In this thesis, two main measuring methods are used to evaluate the candidate of the tip-over axis:

- Moment stability measure (MSM) [116]

  The tip-over prediction is performed based on the measurement of moments at the candidate of the tip-over axes. This principle can be illustrated using the general form of an imaginary support polygon with n-contact points as shown in Fig. 4.5. Each point represents the contact point of each wheel with the plane ground. The shape of this support polygon will keep changing according to the current position and the orientation of both dual-wheel casters. The supporting force, f_{zi} can be computed through the dynamics equations as derived in the previous chapter or measured using force sensors in the actual drive system. The tipping instability may occur in the case when one or more wheels is about to lift off the ground, where the value of the supporting forces is approaching zero. In other cases, the stability may also be affected when the area of the polygon becomes smaller and narrower. In order to estimate the direction and proper presentation of the stability margin, we propose a modified form of the conventional force-angle stability metric where the moment for each tip-over axis is computed using the supporting forces instead of the forces acting at the CoG. At any tipping axis, the total of the moments caused by the supporting forces can be computed by:

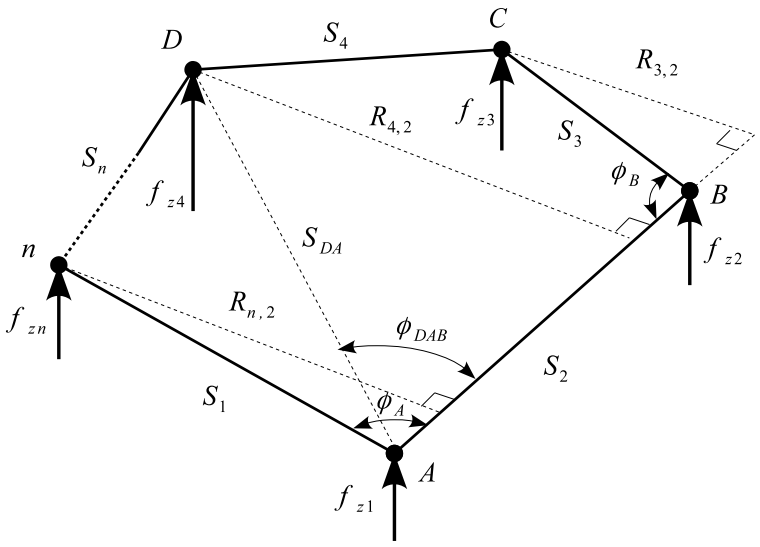

FIGURE 4.5: Moment stability measure

$$\sum \boldsymbol{n}_{S_i} = \begin{cases} \sum_{j=1}^{n-2} f_{z(i+j)} R_{(i+j),i} & \text{if } i \leq 2 \\ \sum_{j=1}^{i-2} f_{zj} R_{j,i} + \sum_{j=1}^{n-i} f_{z(i+j)} R_{(i+j),i} & \text{if } 3 \leq i < n \\ \sum_{j=1}^{i-2} f_{z(j)} R_{(j),i} & \text{if } i = n \end{cases} \tag{4.2}$$

where $i = 1, 2, \ldots n$ and $R_{m,i}$ is the perpendicular distance from the contact point of the supporting force, f_{zm} to the S_i tipping axis. Here, the value of m is either $1 \leq m < i$ or $i < m \leq n$. Therefore, the predicted tip-over axis can be described as the axis with the minimum value of $\Sigma \boldsymbol{n}_{S_i}$.

$$\beta_{msm} = \min_i \sum \boldsymbol{n}_{S_i} \quad \text{for} \quad i = (1, \ldots, n) \tag{4.3}$$

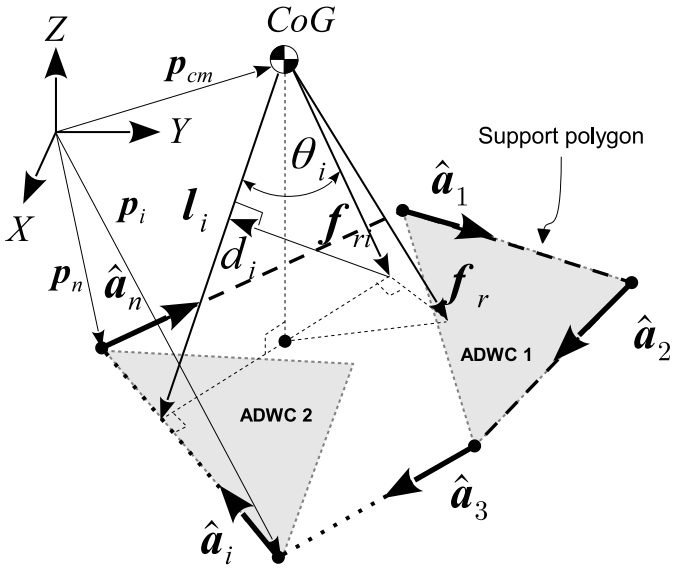

FIGURE 4.6: 3D Force-angle stability measure

- Force-angle stability measure (FASM) [117]

  The force-angle stability measurement is adopted due to the sensitivity of changes by the dynamical effects and the changes in the top heaviness of the robot. The principle of the measurement can be described by the model as shown in Fig. 4.6. The number of edges for the support polygon is $4 \leq n \leq 6$. Here, the dynamic equilibrium of forces at the COG can be obtained using the Newtonian principles by

$$f_r = \Sigma f_g + \Sigma f_d - \Sigma f_{in} = -\Sigma f_s \tag{4.4}$$

  where, the subscripts r, g, d, in and s denote the effective net force, gravitational, external disturbances, inertial and support forces, respectively. Thus, the net force, f_r, can easily obtained if all support or reaction forces are known. In the case of stationary condition, the value of f_s is equal to the ground reaction forces which caused by the gravitational force only. Here, the stability metric is measured by

$$\beta_{fasm} = \min_i(\theta_i \cdot \parallel \boldsymbol{d}_i \parallel \cdot \parallel \boldsymbol{f}_{ri} \parallel) \quad \text{for} \quad i = (1, \ldots, n). \tag{4.5}$$

  where f_{ri} is the component of the net force perpendicular to the $i-$th edge of the support polygon, θ_i is the angle between the resultant force and the vector l_i,

and d_i is the vector from the position of the resultant force acting on the ground perpendicular to the vector l_i. Here, the positive magnitude of β_{fasm} indicates the tip-over stability margin of a stable system. Critical tip-over stability condition occurs when one of the components becoming zero, where the tip-over stability margin $\beta_{fasm} = 0$. Here, the net-force f_r can be obtained from the dynamical model by

$$f_r = -\frac{\sum_{i=1}^{n} f_{zi}}{\cos\phi_r} \tag{4.6}$$

where ϕ_r is the angle between the net-force and the $z-$axis. Meanwhile, the position of the action point of the net force on the ground can be calculated by

$$x_r = \frac{\sum_{i=1}^{n} f_{zi}x_i}{\sum_{i=1}^{n} f_{zi}}, y_r = \frac{\sum_{i=1}^{n} f_{zi}y_i}{\sum_{i=1}^{n} f_{zi}}, \tag{4.7}$$

Assuming the set of stability metrics as $\boldsymbol{\beta} = [\beta_1\ \beta_2\ ...\ \beta_n]^T$, the minimum stability metrics as β_{min} and the set of the support polygon edges as $\boldsymbol{S} = [S_1\ S_2\ ...\ S_n]^T$, the estimated tip-over axis can be found by the following algorithm:

Algorithm 2: Finding the tip-over axis (S_{tip})

for $i = 1$ to n
  if $\boldsymbol{\beta}(i) == \beta_{min}$
    return $a = i$
  end if
end for
$S_{tip} = \boldsymbol{S}(a)$

4.2.3 Tip-over direction and tip-over angle

With the assumption that the S_{tip} is the line connected two of the ground contact points $\boldsymbol{p}_j$ and $\boldsymbol{p}_{j+1}$, then the tip-over direction can be described by the direction of the line which connected the CoG perpendicularly to the S_{tip} as shown in Fig. 4.7.

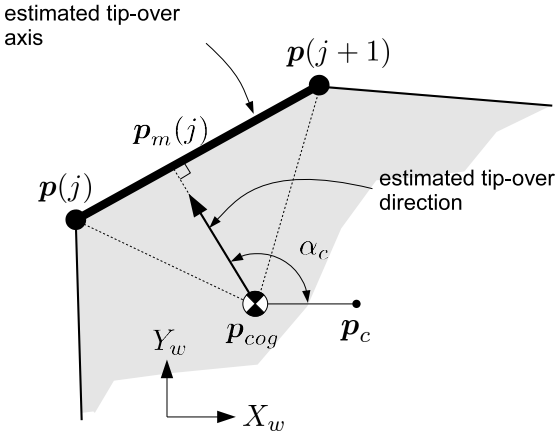

FIGURE 4.7: Tip-over axis and tip-over direction

By defining $\boldsymbol{P}_g = [x_g \ y_g]^T$ and the virtual point in its longitudinal direction as $\boldsymbol{P}_c = [(x_g + a) \ y_g]^T$, the tip-over direction can be described by the angle of α_c. The value of α_c can be calculated using cosine rule by

$$\alpha_c = \cos^{-1}\left(\frac{|p_g p_c|^2 + |p_g p_m|^2 - |p_c p_m|^2}{|p_g p_c||p_g p_m|}\right) \tag{4.8}$$

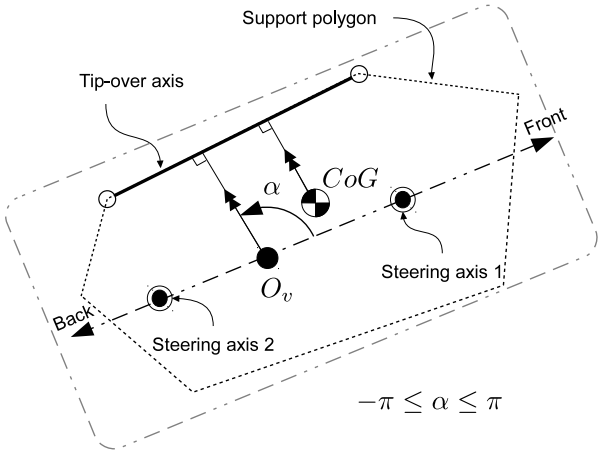

FIGURE 4.8: Tip-over angle

This angle also can be represented according to the coordinate frame of the mobile platform by a tip-over angle α which described by

$$\alpha = \alpha_c - \phi. \tag{4.9}$$

4.3 Simulation 1: Tip-over prediction for four-wheeled personal mobility robot

In this section, the simulation was performed to demonstrate and verify the effectiveness of the prediction system for the four-wheeled personal mobility robot. The results of this simulation were also presented in [116]. The moment stability measure (MSM) is used in this simulation to measure the tip-over stability measure. The simulation time is 35 s, sampling period 20 ms, the initial pose of the personal mobility robot was $x = [0\ 0\ 0]^T$ and the initial orientation of each dual-wheel caster is set to 0 rad. The reference trajectory is shown in Fig. 4.9(a). The personal mobility robot is set to move from a stationary state to the velocity of 0.2 m/s in the first 6 s and maintains the velocity constantly to the end of simulation. The personal mobility robot also is set to rotate at the angular velocity of $\frac{\pi}{12}$ rad/s on the last 8 s. The physical parameters of this simulation are listed in Table 4.1.

TABLE 4.1: Physical parameters of the tip-over prediction simulation 1

d_1, d_2	0.13	[m]	r_1, r_2	0.05	[m]
s_1, s_2	0.075	[m]	s_{g1}, s_{g2}	0.0155	[m]
s_{f1}, s_{f2}	0.08	[m]	I	12.708	[kgm^2]
M_a	122	[kg]	m_1, m_2	6.5	[kg]
L_1,L_2	0.3	[m]	h_{s1}, h_{s2}	0.4	[m]
h_{m1}, h_{m2}	0.15	[m]	h_{M_a}	0.7	[m]

Presented in Figs. 4.9 and 4.10 are the result of the conducted simulation for estimating the supporting forces and moments stability measure (MSM). The estimated supporting forces change according to the given velocity and acceleration. In the existence of acceleration or deceleration, for example in the first 6 s, it is observed that the reaction forces for the front ADWC are greater than those for the back ADWC. Here, the same drive pattern as the conventional vehicle can be seen because all wheels are aligned in parallel without any changes in orientation. However, in other situation, the forces are distributed according to the current position and orientation of the ADWC assemblies. In a constant velocity mode, the reaction forces for all wheels are identical if both of the ADWC assemblies have the same orientation and direction. As shown in Fig. 4.10(b), the moment values are reflected to the dynamics effect and the shape of supporting polygon. These values represent the tendency of a tip-over occurrence at the respective edge

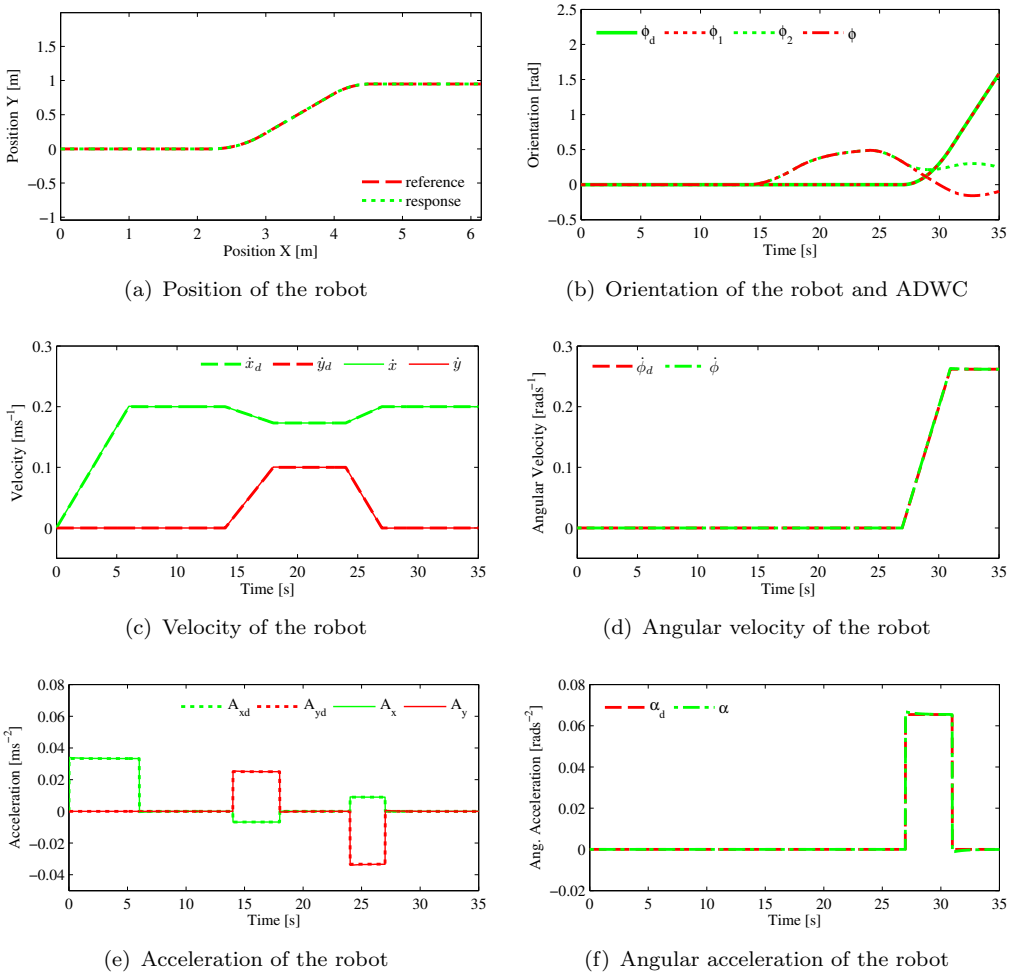

(a) Position of the robot

(b) Orientation of the robot and ADWC

(c) Velocity of the robot

(d) Angular velocity of the robot

(e) Acceleration of the robot

(f) Angular acceleration of the robot

FIGURE 4.9: References and responses

(tipping axis). In this simulation, we found that the personal mobility robot has more tendencies to tip-over at S_1 and S_3 axis compared to S_2 and S_4 axis. However, at a certain time the shape of the supporting polygon may change to triangle, so the candidate of the tip-over axis may be reduced to three or less. This can be seen from the value of n_{S_4} at the time of 34.5 s. The value of 0 Nm here does not represent an actual tip-over occurrence. The number of edges has been reduced into three, therefore the fourth axis possess zero value. At the final stage of the trajectory, the moment's value is decreasing due to the narrow supporting polygon. Here, a tip-over occurrence may easily happen if any external forces due to disturbances or else were applied. Figure 4.11 shows the robot trajectory with an actual position of ADWC assemblies and the comparison of the stability measurement between the static stability margin (SSM) and MSM. In most situations along this trajectory, the tip-over prediction by SSM and MSM are identical. However, in the final position of the personal mobility robot, the MSM shows better estimation. The personal mobility robot tends to tip-over at the axis with the MSM estimation, even though the distance to the SSM's estimated axis is nearer.

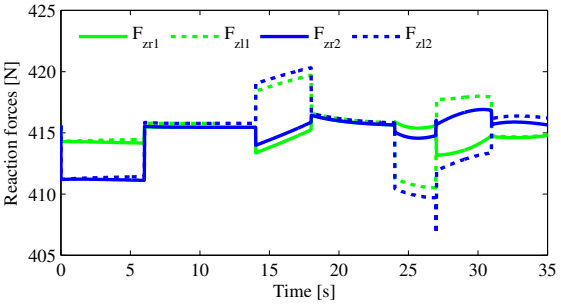

(a) Reaction forces

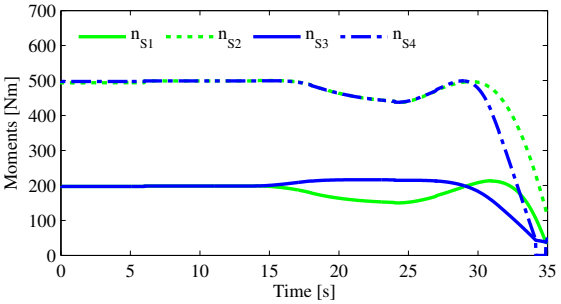

(b) Moments

FIGURE 4.10: Reaction forces and moments

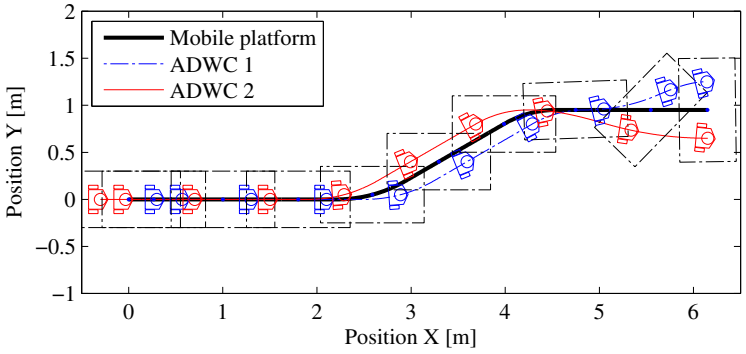

(a) Estimated trajectory

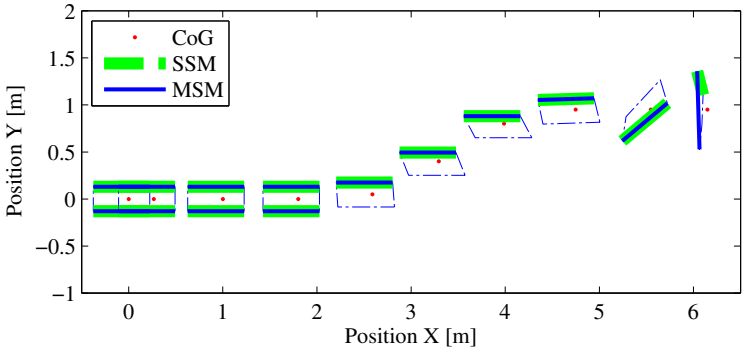

(b) Estimated tip-over axis

FIGURE 4.11: Trajectory and tip-over axis prediction

4.4 Simulation 2: Tip-over prediction for six-wheeled personal mobility robot

In this section, the simulation was performed to demonstrate and verify the effectiveness of the prediction system for the six-wheeled personal mobility robot. The force-angle stability measure (FASM) is used in this simulation to measure the tip-over stability measure. The results of these simulations were also presented in [108, 118].

These simulations were conducted under the resolved velocity control. The simulation time is 10 s and the sampling period is 20 ms. The experiments were conducted in three different cases with the same input of linear velocity. In order to evaluate the dynamic effects, both velocity inputs for each case were set to be different in acceleration and deceleration but have the same maximum velocity of 0.6 ms^{-1}. The physical parameters of the omnidirectional personal mobility robot are listed in Table 4.2.

TABLE 4.2: Physical parameters of the tip-over prediction simulation 2

d_1, d_2	0.13	[m]	r_1, r_2	0.05	[m]
s_1, s_2	0.075	[m]	s_{g1}, s_{g2}	0.0155	[m]
s_{f1}, s_{f2}	0.08	[m]	I	12.708	[kgm^2]
M_a	120	[kg]	m_1, m_2	6.5	[kg]
L_1	0.3	[m]	L_2	0.35	[m]
h_{s1}, h_{s2}	0.15	[m]	h_{m1}, h_{m2}	0.08	[m]
h_{M_a}	0.7	[m]			

4.4.1 Translational motion in longitudinal direction

The basic movement of any mobile robot is to perform a straight trajectory motion in its longitudinal direction. In this experiment, the initial pose of the personal mobility robot was set to $\boldsymbol{x} = [0\ 0\ 0]^T$and the initial orientation of each dual-wheel caster was set to 0 rad. Presented in Fig. 4.12 is the result for this simulation. From Fig. 4.12(i), it is found that both longitudinal motions are stable and there is no possibility of tip-over occurrence. However, the second motion with a lower acceleration and deceleration poses better stability compared with the first motion. The estimated tip-over direction is maintained through the simulation at the angle of -1.5708 rad or equal to -90 deg, which is the right side of the personal mobility robot.

4.4.2 Translational motion in sideway direction

A special feature of a holonomic and omnidirectional mobile robot is the capability to move to the sideway direction without changing its orientation. To evaluate this property and its stability measurement, the personal mobility robot is set to move to its sideway direction from an initial pose of $\boldsymbol{x} = [0\ 0\ \frac{\pi}{2}]^T$ and the initial orientation of both ADWCs were set to $\frac{\pi}{2}$ rad. Fig. 4.13 shows the result for the sideway motion of the personal mobility robot. As referred to Figs. 4.13(a) and 4.13(b), both ADWCs keep changing their direction from $\frac{\pi}{2}$ rad to 0 rad in the first 2 m. The effects of this change can be seen from the FASM value as shown in Fig. 4.13(i) for the first 4 s. It is clear that this rapid change did not cause any tip-over occurrences. In the second stage of constant velocity, both motions are in a stable condition. However, the stability value decreased in the final stage when the personal mobility robot begins to decelerate. This deceleration or braking possibly leads the personal mobility robot in motion 1 to tip-over as the FASM 1 becomes zero. The estimated direction of this tip-over incident may occur on the left side of the personal mobility robot as shown in Fig. 4.13(j).

4.4.3 Translational and rotational motion

Another feature of the holonomic omnidirectional mobile robot is the capability to rotate while performing any translational motion. To analyze the stability with this property, the personal mobility robot is set to move to its longitudinal direction while performing rotation. The initial pose of the personal mobility robot was set to $\boldsymbol{x} = [0\ 0\ 0]^T$ and the initial orientation of both ADWCs were set to 0 rad. The additional angular velocity was set to $\frac{\pi}{20}$ rads^{-1}. Fig. 4.14 shows the result of this simulation. As shown in Figs. 4.14(a) and 4.14(b), the personal mobility robot and the ADWCs were observed to change rapidly their orientation along the trajectory. In a lower acceleration effect, this change did not cause the personal mobility robot to tip-over as shown in Fig. 4.14(i). However, in the existence of sudden braking and the final pose as observed in Fig. 4.14(a) or 4.14(b), the personal mobility robot is estimated to tip-over on the left side. This incident is identical to the tip-over incident that is observed in previous case.

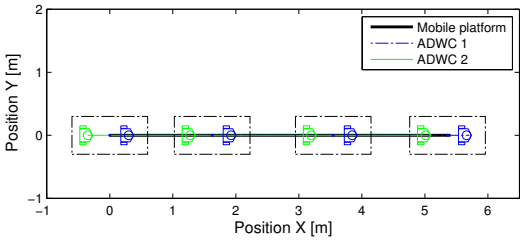

(a) Estimated trajectory (Input velocity=V_{x1})

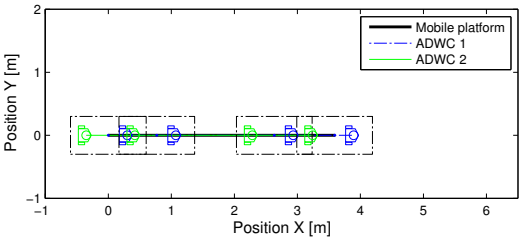

(b) Estimated trajectory (Input velocity=V_{x2})

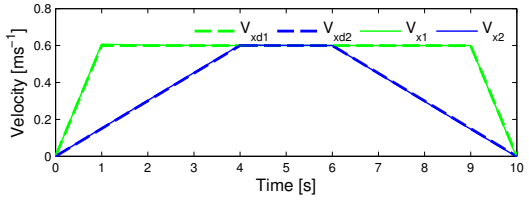

(c) Velocity (V_{xdi}: desired , V_{xi}: response)

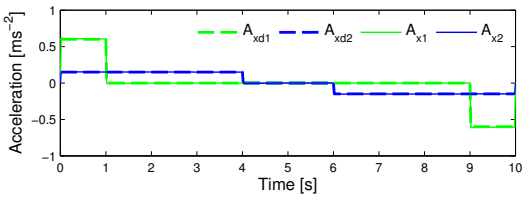

(d) Acceleration (A_{xdi}: desired , A_{xi}: response)

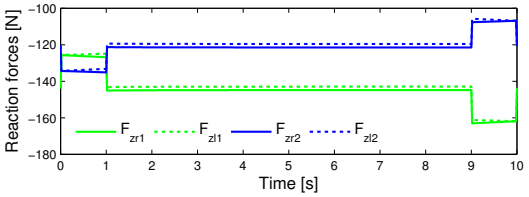

(e) Reaction forces of left and right wheels (Input velocity=V_{x1})

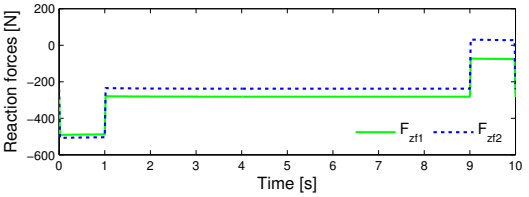

(f) Reaction forces of front wheels (Input velocity=V_{x1})

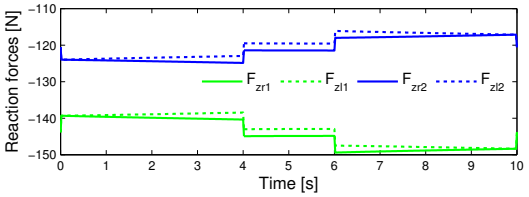

(g) Reaction forces of left and right wheels (Input velocity=V_{x2})

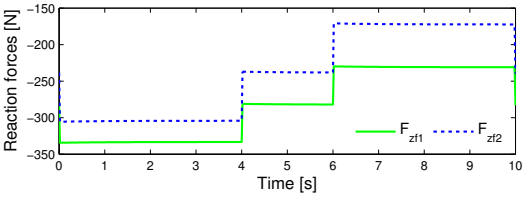

(h) Reaction forces of front wheels (Input velocity=V_{x2})

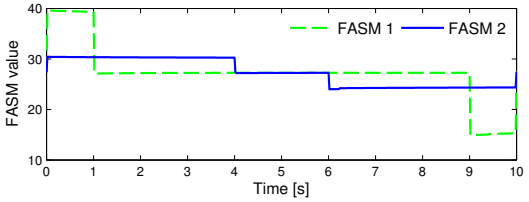

(i) Estimated FASM value of tip-over axis

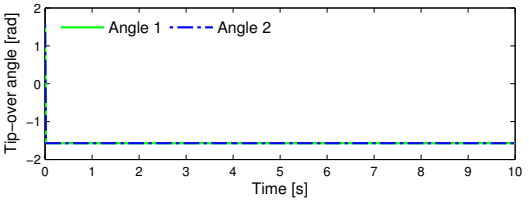

(j) Estimated tip-over angle

FIGURE 4.12: References and responses for translational motion in longitudinal direction

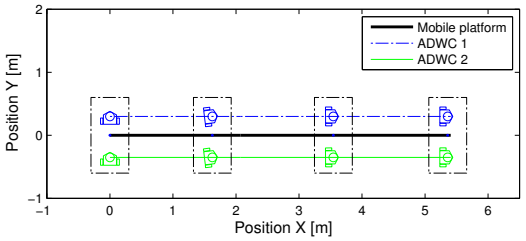

(a) Estimated trajectory (Input velocity=V_{x1})

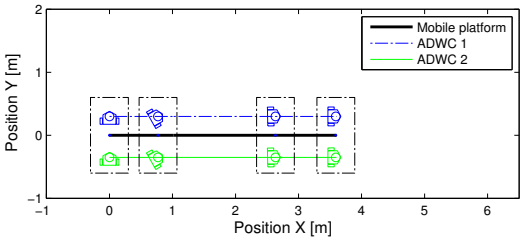

(b) Estimated trajectory (Input velocity=V_{x2})

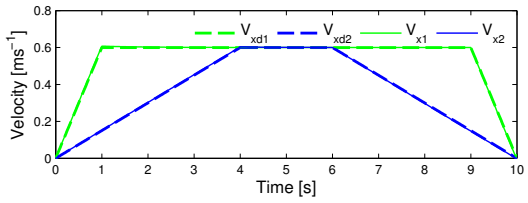

(c) Velocity (V_{xdi}: desired , V_{xi}: response)

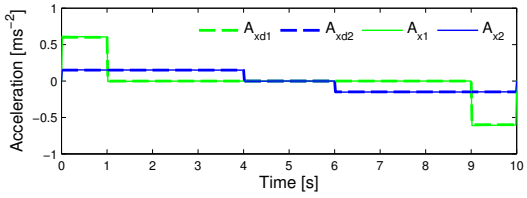

(d) Acceleration (A_{xdi}: desired , A_{xi}: response)

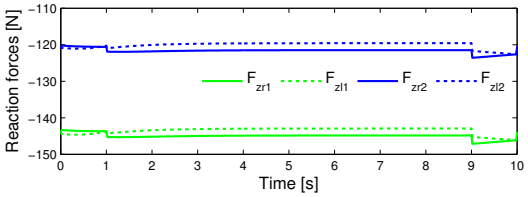

(e) Reaction forces of left and right wheels (Input velocity=V_{x1})

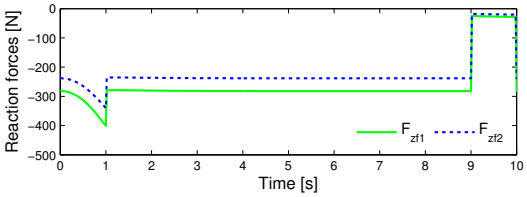

(f) Reaction forces of front wheels (Input velocity=V_{x1})

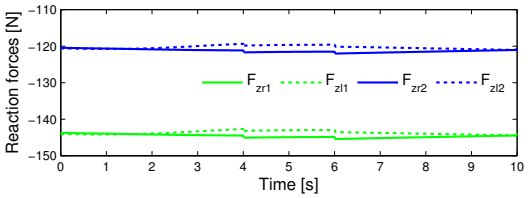

(g) Reaction forces of left and right wheels (Input velocity=V_{x2})

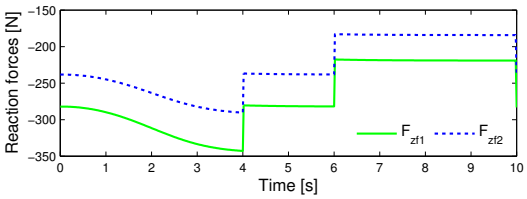

(h) Reaction forces of front wheels (Input velocity=V_{x2})

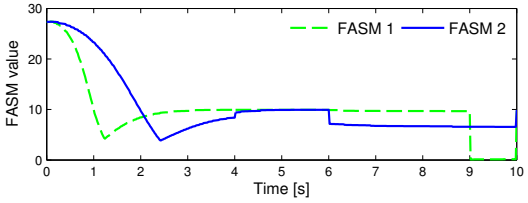

(i) Estimated FASM value of tip-over axis

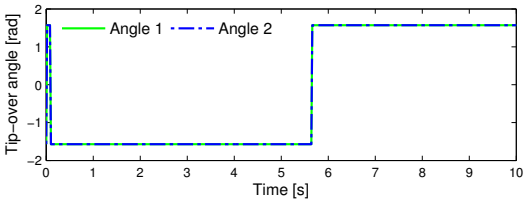

(j) Estimated tip-over angle

FIGURE 4.13: References and responses for translational motion in sideway direction

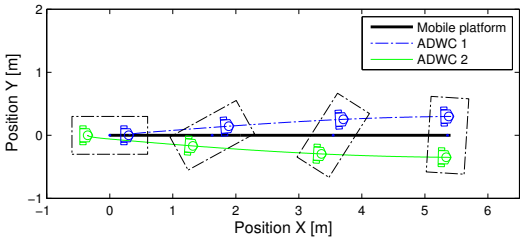

(a) Estimated trajectory (Input velocity=V_{x1})

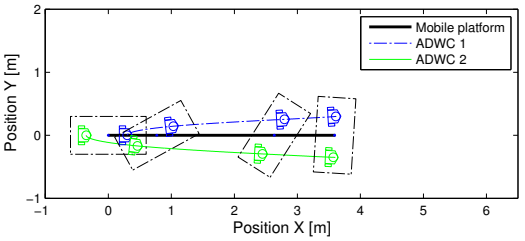

(b) Estimated trajectory (Input velocity=V_{x2})

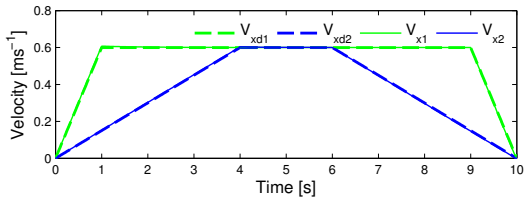

(c) Velocity (V_{xdi}: desired , V_{xi}: response)

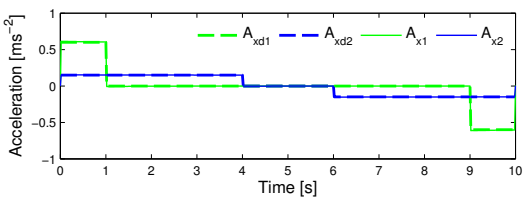

(d) Acceleration (A_{xdi}: desired , A_{xi}: response)

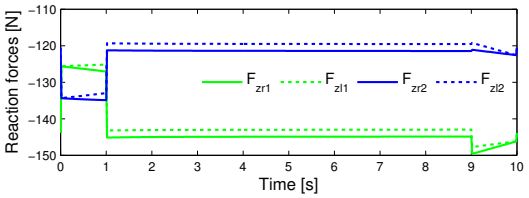

(e) Reaction forces of left and right wheels (Input velocity=V_{x1})

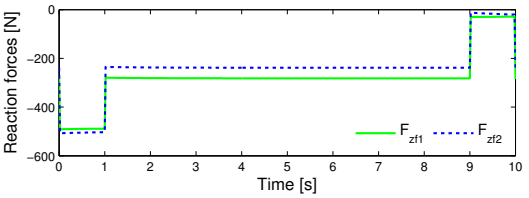

(f) Reaction forces of front wheels (Input velocity=V_{x1})

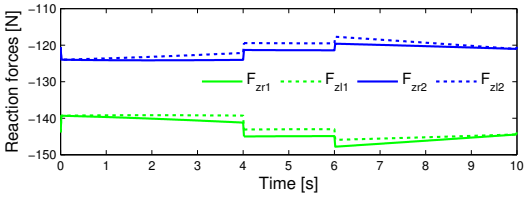

(g) Reaction forces of left and right wheels (Input velocity=V_{x2})

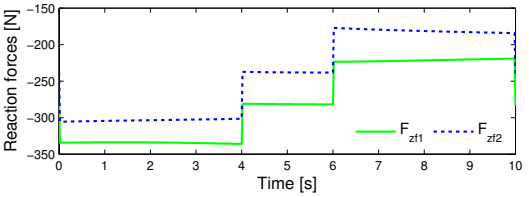

(h) Reaction forces of front wheels (Input velocity=V_{x2})

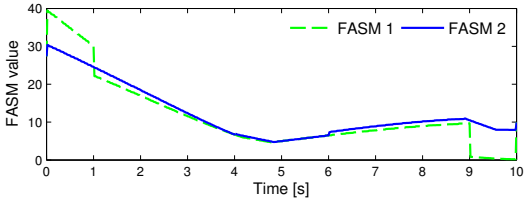

(i) Estimated FASM value of tip-over axis

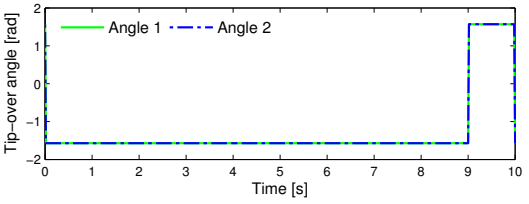

(j) Estimated tip-over angle

FIGURE 4.14: References and responses for translational and rotational motion

4.4.4 Combination trajectories

The simulation was performed to demonstrate and verify the effectiveness of the dynamical model as well as the tipping stability prediction method. This simulation was conducted under the resolved velocity control. The simulation time is 35 s, sampling period 20 ms, the initial pose of the personal mobility robot was $\boldsymbol{x} = [0\ 0\ 0]^T$ and the initial orientation of each dual-wheel caster was set to 0 rad. The reference trajectory and velocity is shown in Fig. 4.15. The personal mobility robot is set to move from a stationary state to the velocity of 0.2 ms^{-1} in the first 6 s and maintains the velocity constantly to the end of simulation. The personal mobility robot also is set to rotate at the angular velocity of $\frac{\pi}{12}$ rads^{-1} on the last 8 s. The physical parameters of this simulation are listed in Table 4.3.

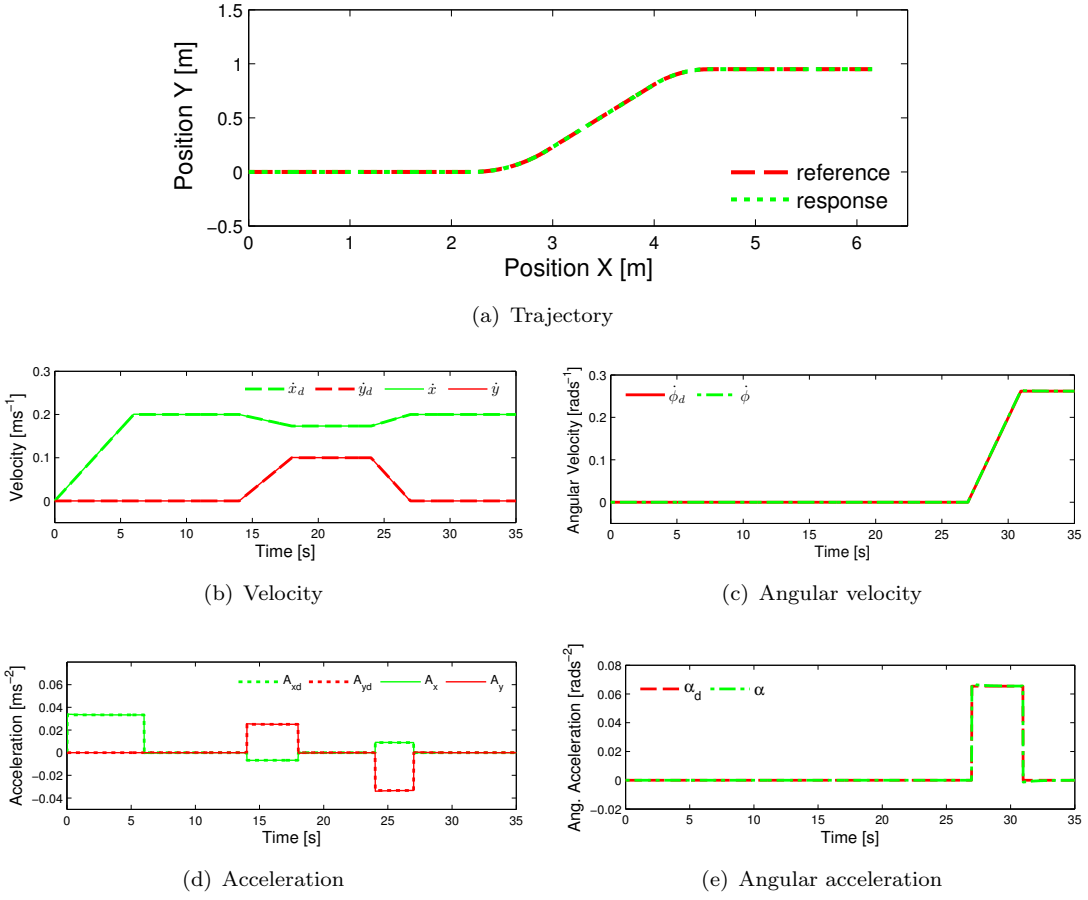

(a) Trajectory

(b) Velocity

(c) Angular velocity

(d) Acceleration

(e) Angular acceleration

FIGURE 4.15: Reference and response

Presented in Figs. 4.16 and 4.17 are the results of the conducted simulation for estimating the supporting forces and FASM. As shown in Figs. 4.16(a) and 4.16(b), the estimated supporting forces are reflected to the given velocity and acceleration. Fig. 4.17(a) shows the response of the overall personal mobility robot system including the position of ADWC. The supporting polygon subjected to this position is shown in Fig. 4.17(b). The shape of the supporting polygon changes rapidly according to the pose of

ADWCs. The prediction of tipping axis is shown by the FASM. Here, we also enclose the result under static stability measurement shown by the SSM.

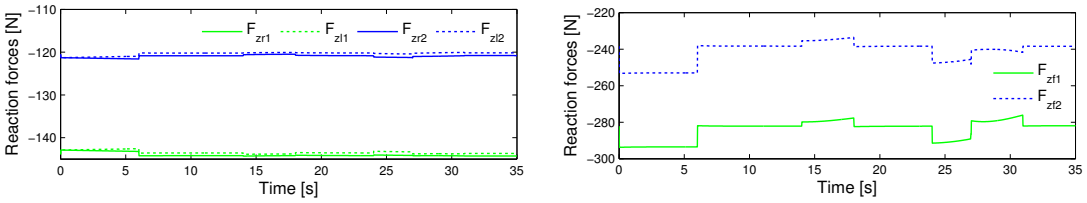

(a) Normal forces for right and left wheels

(b) Normal forces for front wheels

FIGURE 4.16: Estimated supporting forces

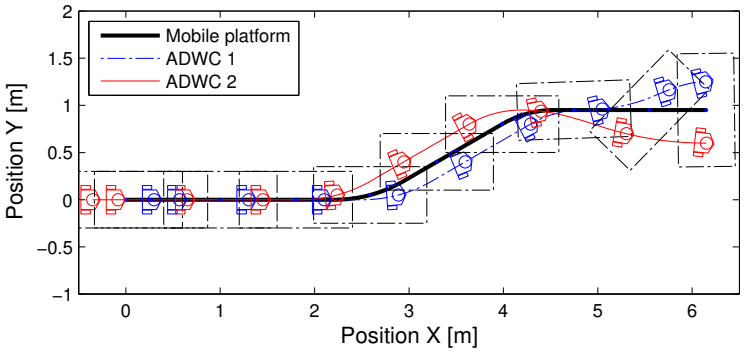

(a) Trajectory

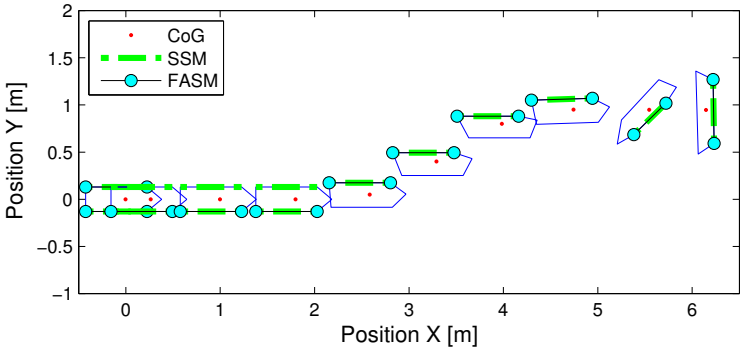

(b) SSM and FASM evaluation

FIGURE 4.17: Supporting polygon and tip-over prediction

4.5 Simulation 3: Relationship between the transport loads and the tip-over stability

In this section, the simulations were conducted to analyze the relationship between the transport loads and the tip-over stability. An increase in the loading weight also leads to the increase in the CoG weight. Thus, these simulations also examined the effects of the changes in the CoG height to the tip-over stability. The simulation results were also presented in [119].

The simulation time is 10 s and the sampling period is 20 ms. The task of the personal mobility robot is to transport several boxes in two simple motion of a holonomic and omnidirectional personal mobility robot. In addition, each transport is simulated under two different acceleration and deceleration but have the same maximum velocity of 0.6 ms^{-1}. The dimension of each box is set to 1.0 m × 0.5 m × 0.2 m with the weight of 20 kg. Assume that the dimension of personal mobility platform is 1.0 m × 0.5 m × 0.1 m. The physical parameters of the omnidirectional personal mobility robot are listed in Table 4.3.

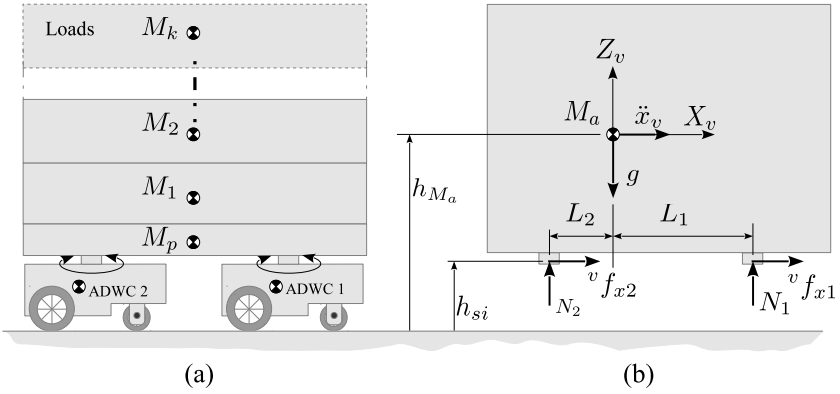

FIGURE 4.18: Transportation for different loads

TABLE 4.3: Physical parameters of the tip-over prediction simulation 3

M_a	120	[kg]	m_1, m_2	6.5	[kg]
L_1	0.3	[m]	L_2	0.35	[m]
h_{s1}, h_{s2}	0.15	[m]	h_{m1}, h_{m2}	0.08	[m]
d_1, d_2	0.13	[m]	r_1, r_2	0.05	[m]
s_1, s_2	0.075	[m]	s_{g1}, s_{g2}	0.0155	[m]
s_{f1}, s_{f2}	0.08	[m]	M_p	5.0	[kg]

4.5.1 Translational motion in sideway direction

A special feature of a holonomic omnidirectional mobile robot is the capability to move to the sideway direction without changing its orientation. To evaluate this property and its stability measurement, the personal mobility robot is set to move to its sideway direction from an initial pose of $\boldsymbol{x} = [0\ 0\ \frac{\pi}{2}]^T$, the initial orientation of ADWC1 is set to $\frac{\pi}{4}$ rad and ADWC2 is set to $-\frac{\pi}{4}$ rad. Fig. 4.19 shows the result for the sideway motion of thepersonal mobility robot. As referred to Figs. 4.19(a) and 4.19(b), both ADWCs keep changing their direction from their initial orientation to 0 rad in the first 2 m before continuing with straight trajectory. This proved that the personal mobility robot is holonomic and capable of driving to its sideway even though the ADWCs is not on the same direction as the required trajectory. Figs. 4.19(e)−4.19(j) show the FASM value and the estimated tip-over angle for each task. From this result, it is noted that the personal mobility robot with no load tends to tip-over more to the left side of the personal mobility robot compared with any load transportation. The transportation for 1 box and 3 boxes shows not much different on its estimated tipping direction. However, the transportation with the maximum of 5 boxes tends to change the tip-over direction from the right to the left side earlier on 6 s. In all cases, the estimated tip-over direction is 90 deg to the left or right side of the personal mobility robot. The tip-over incident is estimated to occur at the end of transportation for the load more than 2 boxes when the velocity is set to V_{x1}. This is referred to the zero FASM value in Figs. 4.19(g)−4.19(j).

4.5.2 Translational and rotational motion

Another feature of the holonomic omnidirectional mobile robot is the capability to rotate while performing any translational motion. To analyze the stability with this property, the personal mobility robot is set to move to its longitudinal direction while performing rotation. The initial pose of the personal mobility robot was set to $\boldsymbol{x} = [0\ 0\ 0]^T$ and the initial orientation of both ADWCs were set to 0 rad. The additional angular velocity was set to $\frac{\pi}{20}$ rads^{-1}. Fig. 4.20 shows the result of this simulation. As shown in Figs. 4.20(a) and 4.20(b), the personal mobility robot and the ADWCs were observed to change rapidly their orientation along the trajectory. In the zero load condition thepersonal mobility robot tends to tip-over in the left side direction during the start of maneuver and between the period of 7 to 9 s. On the other hand, the transportation with load did not tend to tip-over at the left side on the beginning. However, the transportation with load is observed to has the tendency of tip-over in the left direction during the deceleration (braking) period at the end of maneuver. However, the transportation for 1 box is estimated to be

more stable compared with other transportation with load by referencing to the FASM value shown in Figs. 4.20(g)−4.20(j) .

4.6 Summary

This chapter has introduced the tip-over prediction methods for personal mobility robots with active dual-wheel caster assemblies. The prediction of the support polygon for every existing footprints has been discussed and solved using the convex hull algorithm. Two methods for determining the tip-over stability also were introduced: the moment stability measure (MSM) and the force-angle stability measure (FASM). The MSM is novel and used to estimate the tip-over stability for the four-wheeled personal mobility robots. Meanwhile, the FASM superior to the MSM was used later in the six-wheeled personal mobility robots. The performance of these prediction methods has been compared with the standard prediction method using the SSM values. The tip-over stability was also proved to be influenced by changing the loads and the height of the CoG. The prediction method for the six-wheeled structure will be further discussed in the next chapter for the use of the tip-over stability enhancement.

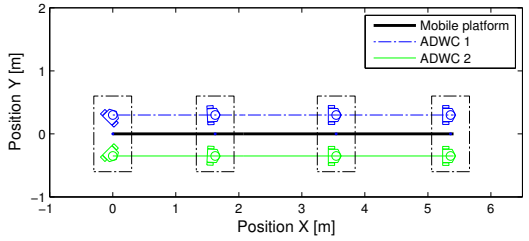

(a) Estimated trajectory (Input velocity=V_{x1})

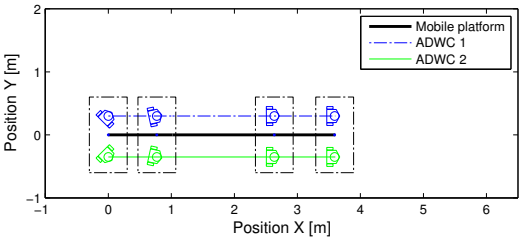

(b) Estimated trajectory (Input velocity=V_{x2})

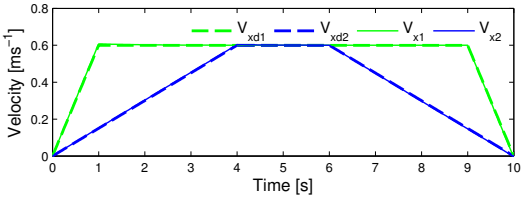

(c) Velocity (V_{xdi}: desired , V_{xi}: response)

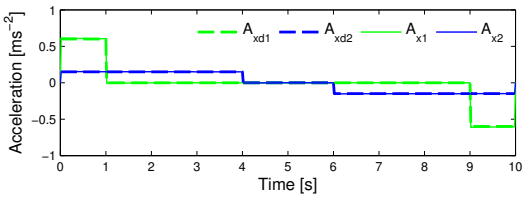

(d) Acceleration (A_{xdi}: desired , A_{xi}: response)

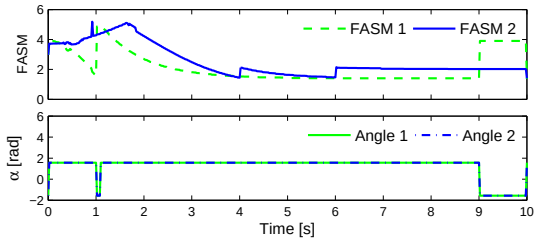

(e) Estimated FASM and tip-over angle without load

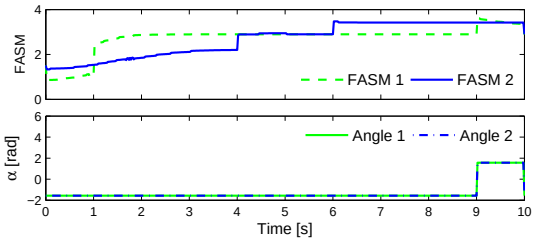

(f) Estimated FASM and tip-over angle with 1 box

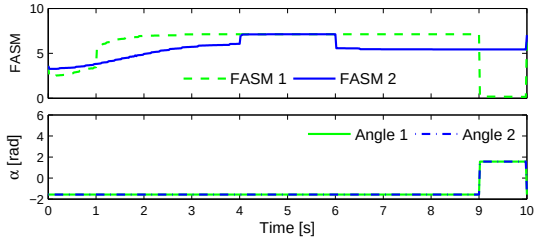

(g) Estimated FASM and tip-over angle with 2 boxes

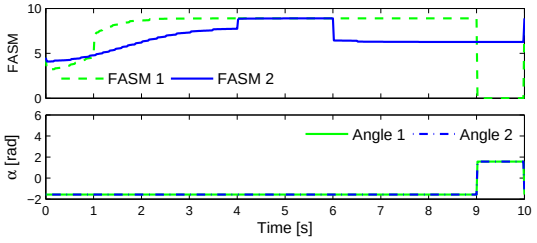

(h) Estimated FASM and tip-over angle with 3 boxes

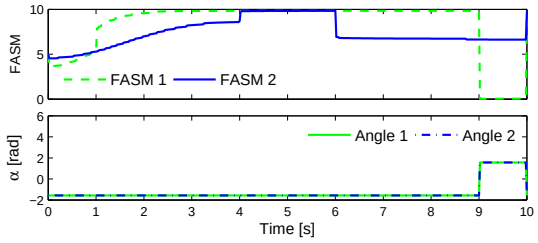

(i) Estimated FASM and tip-over angle with 4 boxes

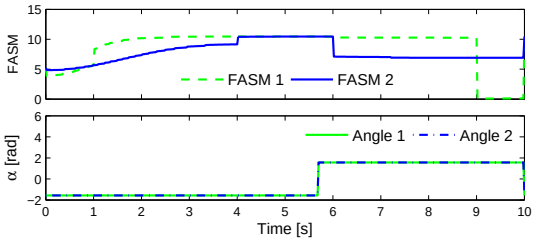

(j) Estimated FASM and tip-over angle with 5 boxes

FIGURE 4.19: References and responses for translational motion in sideway direction

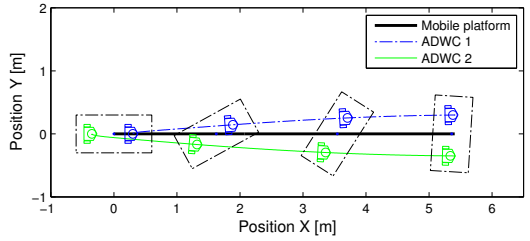

(a) Estimated trajectory (Input velocity=V_{x1})

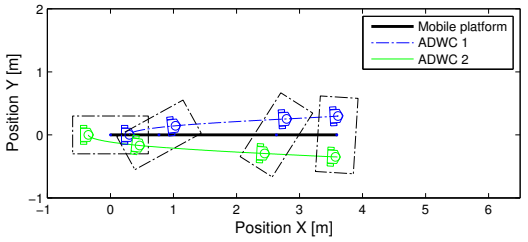

(b) Estimated trajectory (Input velocity=V_{x2})

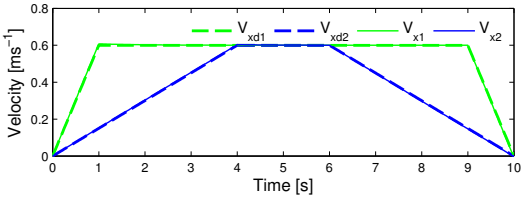

(c) Velocity (V_{xdi}: desired , V_{xi}: response)

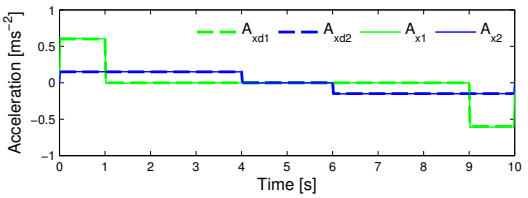

(d) Acceleration (A_{xdi}: desired , A_{xi}: response)

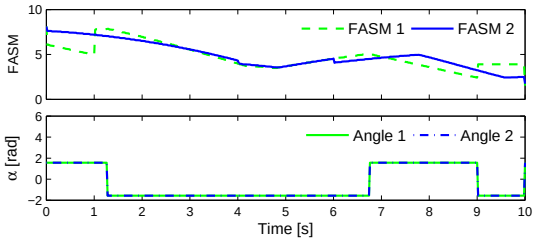

(e) Estimated FASM and tip-over angle without load

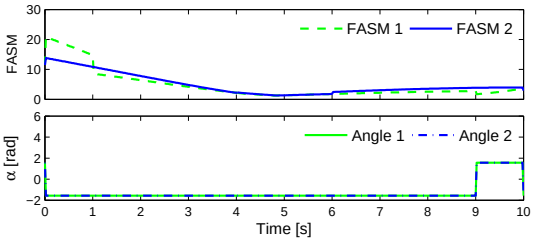

(f) Estimated FASM and tip-over angle with 1 box

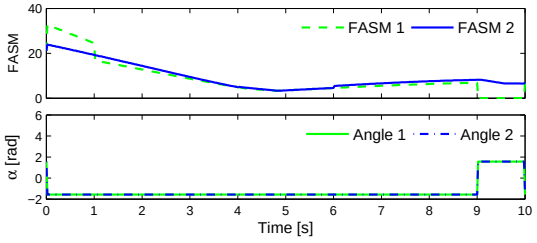

(g) Estimated FASM and tip-over angle with 2 boxes

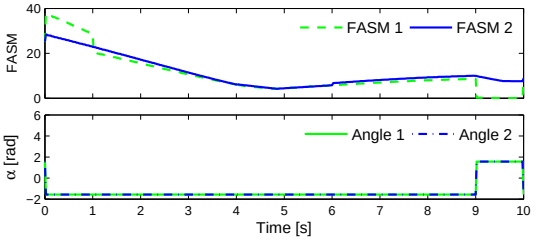

(h) Estimated FASM and tip-over angle with 3 boxes

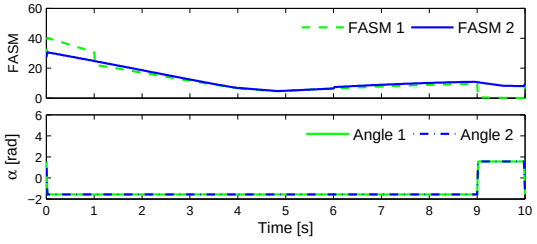

(i) Estimated FASM and tip-over angle with 4 boxes

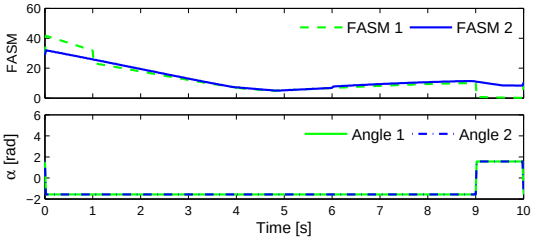

(j) Estimated FASM and tip-over angle with 5 boxes

FIGURE 4.20: References and responses for translational and rotational motion

Chapter 5

Tip-over Stability Enhancement

5.1 Introduction

In general, all vehicles and mobile robots were developed with the consideration of stability. Failure in securing a good stability for the vehicles and mobile robots could lead to heavy injuries and also damage the robot itself [120]. Normally, vehicles and mobile robots with lower CoG, wide supporting area and low velocity disregard the dynamical effects. Most of them were designed with more than three wheels to make sure the CoG position is kept inside the supporting polygon at all times. Meanwhile, statically unstable vehicles and mobile robots usually apply dynamical control such as inverted pendulum model to make sure that they are keeping in balance. The personal mobility robots with active dual-wheel caster assemblies however were statically stable but possible to tip-over when the dynamical effects exist as shown in Fig. 5.1. Thus, it is necessary for the personal mobility robots to be stable either in any static positions or during the existence of dynamics. In the previous chapter, the tip-over stability analysis and the tip-over prediction method have been presented. This chapter will introduce the extended work of the previous chapter by proposing the tip-over prevention systems for the personal mobility robot. The tip-over prevention approaches in this thesis were facilitated by the tip-over stability enhancement.

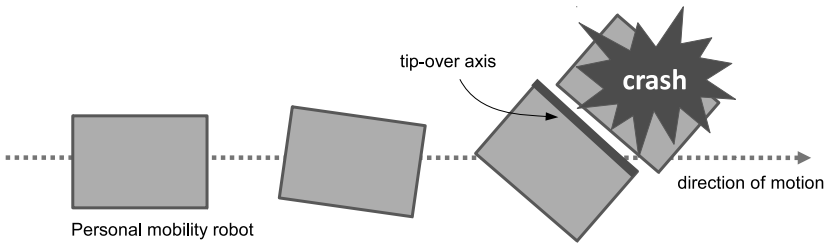

FIGURE 5.1: Personal mobility robots without crash prevention

5.2 Tip-over stability enhancement

A general idea in preventing the tip-over occurrence is providing a motion in the direction of the tip-over as shown in Fig. 5.2. This concept normally implemented for the inverted pendulum model mobile robots [121, 28]. A holonomic and omnidirectional mobile platform is capable to generate an instantaneous planar motion in any direction depending on the estimated tip-over direction. However, the motion may require some free spaces around the personal mobility robot. In actual implementation in a crowded environment, this extra motion may worsen the situation with an unexpected collision between the machines or human. Therefore, enhancing the stability without providing any extra external motion is more preferable for maintaining a stable maneuver. With the existing design of the personal mobility robot, the tip-over incidents tend to occur more in the lateral direction compared with other directions based on the FASM analysis in our previous paper [108]. Thus it is sufficient to provide a preventing mechanism that focused on the lateral instability control only. Here, we proposed two methods: i.e., alteration of acceleration input and gyroscopic torque device as the stability enhancer to improve the stability and prevent a tip-over incident.

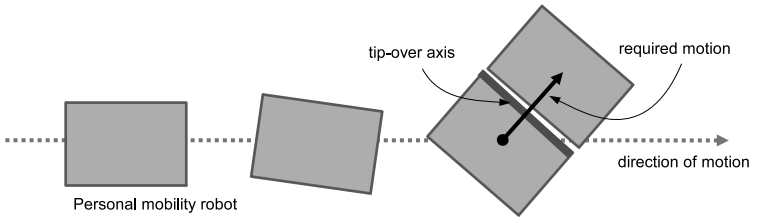

FIGURE 5.2: Personal mobility robots moving towards tipping direction to balance

5.2.1 Alteration of acceleration input

The tip-over stability is very sensitive to the changes in the acceleration and deceleration of the personal mobility robot as shown by the simulation result in the previous chapter. Based on the tip-over stability measure, the unstable region can be identified and correlated with the given velocity and acceleration input. The tip-over stability can be improved by simply altering the related command to surpass the preset tip-over stability threshold. Other parts which passed the preset tip-over stability threshold are maintained like the prior input. This simple method can be explained by Fig. 5.3. Assuming the threshold of the tip-over is set to β_t, the unstable region which is less than the β_t can be recognized and grouped. The given velocity and acceleration are recognized for the same time region and altered as a new command. The alteration can be done by extending the time for acceleration/ braking as shown in Fig. 5.3(b). In this example, the time for

travel is extended from t_j to t_k where $t_k = t_j + \Delta t$. Thus the personal mobility can be kept in stable condition along the predefined trajectory as shown in Fig. 5.4.

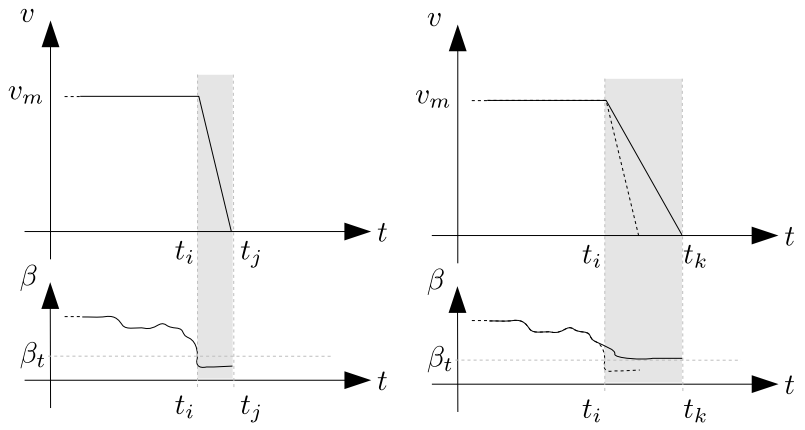

(a) Before alteration (b) After alteration

FIGURE 5.3: Alteration of the acceleration, e.g. by extension of the acceleration/deceleration time

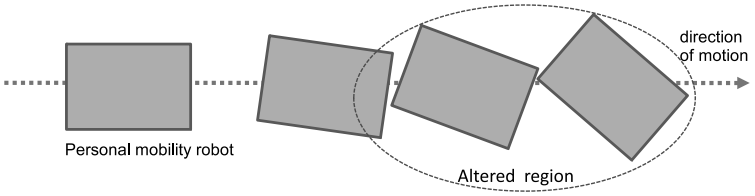

FIGURE 5.4: Personal mobility robots with alteration of acceleration input

5.2.2 Single-gimbal control moment gyro

This thesis also proposed the use of a gyroscopic torque device, i.e. a single-gimbal control moment gyro (SGCMG), to assist the personal mobility robot for maintaining the stability [122, 123, 124]. The control moment gyro (CMG) is a torque generator for attitude control of an artificial satellite and as a roll-over controller device for a ship vessel [125, 126]. A general idea of the CMG for the tip-over prevention is shown in Fig. 5.5. The CMG will generate counter torques against the predicted tip-over axis to maintain the stability. In our approach, single-gimbal CMG is chosen based on the advantages of the simplicity and

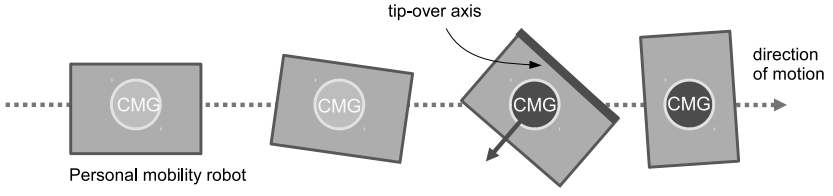

FIGURE 5.5: Personal mobility robots with gyro stabilizer

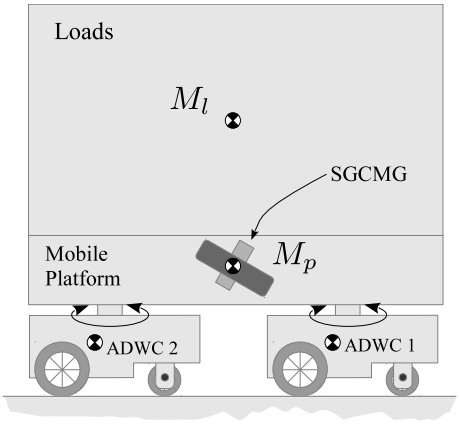

FIGURE 5.6: Overview of the model including the SGCMG unit

higher output torque compared to the double-gimbal CMG (DGCMG). In addition, it also enables a higher instantaneous torque compared with the reaction wheel where CMG can store higher momentum in every second. The SGCMG unit is installed at the center of the mobile platform as shown in Fig. 5.6.

A simple SGCMG system consists of a flywheel rotating at a constant speed and one gimbal motor as shown in Fig. 5.7. The spinning flywheel produces an angular momentum H_f in the $z-$axis direction. If a rotational precession rate of ω_p is applied to the spinning flywheel about the gimbal axis, a precession output torque, τ_p which is perpendicular to the direction of H_f and ω_p will be generated.

Defining the angular velocity of the spinning flywheel as ω_f and the moment of inertia of the flywheel as I_f, the angular momentum produced by the spinning flywheel in the $z-$axis is

$$H_f = I_f \omega_f \tag{5.1}$$

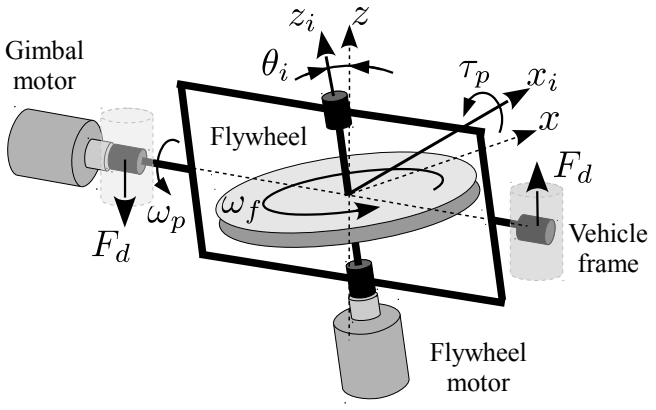

FIGURE 5.7: Single-gimbal control moment gyro

Thus, the gyroscopic torque produced by the existing rotational precession rate of ω_p is

$$\tau_p = H_f \omega_p = I_f \omega_f \omega_p \tag{5.2}$$

Due to the changes in the gimbal angle, the acting torque around the x- axis can be represented by

$$\tau_{px} = \tau_p \cos(\theta_i) \tag{5.3}$$

The production of this gyroscopic torque induced a force to the center of mass on the y-axis direction which later use to provide a counter force to the predicted tip-over direction. The overview of the tip-over stability enhancement system is shown in Fig. 5.8. The value of $\boldsymbol{\omega}_a$ depends on the control method, whether it is set to $\boldsymbol{\omega}_a = \omega_f$ or $\boldsymbol{\omega}_a = \omega_p$.

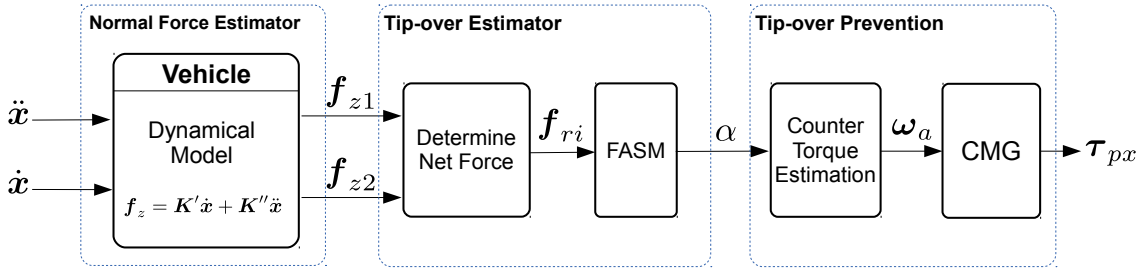

FIGURE 5.8: Overview of a tip-over prediction and tip-over stability enhancement system

5.3 Simulation

In order to verify the performance of the proposed SGCMG for the tip-over stability enhancement system, some simulations were conducted using simple motions of the holonomic and omnidirectional mobile platform. The simulations were conducted under the resolved velocity control for the transportation task which is divided into two: (1) translational motion in sideway direction, (2) simultaneous translational and rotational motion. The transportation load is set to 80 kg with the dimension of 1.0 m × 0.5 m × 0.8 m and the dimension of the mobile platform is set to 1.0 m × 0.5 m × 0.1 m. Other physical parameters of the personal mobility robot are listed in Table 5.1. The sampling interval for all simulation is set to 20 ms.

5.3.1 Translational motion in sideway direction

The personal mobility robot is set to move to the sideway direction from an initial pose of $x = [0\ 0\ \frac{5}{9}\pi]^T$, the initial orientation of ADWC1 is set to $\frac{3}{4}\pi$ rad and ADWC2 is set

TABLE 5.1: Physical parameters of the tip-over stability enhancement simulation

M_a	87	[kg]	m_1, m_2	6.5	[kg]
L_1	0.28	[m]	L_2	0.28	[m]
h_{s1}, h_{s2}	0.15	[m]	h_{m1}, h_{m2}	0.08	[m]
d_1, d_2	0.152	[m]	r_1, r_2	0.05	[m]
s_1, s_2	0.0875	[m]	s_{g1}, s_{g2}	0.028	[m]
s_{f1}, s_{f2}	0.175	[m]			

to $-\frac{3}{4}\pi$ rad. In this simulation, the SGCMG is set to produce a gimbal rate of 1 rad/s when the FASM ≤ 6. The velocity and acceleration profiles for this simulation are shown in Fig. 5.9. The simulation time is 13 s and the maximum velocity is set to 0.7 m/s.

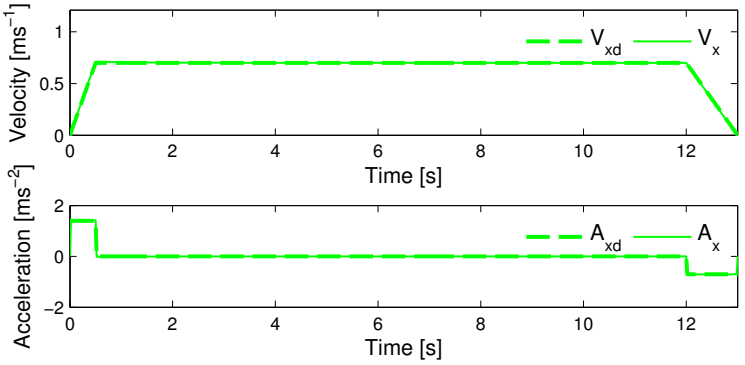

FIGURE 5.9: Velocity and acceleration profile (desired and actual)

Figure 5.10 shows the result of this simulation. The personal mobility robot performed the trajectory as shown in Fig. 5.10(a) without any tip-over incident was estimated where the stability is measured above zero as shown in Fig. 5.10(c). However, low tip-over stability is measured for the FASM ≤ 6 at two intervals: (1) the first 0.16 s, (2) between 12 s to 13 s. Both intervals of lower stability were measured during the acceleration and deceleration (braking) of the personal mobility robot where the dynamical effect was exists. A more stable maneuver is estimated during the constant velocity between 0.5 s to 12 s. Although the first acceleration is greater than the deceleration during braking, the stability during the acceleration is more stable. From our observation, more than half of the acceleration interval is stable (FASM > 6). The low stability in this period is not purely caused by the acceleration but also due to the rapid changes in the footprint shape. The stability enhancement by the SGCMG is effectively accomplished as shown by the FASM$_{cmg}$ value in Fig. 5.10(c). The stability in both intervals is improved. Fig. 5.10(d) shows the responses of the SGCMG. The flywheel of the SGCMG is initially rotating at 287.03 rad/s and changing rapidly at the end of the trajectory in parallel to the changes in gimbal angle to maintain the output torque.

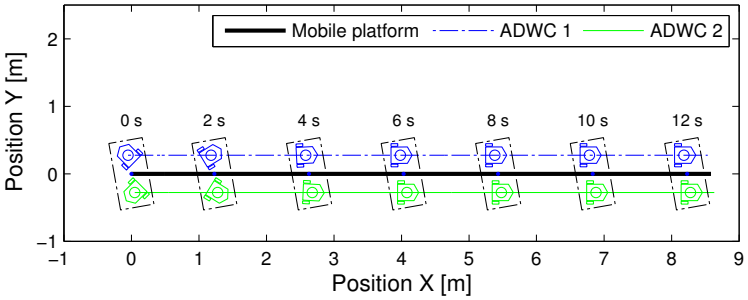

(a) Trajectory path

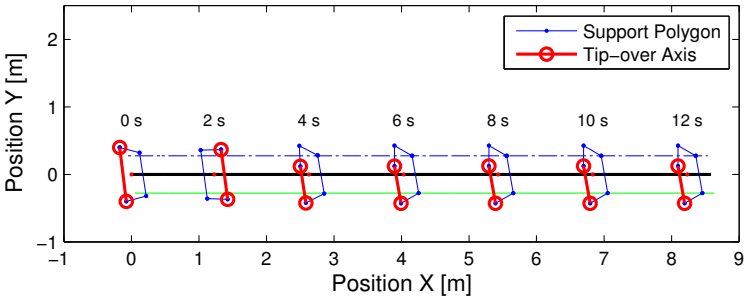

(b) Support polygon and tip-over axis

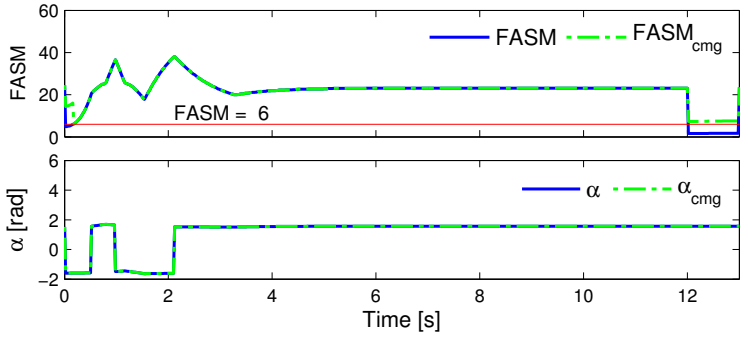

(c) FASM metric and tip-over angle

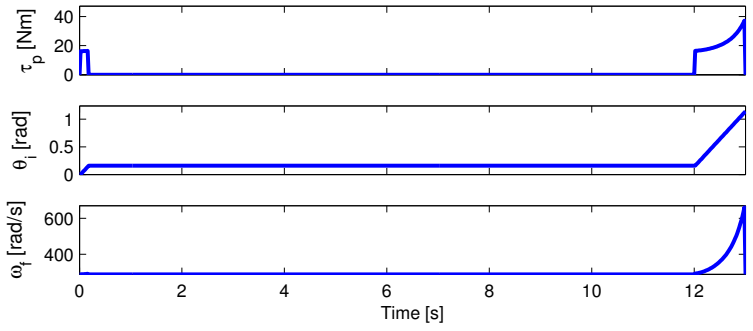

(d) SGCMG responses

FIGURE 5.10: Response for translational motion in sideway direction

5.3.2 Simultaneous translational and rotational motion

The personal mobility robot is set to perform a simultaneous translational and rotational motion from an initial pose of $x = [0\ 0\ \frac{\pi}{2}]^T$, the initial orientation of ADWC1 is set to $\frac{\pi}{2}$ rad and ADWC2 is set to $\frac{\pi}{4}$ rad. In this simulation, the SGCMG is set to produce a gimbal rate of 1 rad/s when the FASM ≤ 5. The velocity and acceleration profile for this simulation is shown in Fig. 5.11. The simulation time is 12.5 s and the maximum translational velocity is set to 0.6 m/s. An additional rotational motion of $\frac{\pi}{10}$ rad/s is also included while performing the translational motion.

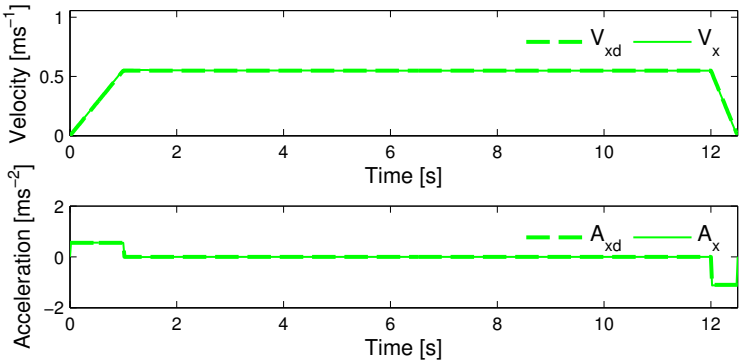

FIGURE 5.11: Velocity and acceleration profile (desired and actual)

Figure 5.12 shows the result of this simulation. The personal mobility robot was observed to be stable along the trajectory except at 12 s where the FASM has reached zero. As shown in Fig. 5.12(c) , the unstable region only measured at the final period during deceleration between 12 s to 12.5 s. In comparison with a normal translational motion, the stability of the personal mobility robot is keep changing along the trajectory due to the rapid changes in the ADWCs orientation (footprint). We also observed that the tip-over stability between 12 s to 12.5 s is improved by the SGCMG. The response of the SGCMG during the stability enhancement is shown in Fig. 5.12(d) . The flywheel of the SGCMG which is initially rotating at 287.03 rad/s changed in the final 0.5 s to 321.22 rad/s.

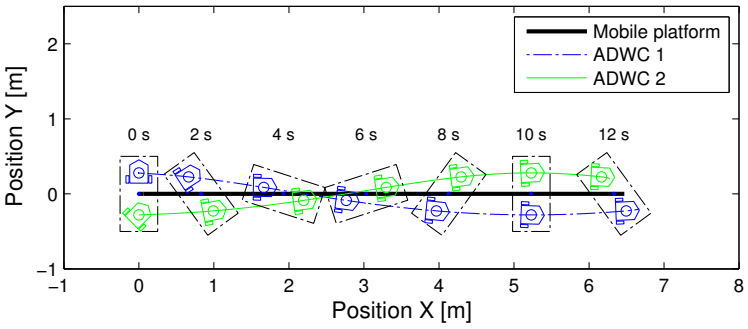

(a) Trajectory path

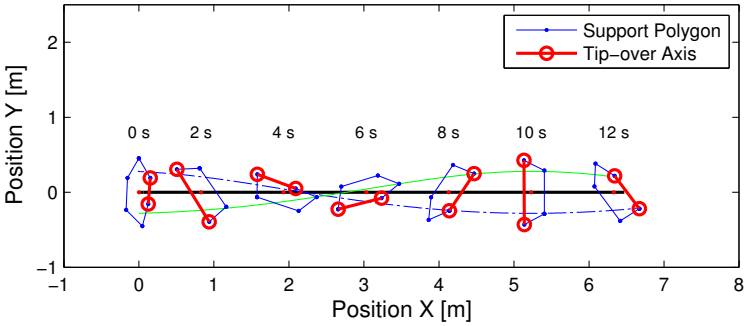

(b) Support polygon and tip-over axis

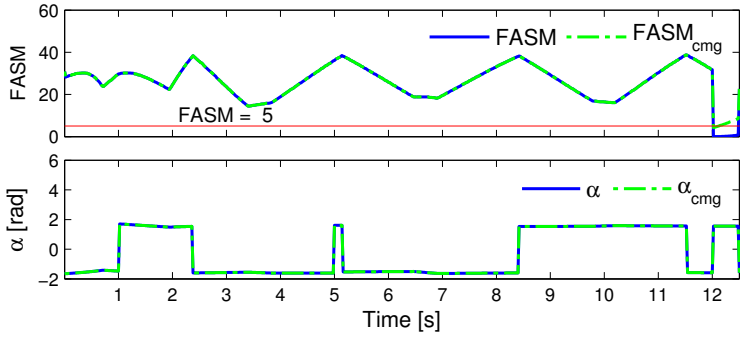

(c) FASM metric and tip-over angle

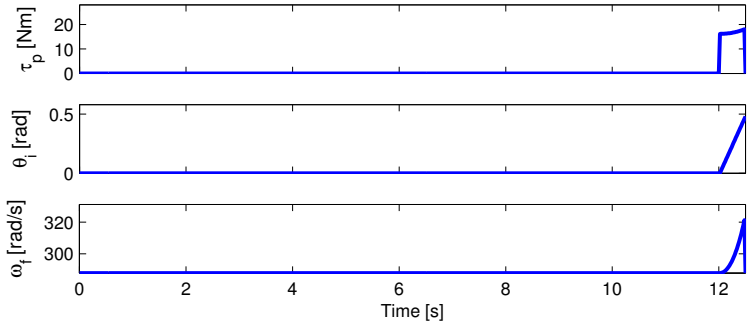

(d) SGCMG responses

FIGURE 5.12: Response for simultaneous translational and rotational motion

5.3.3 Alteration of acceleration and deceleration

Another method for enhancing the tip-over stability is by finding the safest acceleration and deceleration limit for the specific motion before the actual motion. Here, we moderated the acceleration and deceleration input before departure by finding the best solution of FASM value that passed the requirement of FASM>6. Figure 5.13 shows the comparison of the stability enhancement between the SGCMG method and the acceleration moderation method. We observed that the SGCMG method has shorter traveling time in comparison with the acceleration moderation method. In the first translational motion, the time is reduced by 0.46 s. Meanwhile, the time for simultaneous translational and rotational motion is reduced by 0.18 s. Thus, the SGCMG method is more desirable in term of advantage in the shorter travel time cost.

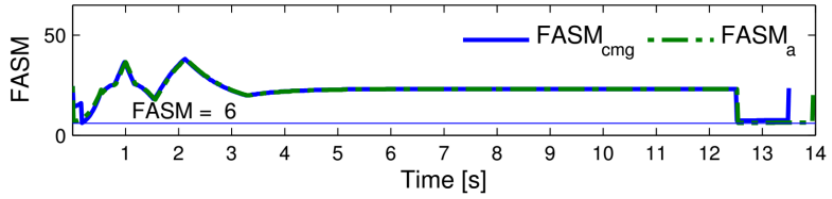

(a) Traslational motion

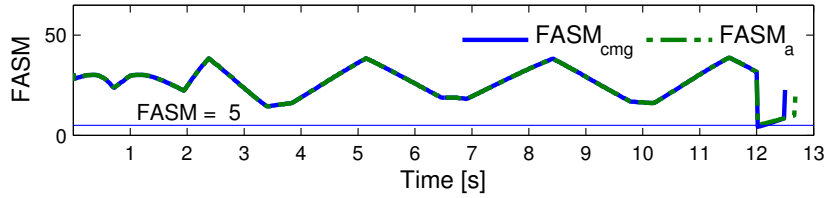

(b) Simultaneous translational and rotational motion

FIGURE 5.13: Comparison between the alteration of acceleration method and the SGCMG

5.4 Summary

In this chapter, we have examined two methods for the tip-over stability enhancement: i.e., alteration of acceleration input and gyroscopic torque device using the single-gimbal control moment gyro (SGCMG). From the simulation results, we found that both methods were capable of enhancing the tip-over stability and of preventing the personal mobility robots from the tip-over occurrence. The alteration of acceleration input method is more suitable for the robot path planning instead of instantaneous tip-over prevention. Meanwhile, the latter method using the SGCMG is more suitable for the real-time operation.

The performance of the SGCMG method is also proven to be superior in travel time cost to the alteration of the acceleration input method.

Chapter 6

Conclusion

This chapter summaries the contributions of this thesis and describes possible future directions for completion and extension of this work.

6.1 Summary of contribution

The primary theoretical contributions which have been presented in this thesis can be summarized as follows:

1. Most of the personal mobility robots introduced by several companies and universities were unique and have their own specialty. However, most of them require large spaces for rotation and turning, and is not capable of moving laterally. In consideration to the needs of motion in a crowded area, this thesis has presented a new approach to a personal mobility robot with holonomic and omnidirectional capabilities. The personal mobility robot was structured with two units of active dual-wheel caster assemblies. The locomotion mechanism provided by the active dual-wheel caster has advantages over that with the specialized wheel in the fact that it has better traction force and is able to handle the motion for indoor and outdoor applications. The use of the standard wheel also has a merit for overcoming the steps and uneven terrain.

2. Two basic designs for the personal mobility robot were proposed: i.e., four-wheeled architecture and six-wheeled architecture. The six-wheeled architecture has better stability in comparison with the four-wheeled architecture because of larger support polygon area. The personal mobility robot with four-wheeled structure also requires dynamical control when both active dual-wheel casters were aligned 90 deg to the

right or left of the robot's body. The six-wheeled architecture was more preferable for the personal mobility robot and discussed in detail for the tip-over prediction and prevention.

3. Dynamical models for both architectures were derived to predict the wheel reaction forces which were later used for estimating the net-forces in the tip-over prediction.

4. A novel method named Moment Stability Measure (MSM) was introduced to measure the tip-over stability. The performance of the MSM was shown to be equal to the existing measurement technique as proven by simulations.

5. The tip-over prediction system has been developed using the stability metrics, i.e., MSM and the Force-angle Stability Measure, and the derived dynamical model. The candidate of the tip-over occurrence was described using the tip-over angle.

6. Two methods for the tip-over stability enhancements were proposed: i.e., alteration of acceleration input and gyroscopic torque device using the single-gimbal control moment gyro (SGCMG). Both methods were capable of enhancing the tip-over stability and preventing the personal mobility robots from the tip-over occurrence. The alteration of acceleration input method was more suitable for considering the robot path planning instead of instantaneous tip-over prevention. Meanwhile, the latter method using the SGCMG was more suitable for the real-time operation. The performance of the SGCMG method was also proven to be superior in travel time cost to the alteration of the acceleration input method.

6.2 Future works

This section describes several suggestions for the completion and extension of this research.

1. *Development of prototype:*
   A prototype for the personal mobility robot with active dual-wheel caster assemblies should be developed. Real experiments for this prototype are necessary for real applications.

2. *Development of advanced control system for the SGCMG:*
   The basic control system for the SGCMG was discussed in Chapter 5. More advanced system to control the gimbal rate of the SGCMG is necessary especially for more complicated trajectories.

3. *Human dynamics:*

   The dynamical model for the personal mobility robots also should consider the human dynamics in the passenger model.

List of publications

Articles Published/Accepted/Submitted in Refereed International Journals

[1] M. J. A. Safar, K. Watanabe, S. Maeyama, and I. Nagai, "A study of tipping stability for omnidirectional mobile robot with active dual-wheel caster assemblies," *Artif. Life Robot.*, vol. 17, no. 1, pp. 145–151, Aug. 2012.

[2] M. J. A. Safar, K. Watanabe, S. Maeyama, and I. Nagai, "Tip-over stability enhancement for omnidirectional mobile robot," *Int. J. Intell. Unmanned Syst.*, (Submitted Dec. 2013).

International Conferences/Symposiums

[1] M. J. A. Safar, K. Watanabe, S. Maeyama, and I. Nagai, "Tip-over stability control for a holonomic omnidirectional mobile robot with active dual-wheel caster assemblies using SGCMG," in *Proc. IEEE/RSJ Int. Conf. Intell. Robot. Syst.*, Nov. 2013, pp. 4866–4871.

[2] M. J. A. Safar, K. Watanabe, S. Maeyama, and I. Nagai, "Tip-over prevention for a holonomic omnidirectional mobile robot with ADWCs," in *Proc. SICE Annu. Conf. 2013*, Sep. 2013, pp. 2738–2742.

[3] M. J. A. Safar, K. Watanabe, S. Maeyama, and I. Nagai, "Tip-over stability enhancement for omnidirectional mobile robot with ADWCs," in *Proc. 2nd Int. Conf. Electr. Control Comput. Eng.*, Aug. 2013, pp. 273–278.

[4] M. J. A. Safar, K. Watanabe, S. Maeyama, and I. Nagai, "Tip-over prevention for a holonomic omnidirectional mobile robot with ADWCs using SGCMG," in *Proc. IEEE Int. Conf. Mechatronics Autom.*, Aug. 2013, pp. 704–709.

[5] M. J. A. Safar, K. Watanabe, S. Maeyama, and I. Nagai, "Tip-over stability prediction for a holonomic omnidirectional transport mobile robot," in *6th Int. Conf. Soft Comput. Intell. Syst. 13th Int. Symp. Adv. Intell. Syst.*, Nov. 2012, pp. 763–768.

[6] M. J. A. Safar, K. Watanabe, S. Maeyama, and I. Nagai, "Tip-over Prediction for Omnidirectional Mobile Robot," *Procedia Eng.*, vol. 41, pp. 1085–1094, 2012.

[7] M. J. A. Safar, K. Watanabe, S. Maeyama, and I. Nagai, "Tip-over prediction for an omnidirectional mobile robot with dynamic supporting polygon," in *Proc. SICE Annu. Conf. 2012*, Aug. 2012, pp. 149–154.

[8] M. J. A. Safar, K. Watanabe, S. Maeyama, and I. Nagai, "A study of tipping stability for omnidirectional mobile robot with active dual-wheel caster assemblies," in *Proc. 17th Int. Symp. Artif. Life Robot.*, Jan. 2012, pp. 192–195.

References

[1] International Federation of Robotics, "Executive summary world robotics 2013," *World Robot. 2013*, pp. 10–21, 2013.

[2] B. Sawatzky, I. Denison, S. Langrish, S. Richardson, K. Hiller, and B. Slobogean, "The segway personal transporter as an alternative mobility device for people with disabilities: a pilot study." *Arch. Phys. Med. Rehabil.*, vol. 88, no. 11, pp. 1423–8, Nov. 2007.

[3] M. Bengel, K. Pfeiffer, B. Graf, A. Bubeck, and A. Verl, "Mobile robots for offshore inspection and manipulation," in *Proc. of IEEE/RSJ Int. Conf. Intell. Robot. Syst.*, Oct. 2009, pp. 3317–3322.

[4] P. Dutkiewicz, M. Kowalski, B. Krysiak, J. Majchrzak, M. Michalski, and W. Wr, "Design and control of a heating-pipe duct inspection mobile robot," in *Robot Motion Control*, 2007, no. 3, pp. 361–370.

[5] D. D. Paola, A. Milella, G. Cicirelli, and A. Distante, "An autonomous mobile robotic system for surveillance of indoor environments," *Int. J. Adv. Robot. Syst.*, vol. 7, no. 1, pp. 19–26, 2010.

[6] M. K. Habib and Y. Baudoin, "Robot-assisted risky intervention, search, rescue and environmental surveillance," *Int. J. Adv. Robot. Syst.*, vol. 7, no. 1, pp. 1–8, 2010.

[7] K. Zafar and I. M. Hussain, "Rope climbing robot with surveillance capability," *Int. J. Intell. Syst. Appl.*, vol. 5, no. 9, pp. 1–9, Aug. 2013.

[8] International Energy Agency, "CO2 emissions from fuel combustion - highlights," *IEA Stat.*, 2013.

[9] National Institute for Environmental Studies, "Japan's national greenhouse gas emissions in fiscal year 2012," pp. 1–7, 2013. [Online]. Available: http://www.nies.go.jp/whatsnew/2013/20131119/20131119-e.html

[10] M. Morita and A. Motojima, "Toyota i-unit: future "personal mobility"," pp. 3–6.

[11] G. S. Serv, L. Miguel, and S. Vera, "Prototype for a self-balanced personal transporter," in *2012 Work. Eng. Appl.*, May 2012, pp. 1–6.

[12] M. Strand, T. Schamm, A. Benazza, T. Kerscher, M. Zollner, and R. Dillmann, "Control of an autonomous personal transporter towards moving targets," in *Proc. of IEEE Work. Adv. Robot. its Soc. Impacts*, Nov. 2009, pp. 18–23.

[13] S. Ajisaka, T. Kubota, and H. Hashimoto, "Human balance control ability for affinitive personal vehicle," in *Proc. of the 10th Int. Conf. Ubiquitous Robot. Ambient Intell.*, Oct. 2013, pp. 503–508.

[14] K. Ulrich, "Estimating the technology frontier for personal electric vehicles," *Transp. Res. Part C Emerg. Technol.*, vol. 13, no. 5-6, pp. 448–462, Oct. 2005.

[15] L. D. Ballard, "Human-scaled personal mobility device performance characteristics," Georgia Institute of Technology, Tech. Rep., 2012.

[16] S. Nakajima and T. Fujikawa, "Proposal for personal mobility vehicle supported by mobility support system," in *Proc. of IEEE Int. Electr. Veh. Conf.*, Mar. 2012, pp. 1–6.

[17] R. Ando and A. Li, "An analysis on users' evaluation for self-balancing two-wheeled personal mobility vehicles," in *Proc. of the 15th Int. IEEE Conf. Intell. Transp. Syst.*, no. 9, 2012, pp. 1525–1530.

[18] J. Masood, M. Zoppi, and R. Molfino, "Investigation of personal mobility vehicle stability and maneuverability under various road scenarios," in *Proc. of IEEE/RSJ Int. Conf. Intell. Robot. Syst.*, Oct. 2012, pp. 4859–4864.

[19] N. Tomokuni and M. Shino, "Wheeled inverted-pendulum-type personal mobility robot with collaborative control of seat slider and leg wheels," in *Proc. of IEEE/RSJ Int. Conf. Intell. Robot. Syst.*, Oct. 2012, pp. 5367–5372.

[20] N. Hirose, R. Tajima, K. Sukigara, and Y. Tsusaka, "Posture stabilization for a personal mobility robot using feedback compensation with an unstable pole," in *Proc. of IEEE Int. Conf. Mechatronics*, Feb. 2013, pp. 804–809.

[21] T. Ienaga, Y. Senta, D. Arita, Y. Kimuro, K. Murakami, and T. Hasegawa, "A method for event handling on robot town platform and a sharable personal mobility robot," in *Proc. of Int. Conf. Broadband, Wirel. Comput. Commun. Appl.*, Nov. 2010, pp. 749–754.

[22] D. E. Kramer, "US . Patent Feb . 18 , 1986," 1986.

[23] Hoverround Corp., "Hoverround - Personal Mobility Solutions." [Online]. Available: http://www.hoverround.com/

[24] Segway Inc., "Segway Company Milestones." [Online]. Available: http://www.segway.com/about-segway/segway-milestones.php

[25] Segway Inc., "Project P.U.M.A." [Online]. Available: http://www.segway.com/puma/

[26] General Motors, "GM Unveils EN-V Concept A Vision for Future Urban Mobility." [Online]. Available: http://media.gm.com/content/autoshows/Shanghai/2010/public/cn/en/env/news.html

[27] Segway Inc., "Segway PT i2." [Online]. Available: http://www.segway.com/individual/models/i2.php

[28] S.-C. Lin, C.-C. Tsai, and H.-C. Huang, "Adaptive robust self-balancing and steering of a two-wheeled human transportation vehicle," *J. Intell. Robot. Syst.*, vol. 62, pp. 103–123, Aug. 2011.

[29] N. Hatao, R. Hanai, K. Yamazaki, and M. Inaba, "Real-time navigation for a personal mobility in an environment with pedestrians," in *Proc. of the 18th IEEE Int. Symp. Robot Hum. Interact. Commun.*, Sep. 2009, pp. 619–626.

[30] L. J. Pinto, D.-H. Kim, J. Y. Lee, and C.-S. Han, "Development of a Segway robot for an intelligent transport system," in *Proc. of IEEE/SICE Int. Symp. Syst. Integr.*, Dec. 2012, pp. 710–715.

[31] Toyota Motor Corp., "Toyota Personal Mobility." [Online]. Available: http://www.toyota-global.com/innovation/personal_mobility/

[32] Toyota Motor Corp., "Toyota exhibited a new concept of fuel cell hybrid vehicles and personal mobility at the Tokyo Motor Show (in Japanese)." [Online]. Available: http://www.toyota.co.jp/jp/news/03/Oct/nt03_082.html

[33] Toyota Motor Corp., "Toyota presents a new concept fuel cell hybrid vehicles, personal mobility at the Tokyo Motor Show (in Japanese)." [Online]. Available: http://www.toyota.co.jp/jp/news/05/Oct/nt05_060.html

[34] Toyota Motor Corp., "Toyota i-Real." [Online]. Available: http://www.toyota-global.com/innovation/personal_mobility/i-real.html

[35] Toyota Motor Corp., "Toyota develops personal transport assistance robot 'Winglet'." [Online]. Available: http://www.toyota.co.jp/en/news/08/0801_1.html

[36] Toyota Motor Corp., "Toyota i-Road (in Japanese)." [Online]. Available: http://www.toyota.co.jp/jpn/tokyoms2013/iroad/

[37] Toyota Motor Corp., "Toyota personal mobility)." [Online]. Available: http://www.toyota-global.com/events/motor_show/2013/geneva/booth/pmobility.html

[38] Honda Motor Co. Ltd., "The U3-X challenge: Mobility that unites rider and vehicle." [Online]. Available: http://world.honda.com/U3-X/BackStory/index.html

[39] Honda Motors Co. Ltd., "U3-X." [Online]. Available: http://www.honda.co.jp/robotics/u3x/

[40] Honda Motors Co. Ltd., "UNI-CUB (in Japanese)." [Online]. Available: http://www.honda.co.jp/UNI-CUB/

[41] Honda Motors Co. Ltd., "Overview of exhibited car at Geneva Motor Show (in Japanese)." [Online]. Available: http://www.honda.co.jp/news/2010/4100224.html

[42] T. Hayashi, "Hyundai Unveils 'E4U' Personal Mobility Vehicle." [Online]. Available: http://techon.nikkeibp.co.jp/english/NEWS_EN/20130402/274491/

[43] Hitachi Ltd., *Hitac Magazine (Sep. 2013) - in Japanese*, pp. 13–14.

[44] City of Tsukuba, "Robot Demonstration Zone Promotion Council." [Online]. Available: http://www.rt-tsukuba.jp/council/

[45] Toyota Motor Corp., "Sustainability Report 2010."

[46] M. Hashimoto, N. Suizu, I. Fujiwara, and F. Oba, "Path tracking control of a non-holonomic modular omnidirectional vehicle," in *Proc. IEEE Int. Conf. Syst. Man, Cybern.*, 1999, pp. 637–642.

[47] L. Clavien and J. Fr, "Teleoperation of AZIMUT-3 , an Omnidirectional Non-Holonomic Platform with Steerable Wheels," *IEEE Trans. Robot.*, pp. 2515–2516, 2010.

[48] B. E. Ilon, "Wheels for a course stable selfpropelling vehicle movable in any desired direction on the ground or some other base," 1975.

[49] J. Batlle and A. Barjau, "Holonomy in mobile robots," *Rob. Auton. Syst.*, vol. 57, no. 4, pp. 433–440, Apr. 2009.

[50] H. Asama, M. Sato, H. Kaetsu, K. Ozaki, A. Matsumoto, and I. Endo, "Development of an omni-directional mobile robot with 3 dof decoupling drive mechanism," *Journal of the Robotics Society of Japan*, vol. 14, no. 2, pp. 249–254, 1996.

[51] D. Chugo, K. Kawabata, H. Kaetsu, H. Asama, and T. Mishima, "Development of omnidirectional vehicle with step-climbing ability," in *Proc. of IEEE Int. Conf. Robot. Autom.*, 2003, pp. 3849–3854.

[52] D. Chugo, H. Asama, K. Kawabata, H. Kaetsu, and T. Mishima, "Plural Wheels Control based on Slip Estimation," in *Proc. of IEEE/RSJ Int. Conf. Intell. Robot. Syst.*, Oct. 2006, pp. 5558–5563.

[53] M. Komori, "Movable to sideways and in any direction! Development of future vehicles - the omnidirectional wheel made the movement easier and convenient (in Japanese)." [Online]. Available: http://www.kyoto-u.ac.jp/ja/news_data/h/h1/news6/2011/120322_1.htm

[54] F. Pin and S. Killough, "A new family of omnidirectional and holonomic wheeled platforms for mobile robots," *IEEE Trans. Robot. Autom.*, vol. 10, no. 4, pp. 480–489, 1994.

[55] G. Mourioux, C. Novales, G. Poisson, and P. Vieyres, "Omni-directional robot with spherical orthogonal wheels: concepts and analyses," in *Proc. 2006 IEEE Int. Conf. Robot. Autom. 2006. ICRA 2006.*, vol. 2, no. May, 2006, pp. 3374–3379.

[56] K. Watanabe, "Control of an mnidirectional Mobile Robot," *Rev. Lit. Arts Am.*, no. April, pp. 21–23, 1998.

[57] J. Tang, K. Watanabe, K. Kuribayashi, and Y. Shiraishi, "Autonomous Control for an Omnidirectional Mobile Robot with the Orthogonal-Wheel Assembly (In Japanese)," *J. Robot. Soc. Japan*, vol. 17, no. 1, pp. 51–60, 1999.

[58] C. Ye and S. Ma, "Development of an omnidirectional mobile platform," in *Proc. of Int. Conf. on Mechatronics and Automation*, 2009, pp. 1111–1115.

[59] S. Ma, C. Ren, and C. Ye, "An omnidirectional mobile robot: Concept and analysis," in *Proc. of IEEE Int. Conf. on Robotics and Biomimetics (ROBIO)*, 2012, pp. 920–925.

[60] M. West and H. Asada, "Design and control of ball wheel omnidirectional vehicles," in *Proc. IEEE Int. Conf. Robot. Autom.*, 1995, pp. 1931–1938.

[61] L. Ferriere and B. Raucent, "ROLLMOBS, a new universal wheel concept," in *Proceedings IEEE Int. Conf. Robot. Autom.*, 1998, pp. 1877–1882.

[62] H. Ghariblu, "Design and modeling of a ball wheel omni-directional mobile robot," in *Proc. of Second Int. Conf. Comput. Eng. Appl.*, 2010, pp. 571–575.

[63] S. Ishida and H. Miyamoto, "Ball wheel drive mechanism for holonomic omnidirectional vehicle," in *Proc. of World Autom. Congr.*, 2010, pp. 1–6.

[64] S. Mascaro, J. Spano, and H. H. Asada, "A reconfigurable holonomic omnidirectional mobile bed with unified seating (RHOMBUS) for bedridden patients," in *Proc. IEEE Int. Conf. Robot. Autom.*, 1997, pp. 1277–1282.

[65] S. Mascaro and H. H. Asada, "Docking control of holonomic omnidirectional vehicles with applications to a hybrid wheelchair/bed system," in *Proc. IEEE Int. Conf. Robot. Autom.*, 1998, pp. 399–405.

[66] M. Wada and H. Asada, "Design of a holonomic omnidirectional vehicle using a reconfigurable footprint mechanism and its application to a wheelchair (In Japanese)," *J. Robot. Soc. Japan*, vol. 16, no. 6, pp. 816–823, 1998.

[67] M. Wada and H. H. Asada, "A holonomic vehicle with a reconfigurable footprint mechanism and its application to wheelchairs," in *Proc. IEEE Int. Conf. Robot. Autom.*, 1998, pp. 774–780.

[68] M. Wada, A. Takagi, and S. Mori, "A mobile platform with a dual-wheel caster-drive mechanism for holonomic and omnidirectional mobile robots (in Japanese)," *J. Robot. Soc. Japan*, vol. 18, no. 8, pp. 1166–1172, 2000.

[69] S. Ok, A. Kodama, Y. Matsumura, and Y. Nakamura, "SO(2) and SO(3), omni-directional personal mobility with link-driven spherical wheels," in *Proc. of IEEE/RSJ Int. Conf. Intell. Robot. Syst.*, no. 2, Sep. 2011, pp. 268–273.

[70] K. Tadakuma and R. Tadakuma, "Mechanical design of "omni-ball": spherical wheel for holonomic omnidirectional motion," in *Proc. IEEE Int. Conf. Autom. Sci. Eng.*, vol. 788, 2007, pp. 788–794.

[71] K. Tadakuma, R. Tadakuma, and J. Berengeres, "Development of holonomic omnidirectional vehicle with "omni-ball": spherical wheels," in *Proc. IEEE Int. Conf. Intell. Robot. Syst.*, Oct. 2007, pp. 33–39.

[72] U. Nagarajan, A. Mampetta, G. a. Kantor, and R. L. Hollis, "State transition, balancing, station keeping, and yaw control for a dynamically stable single spherical wheel mobile robot," in *Proc. of 2009 IEEE Int. Conf. Robot. Autom.*, vol. 2, 2009, pp. 998–1003.

[73] M. Wada and H. Asada, "A holonomic omnidirectional vehicle with a reconfigurable footprint mechanism and its application to wheelchairs," in *Proc. IEEE Int. Conf. Robot. Autom.*, 1998, pp. 774–780.

[74] A. Nishikawa, M. West, and H. Asada, "Development of a Holonomic Omnidirectional Vehicle and an Accurate Guidance Method of the Vehicles (In Japanese)," *J. Robot. Soc. Japan*, vol. 13, no. 2, pp. 249–256, 1995.

[75] S. Hirose and S. Amano, "The VUTON: High Payload, High Efficiency Holonomic Omni-Directional Vehicle," in *Proc. 6th Int. Symp. Robot. Res.*, 1993, pp. 253–260.

[76] R. Damoto, W. Cheng, and S. Hirose, "Holonomic omnidirectional vehicle with new omni-wheel mechanism," in *Proc. IEEE Int. Conf. Robot. Autom.*, 2001, pp. 773–778.

[77] M. Wada, "A synchro-caster drive system for holonomic and omnidirectional mobile robots," in *Proc. IEEE 26th Annu. Conf. Ind. Electron. Soc.*, 2000, pp. 1937–1942.

[78] M. Wada and S. Mori, "Holonomic and omnidirectional vehicle with conventional tires," in *Proc. IEEE Int. Conf. Robot. Autom.*, 1996, pp. 3671–3676.

[79] M. Wada and S. Mori, "Modeling and control of a new type of omnidirectional holonomic vehicle," in *Proc. of the 4th Int. Work. Adv. Motion Control*, 1996, pp. 265–270.

[80] F. Han, T. Yamada, K. Watanabe, and K. Izumi, "Construction of an omnidirectional mobile robot platform based on active dual-wheel caster mechanisms and development of a control simulator," *J. Intell. Robot. Syst.*, vol. 29, no. 3, pp. 257–275, 2000.

[81] F. Han, T. Yamada, K. Watanabe, and K. Izumi, "An omnidirectional mobile robot using multiple dual-wheel caster assemblies (in Japanese)," *JSME Trans. Ser. C*, vol. 67, no. 653, pp. 154–161, 2001.

[82] H. Yu, M. Spenko, and S. Dubowsky, "Omni-directional mobility using active split offset castors," *ASME J. Mech. Des.*, vol. 126, no. 7, pp. 822–829, 2004.

[83] M. Udengaard and K. Iagnemma, "Analysis, design, and control of an omnidirectional mobile robot in rough terrain," *ASME J. Mech. Des.*, vol. 131, no. 12, pp. 121 002 (1–11), 2009.

[84] I. Karl, U. Martin, I. Genya, S. Matthew, O. Sinan, K. Imad, J. Overholt, and G. Hudas, "Design and development of an agile, man portable unmanned ground vehicle," in *Proceedings of the 26th Annual Army Science Conference*, 2008.

[85] M. Wada, "Holonomic and omnidirectional wheelchairs with synchronized 4WD mechanism," in *Proc. IEEE Int. Conf. Intell. Robot. Syst.*, Oct. 2007, pp. 1196–1202.

[86] M. Wada, "Mechanism and control of a 4WD robotic platform for omnidirectional wheelchairs," in *Proc. of IEEE/RSJ Int. Conf. Intell. Robot. Syst.*, Oct. 2009, pp. 4855–4862.

[87] M. C. Walz, "Trends in the static stability factor of passenger cars, light trucks, and vans," U.S. Department of Transportation, Tech. Rep. June, 2005.

[88] J. P. Chrstos and D. A. Guenther, "Measurement of static rollover metrics," *SAE Technical Paper Series*, no. 920582, pp. 123–134, 1992.

[89] S.-k. Chen, N. Moshchuk, F. Nardi, and J. Ryu, "Vehicle rollover avoidance," *IEEE Control Syst.*, pp. 70–85, 2010.

[90] B. Schofield, T. Hä gglund, and A. Rantzer, "Vehicle dynamics control and controller allocation for rollover prevention," in *2006 IEEE Conference on Computer Aided Control System Design, 2006 IEEE International Conference on Control Applications, 2006 IEEE International Symposium on Intelligent Control*, 2006, pp. 8–13.

[91] R. McGhee and A. Frank, "On the stability properties of quadruped creeping gaits," *Mathematical Biosciences*, vol. 3, pp. 331–351, 1968.

[92] R. B. Mcghee and G. I. Iswandhi, "Adaptive locomotion of a multilegged robot over rough terrain," *IEEE Trans. Syst. Man Cybern.*, vol. 9, no. 4, pp. 176–182, 1979.

[93] C. de Zhang and S.-M. Song, "Gaits and geometry of a walking chair for the disabled," *Journal of Terramechanics*, vol. 26, no. 3–4, pp. 211 – 233, 1989.

[94] C.-D. Zhang and S.-M. Song, "Stability analysis of wave-crab gaits of a quadruped," *Journal of Robotic Systems*, vol. 7, no. 2, pp. 243–276, 1990.

[95] T.-t. Lee and C.-l. Shih, "A study of the gait control of a quadruped walking vehicle," *IEEE J. Robot. Autom.*, vol. RA-2, no. 2, pp. 61–69, 1986.

[96] T.-T. Lee, C.-M. Liao, and T. Chen, "On the stability properties of hexapod tripod gait," *Robotics and Automation, IEEE Journal of*, vol. 4, no. 4, pp. 427–434, 1988.

[97] D. A. Messuri and C. A. Klein, "Automatic body regulation for maintaining stability of a legged vehicle," *Robotics*, vol. RA-1, no. 3, pp. 132–141, 1985.

[98] P. V. Nagy, S. Desa, and W. L. Whittaker, "Energy-based stability measures for reliable locomotion of statically stable walkers: Theory and application." *Int. J. Robotic Res.*, no. 3, pp. 272–288, 1994.

[99] S. Hirose, H. Tsukagoshi, and K. Yoneda, "Normalized energy stability margin and its contour of walking vehicles on rough terrain," in *Proceedings of IEEE International Conference on Robotics and Automation*, vol. 1, 2001, pp. 181–186.

[100] D. Orin, R. Mcghee, and V. Jaswa, "Interactive compute-control of a six-legged robot vehicle with optimization of stability, terrain adaptibility and energy," in *Proc. of IEEE Conf. on Decision and Control and the 15th Symposium on Adaptive Processes*, vol. 15, 1976, pp. 382–391.

[101] B.-S. Lin and S.-M. Song, "Dynamic modeling, stability and energy efficiency of a quadrupedal walking machine," in *Robotics and Automation, 1993. Proceedings., 1993 IEEE International Conference on*, 1993, pp. 367–373 vol.3.

[102] K. Yoneda and S. Hirose, "Tumble stability criterion of integrated locomotion and manipulation," in *Proc. of IEEE/RSJ International Conference on Intelligent Robots and Systems. IROS '96*, vol. 2, 1996.

[103] D. Zhou, K. H. Low, and T. Zielinska, "A stability analysis of walking robots based on leg-end supporting moments," in *Proceeding of IEEE International Conference on Robotics and Automation*, vol. 3, 2000, pp. 2834–2839.

[104] E. Papadopoulos and D. Rey, "A new measure of tipover stability margin for mobile manipulators," in *Proc. IEEE Int. Conf. Robot. Autom.*, no. April, 1996, pp. 3111–3116.

[105] T. Yamada, K. Watanabe, K. Izumi, and K. Kiguchi, "Dynamics-based control for an omnidirectional mobile robot with active dual-wheel caster cssemblies (in Japanese)," *JSME Trans. Robot. Mechatronics*, pp. 2P1–41–057 (1–2), 2000.

[106] F. Han, T. Yamada, K. Watanabe, and K. Izumi, "An omnidirectional mobile robot using multiple dual-wheel caster assemblies (in Japanese)," *JSME Trans. Ser. C*, vol. 67, no. 653, pp. 154–161, 2001.

[107] M. J. A. Safar, K. Watanabe, S. Maeyama, and I. Nagai, "A study of tipping stability for omnidirectional mobile robot with active dual-wheel caster assemblies," in *Proc. 17th Int. Symp. Artif. Life Robot.*, Jan. 2012, pp. 192–195.

[108] M. J. A. Safar, K. Watanabe, S. Maeyama, and I. Nagai, "Tip-over Prediction for Omnidirectional Mobile Robot," *Procedia Eng.*, vol. 41, pp. 1085–1094, 2012.

[109] S. Peters and K. Iagnemma, "An analysis of rollover stability measurement for high-speed mobile robots," in *Proc. 2006 IEEE Int. Conf. Robot. Autom. 2006. ICRA 2006.*, May 2006, pp. 3711–3716.

[110] S. C. Peters and K. Iagnemma, "Stability measurement of high-speed vehicles," *Veh. Syst. Dyn.*, vol. 47, no. 6, pp. 701–720, Jun. 2009.

[111] C. H. Thomas, C. E. Leiserson, R. L. Rivest, and C. Stein, *Introduction to Algorithms*, 3rd ed. Massachusetts Institute of Technology, Jun. 2009, vol. 1, no. 2.

[112] R. F. Abo-Shanab and N. Sepehri, "Dynamic modeling of tip-over stability of mobile manipulators considering the friction effects," *Robotica*, vol. 23, no. 2, pp. 189–196, Mar. 2005.

[113] Q. Huang, S. Sugano, and I. Kato, "Stability control for a mobile manipulator using a potential method," in *Proc. IEEE/RSJ Int. Conf. Intell. Robot. Syst.*, 1994, pp. 839–846.

[114] M. Mann and Z. Shiller, "Dynamic stability of off-road vehicles: a geometric approach," in *Proc. IEEE Int. Conf. Robot. Autom.*, vol. 2, May 2006, pp. 3705–3710.

[115] E. Garcia, J. Estremera, and P. G. de Santos, "A comparative study of stability margins for walking machines," *Robotica*, vol. 20, no. 06, pp. 595–606, Nov. 2002.

[116] M. J. A. Safar, K. Watanabe, S. Maeyama, and I. Nagai, "A study of tipping stability for omnidirectional mobile robot with active dual-wheel caster assemblies," *Artif. Life Robot.*, vol. 17, no. 1, pp. 145–151, Aug. 2012.

[117] E. Papadopoulos and D. A. Rey, "The force-angle measure of tipover stability margin for mobile manipulators," *System*, pp. 29–48, 2000.

[118] M. J. A. Safar, K. Watanabe, S. Maeyama, and I. Nagai, "Tip-over prediction for an omnidirectional mobile robot with dynamic supporting polygon," in *Proc. SICE Annu. Conf. 2012*, Aug. 2012, pp. 149–154.

[119] M. J. A. Safar, K. Watanabe, S. Maeyama, and I. Nagai, "Tip-over stability prediction for a holonomic omnidirectional transport mobile robot," in *6th Int. Conf. Soft Comput. Intell. Syst. 13th Int. Symp. Adv. Intell. Syst.*, Nov. 2012, pp. 763–768.

[120] K. Boniface, M. P. McKay, R. Lucas, A. Shaffer, and N. Sikka, "Serious injuries related to the segway® personal transporter: a case series," *Annals of emergency medicine*, vol. 57, no. 4, pp. 370–374, 2011.

[121] M. Kumagai and T. Ochiai, "Development of a robot balancing on a ball," in *Proc. of Int. Conf. Control. Autom. Syst.*, 2008, pp. 433–438.

[122] M. J. A. Safar, K. Watanabe, S. Maeyama, and I. Nagai, "Tip-over stability control for a holonomic omnidirectional mobile robot with active dual-wheel caster assemblies using SGCMG," in *Proc. IEEE/RSJ Int. Conf. Intell. Robot. Syst.*, Nov. 2013, pp. 4866–4871.

[123] M. J. A. Safar, K. Watanabe, S. Maeyama, and I. Nagai, "Tip-over prevention for a holonomic omnidirectional mobile robot with ADWCs using SGCMG," in *Proc. IEEE Int. Conf. Mechatronics Autom.*, Aug. 2013, pp. 704–709.

[124] M. J. A. Safar, K. Watanabe, S. Maeyama, and I. Nagai, "Tip-over stability enhancement for omnidirectional mobile robot with ADWCs," in *Proc. 2nd Int. Conf. Electr. Control Comput. Eng.*, Aug. 2013, pp. 273–278.

[125] K. Omagari, T. Usuda, and S. Matunaga, "Research of control momentum gyros for micro-satellites and 3-DOF attitude dynamics simulator experiments," in *Proc. 8th Int. Symp. Artif. Intell., Robot. Autom. Sp.*, 2005.

[126] N. Townsend, A. Murphy, and R. Shenoi, "A new active gyrostabiliser system for ride control of marine vehicles," *Ocean Eng.*, vol. 34, no. 11-12, pp. 1607–1617, Aug. 2007.